UNIVERSITY OF MINNESOTA

This is to certify that I have examined this bound copy of a doctoral thesis by

Christopher L. Moore

and have found that it is complete and satisfactory in all respects,
and that any and all revisions required by the final
examining committee have been made.

Dr. Homayoon Kazerooni

Name of Faculty Adviser(s)

H. Kazerooni

Signature of Faculty Adviser(s)

November 14, 1991

Date

GRADUATE SCHOOL

PERFORMANCE AND STABILITY OF TELEMANIPULATORS USING BILATERAL IMPEDANCE CONTROL

A THESIS
SUBMITTED TO THE FACULTY OF THE GRADUATE SCHOOL
OF THE UNIVERSITY OF MINNESOTA
BY

CHRISTOPHER LANE MOORE

IN PARTIAL FULFILLMENT OF THE REQUIREMENTS
FOR THE DEGREE OF
DOCTOR OF PHILOSOPHY

DECEMBER, 1991

PERFORMANCE AND STABILITY OF TELEMANIPULATORS USING BILATERAL IMPEDANCE CONTROL

ABSTRACT

The research investigates a new method of control for telemanipulators called bilateral impedance control. This new method differs from previous approaches in that interaction forces are used as the communication signals between the master and slave robots. The new control architecture has several advantages:

1. It allows the master robot and the slave robot to be stabilized independently without becoming involved in the overall system dynamics.
2. It permits the system designers to arbitrarily specify desired performance characteristics such as the force and position ratios between the master and slave.
3. The impedance at both ends of the telerobotic system can be modulated to suit the requirements of the task.

The main goals of the research are to characterize the performance and stability of the new control architecture. The dynamics of the telerobotic system are described by a bond graph model that illustrates how energy is transformed, stored, and dissipated.

Performance can be completely described by a set of three independent parameters. These parameters are fundamentally related to the structure of the H matrix that regulates the communication of force signals within the system. By tailoring the H matrix, the performance parameters can be arbitrarily specified to achieve desired performance characteristics. The only limitations on the choice of these parameters are imposed by system stability.

Stability is analyzed with two mathematical techniques: the Small Gain Theorem and the Multivariable Nyquist Criterion. The Small Gain Theorem is used to arrive at a general set of stability conditions that is equally valid for linear as well as nonlinear systems. The Multivariable Nyquist Criterion is used to analyze the stability of linear systems with transfer function matrix operators.

The theoretical predictions for performance and stability are experimentally verified by implementing the new control architecture on a multi-degree-of-freedom telemanipulator. The frequency response of the performance parameters are measured, and the absolute stability bounds are determined. Robustness to modeling uncertainties is demonstrated from the shape of the frequency response.

ACKNOWLEDGMENTS

I wish to thank my adviser, Dr. Homayoon Kazerooni, for his guidance and support. His ideas on new methods of telerobotic control were the foundation of my research. I am grateful to the members of my thesis review committee, Dr. Arthur G. Erdman, Dr. Darrell A. Frohrib, Dr. William L. Garrard, and Dr. James R. Slagle. Finally, I would like to thank the members of the Automation Technology Branch at NASA Langley Research Center who gave me the opportunity to work in their lab. This work was funded under NASA research grant RTR 590-11-41-01.

TABLE OF CONTENTS

LIST OF FIGURES

LIST OF TABLES

Symbols

α	Small Gain Theorem constant
β	Small Gain Theorem constant
ϕ_{CL}	closed-loop characteristic polynomial
ϕ_{OL}	open-loop characteristic polynomial
θ_m	vector of master robot joint angles
θ_{ref}	reference position command in joint space
θ_s	vector of slave robot joint angles
Δq	position error in joint space
$\dot{\theta}_m$	vector of master robot joint velocities
$\dot{\theta}_{ref}$	reference velocity command in joint space
$\dot{\theta}_s$	vector of slave robot joint velocities
τ_a	actuator torque
τ_m	master robot joint torques
τ_s	slave robot joint torques
ω	angular frequency
adj	matrix adjunct
A(q)	ARX model denominator polynomial
B(q)	ARX model numerator polynomial
C	damping impedance; capacitor
det	matrix determinant
E	environmental dynamics
E(t)	energy
e	error signal
e(t)	effort; random noise
f(t)	vector function; flow
f_{ext}	external forces imposed on slave robot
f_m	force acting on master robot
f_s	force acting on slave robot
$\| f \|_p$	L_p norm of f(t)
$\| f_T \|_p$	truncated L_p norm of f(t)
G	transfer function matrix
G_{CL}	closed-loop transfer function
G_m	master robot primary closed-loop system
G_n	nominal open-loop transfer function

G_{OL}	open-loop transfer function
G_s	slave robot primary closed-loop system
GY	gyrator
g(k)	impulse response function
H	force feedback matrix
H_{11}	element in H matrix that controls master impedance
H_{12}	element in H matrix that controls force reflection
H_{21}	element in H matrix that controls motion coupling
H_{22}	element in H matrix that controls slave impedance
h(k)	random noise filter
I	inertia
J	robot Jacobian matrix
J^T	transpose of Jacobian matrix
j	complex variable
K	stiffness impedance
k	sample number
L_p^n	n x 1 vector space
M	robot mass matrix
m	transformer modulus
N	number of clockwise encirclements; total samples
n	degrees of freedom
na	order of ARX denominator polynomial
nb	order of ARX numerator polynomial
nk	sample delay in ARX model
P	admittance matrix; number of poles
P(t)	power
P_m	master robot pitch position
P_s	slave robot pitch position
P_{11}	admittance $G_mH_{11} + S_m$
P_{12}	admittance G_mH_{12}
P_{21}	admittance G_sH_{21}
P_{22}	admittance $G_sH_{22} + S_s$
ΔP	$P_{11}P_{22} - P_{12}P_{21}$
p(t)	momentum
q	shift operator

$q(t)$	displacement
r	reference input command; gyrator modulus
R	resistor
R_f	ratio of slave force to master force
R_y	ratio of slave position to master position
S	sensitivity matrix
S_e	source of effort
S_f	source of flow
S_h	human arm sensitivity
S_m	master robot sensitivity
S_s	slave robot sensitivity
s	Laplace operator ($j\omega$)
${}^{b}_{h}T$	coordinate frame transformation from hand to base
TF	transformer
t	time
$u(t)$	system input
u_h	thought command from human central nervous system
u_m	electronic input command to G_m
u_s	electronic input command to G_s
$V[\,]$	nonlinear operator
V_N	prediction error
$v(t)$	disturbance
X	vector of state variables
Y_m	master robot yaw position
Y_s	slave robot yaw position
$y(t)$	system output
y_m	position of master robot
y_n	nominal system output
y_s	position of slave robot
Z	impedance; number of zeros
Z_m	impedance telerobotic system presents to human
Z_{ma}	master robot impedance
Z_s	impedance telerobotic system presents to environment
Z_{sa}	slave robot impedance
z	Nyquist conformal mapping variable

Chapter 1
INTRODUCTION

1.1 Introduction

A telerobotic system consists of two robots; the "master," which is driven by a human operator, and the "slave," which performs tasks at a remote location. The motion of the slave robot is a function of the master robot. Figure 1.1 shows the elements of a telerobotic system where the human is pushing against an object.

Teleoperation is greatly enhanced if the forces acting on the slave robot are fed back to the operator. This gives the operator the feeling that she is manipulating the remote object directly. Systems that employ force reflection are called "bilateral" because information flows in two directions between the master and the slave. An historical overview of telerobotics is given in Sheridan (1988).

This research proposes a new method of telerobotic control. The proposed control architecture has several advantages over previous approaches. First, the control method allows the designers to stabilize the master robot and the slave robot independently, without getting involved in the overall system dynamics. It is not necessary to include the dynamics of the human, the dynamics of the object being manipulated, or any cross coupling between the master and the slave.

Second, the control method allows the specification of desired performance characteristics. It is possible to arbitrarily select three independent performance parameters. These may be the force reflection ratio, the master-to-slave position ratio, and the impedance of either robot. Impedance is defined as the ratio of force to position (or velocity), and it is a measure of the robot's resistance to motion. The only limitations on the choice of these parameters are the bounds imposed by system stability.

Finally, the control method works for both direct and non-direct drive systems. A non-direct drive system is one in which gears or chains transfer mechanical power from the motors to the robot links. Present control architectures work well only for direct drive systems where the human can easily overcome the friction and inertia of the master robot. With a non-direct drive system, the human may not be able to exert sufficient force to move the robot. Even with direct drive systems, the master impedance may be significant, and this contributes to operator fatigue. The proposed control architecture overcomes the impedance problem by sensing the interaction forces between the human and the master, and using the forces as input to drive the robot. This method is called "impedance control" because it establishes a relationship between force and position (Kazerooni 1989).

1.2 Dynamic Behavior of the Telerobotic System

The dynamic behavior of a telerobotic system results from the interaction of its components: the master and slave robots, the human, and the environment. A dynamic model for each component will be developed separately. These models will then be combined to form a control architecture that describes the overall system dynamics.

1.2.1 Dynamic Behavior of the Telerobots

It is assumed that both the master and the slave robots are stabilized by independent closed-loop position controllers. The compensators that stabilize the robots may include velocity feedback, but closed-loop velocity control by itself cannot guarantee that the motion of the slave will always follow the motion of the master. There are two significant motivations for using closed-loop position controllers as the primary stabilizing compensators. First, safety dictates that the master remains stable when it is not being manipulated by the human. Closed-loop position controllers keep the master and slave robots stationary when the human is not interacting with the system. Second, the primary stabilizing compensators can be designed without getting involved in the overall dynamics of the system. It is not necessary to include the dynamics of the human, the dynamics of the object being manipulated, or any cross coupling between the master and the slave. A variety of robust control methods can be used to stabilize the master and slave robots independently (Spong and Vidyasagar 1985).

The master position vector, y_m, is a function of two variables: the electronic commands to the master drive motors, and the external forces imposed on the master robot.[1] The operator G_m represents the primary closed-loop system, which consists of the master robot and the stabilizing compensator. The input to the primary closed-loop system is the electronic command, u_m. The output is the master position, y_m. The master sensitivity operator, S_m, relates the force imposed on the master robot, f_m, to its position, y_m. The sensitivity depends on the robot's mechanical characteristics as well as the strength of the stabilizing position controller. Equation 1.1 represents the master robot dynamic behavior in its most general form.

---

[1]For convenience, "position" implies both position and orientation; "force" implies both force and torque.

$$y_m = G_m(u_m) + S_m(f_m) \tag{1.1}$$

Since the master robot is in contact with only the human, f_m represents the forces exerted by the human. The dynamic behavior of the slave robot can be similarly defined by equation 1.2.

$$y_s = G_s(u_s) + S_s(f_s) \tag{1.2}$$

where f_s represents the forces imposed on the slave by the environment, and u_s is the electronic input command to the slave drive motors. G_s and S_s are defined in the same way as G_m and S_m.[2]

1.2.2 Dynamic Behavior of the Human Arm

The internal structure of the human arm is not considered in a dynamic model. A relationship between inputs and outputs implicitly accounts for the dynamics of nerve conduction, muscle contraction, and central nervous system processing. Since the human arm is in contact with the master robot only, the position and velocity disturbances on the human arm are solely from the master robot.

The human arm can be modeled as a non-ideal force control system (Kazerooni 1990). The force imposed on the master robot by the human arm results from two inputs. The first input, u_h, is issued by the human central nervous system, while the motion of the master robot forms the second input. The master robot motion can be thought of as a position or velocity disturbance occurring on the force-controlled human arm. In other words, if the master robot is stationary, the amount of force imposed on the master robot will only be a function of the commands from the central nervous system. However, if the master robot moves, then the force imposed on the master robot is a function of not only the central nervous system, but also the motion of the master robot. It is assumed that the specific form of u_h is not known, other than it is the human thought deciding to impose a force onto the master robot. The human arm "sensitivity" operator, S_h, is defined in equation 1.3 to map the master robot position, y_m, into the imposed force, f_m.

$$f_m = u_h - S_h(y_m) \tag{1.3}$$

---

[2]The subscript "m" signifies the master; "s" refers to the slave.

The minus sign results from the disturbance rejection property of the human arm. The master robot motion decreases the force imposed by the human.

1.2.3 Dynamic Behavior of the Environment

The master-slave system is used for manipulating heavy objects or for imposing large forces on the objects. The term "environment" represents any object being manipulated or pushed by the slave robot. A simple example of environmental interaction is seen in Figure 1.2 where the slave robot is pushing against a compliant object. The object has been modeled as a first-order system with equivalent stiffness and damping. The amount of deformation of the environment is equal to y_s, the position vector of the slave robot. If the positive direction of f_s is defined to be from the environment to the slave, the imposed force on the slave is given by

$$f_s = -(K + Cs)y_s$$

where K, C, and s are the stiffness, damping, and the Laplace operator, respectively. In another example, shown in Figure 1.3, an object with mass m is rotating counterclockwise around the origin with angular acceleration $\ddot{y}_s$. A clockwise constraining torque of f_s acts on the slave such that

$$f_s = -[mL^2 \ddot{y}_s + mgLcos(y_s)]$$

where y_s is the angular orientation of the slave.

The previous examples suggest that the environmental dynamics can be represented by a nonlinear operator, E, which maps the slave position, y_s, into the imposed force on the slave robot, f_s. If f_{ext} is the resultant of all external forces acting on the slave, then a general expression for the total force imposed on the robot is

$$f_s = -E(y_s) + f_{ext} \qquad (1.4)$$

The environment is ususally considered to be a passive element with no independent sources of effort. Thus, in most cases, it is assumed that $f_{ext} = 0$.

1.3 Telerobotic Control Architectures

The dynamic behavior of the overall telerobotic system, including the human and the environment, can be represented by a block diagram. The block diagram traces the flow of signals between the various system components. A block diagram is constructed by combining the dynamic equations for the human, the master and slave robots, and the environment (Equations 1.1-1.4). These equations can be combined in many ways to form different control architectures. The two most common control architectures in present use are the classical position error architecture and the forward flow architecture.

1.3.1 Position Error Control Architecture

In the position error architecture (Figure 1.4), the position of the master is the reference input command to the slave primary control loop. Similarly, the slave position is the input command to the master primary control loop. In other words, the error between the master and slave positions drives the robots (Hannaford 1989). There is no force reflection since no forces are measured. However, a position error is generated whenever the slave robot contacts the environment, and this allows the human to feel the interaction.

The main disadvantage of the position error architecture is that the human must work against the impedance of the master robot. If the sensitivity S_m is small (high impedance), then the human may not be able to exert sufficient force to move the robot. For this reason, the position error architecture is best suited for use in direct-drive systems where the master impedance is relatively low. Another disadvantage of this architecture is that it is extremely sensitive to communication time delays between the master and slave. This results from the feedback signal having to travel in the long loop from the master to the slave and back again (Hannaford 1989).

1.3.2 Forward Flow Control Architecture

The forward flow architecture (Figure 1.5) is similar to the position error architecture in that the master position is used to drive the slave. Position information flows in the forward direction from the master to the slave, giving the architecture its name. The forward flow architecture is an improvement in that it provides true force reflection by sensing the force imposed on the slave robot. The slave force is used as the input command to the master primary control loop (Hannaford 1989). The forward flow architecture suffers from the same disadvantages as the position error architecture: it does not permit

the impedance of the master robot to be adjusted, and it is sensitive to communication time delays.

1.3.3 Local Force Feedback Architectures

Several researchers have noted that in theory, local force feedback on the slave tends to improve stability. In architectures of this type, the input command to the slave stabilizing control system has the form

$$u_s = y_m + \alpha f_s$$

where α is the gain of the force feedback signal. The measured slave force is used to backdrive the robot, generating compliance in interactions with the environment. Anderson and Spong (1989) proved that certain position error architectures with local force feedback are assymtotically stable in the presence of time delay. Hannaford (1989) has shown that local force feedback can improve the stability of the forward flow architecture.

A further enhancement can be made to the basic forward flow architecture if local force feedback is also utilized on the master. This increases the apparent sensitivity of the master robot to input commands from the human. Jansen and Herndon (1990) have explored architectures of this type using robots equipped with joint torque sensors.

In addition to having local force feedback on both robots, it is conceptually desirable to have a symmetric system in which force information is communicated in both directions. Bilateral impedance control is the most general extension of these ideas. In this new architecture, impedance is modulated at both ends of the system.

1.3.4 Bilateral Impedance Control

Figure 1.6 is the block diagram for the proposed bilateral impedance control architecture. The central difference between this new control method and previous architectures is that interaction forces are used as the communication signals between the master and the slave. The communication of forces within the system is regulated by the H matrix. This matrix permits the arbitrary specification of system performance.

Hannaford (1989) proposed a bilateral impedance control architecture that employs estimators to predict the dynamic behavior of the human and the environment. The bilateral impedance control architecture proposed here does not require complex estimators, and it allows a more general specification of performance characteristics.

Suppose that both the master and the slave robots are initially at rest with no forces imposed on the system. Then u_h, u_m, u_s, and f_{ext} are all zero. Now, if the human decides to move her hand, u_h becomes nonzero, and the master robot starts to move. This motion is a result of the interaction force between the master and the human. Even though the interaction force may be very large, the master robot motion will be small if the sensitivity S_m is small. In other words, the human may not have enough strength to overcome the master robot's primary control loop.

To increase the human's effective strength, the apparent sensitivity of the master robot is increased by measuring the interaction force, f_m, and using it as an input to the master primary control loop. The interaction force is modified by the compensator H_{11} which produces as its output the master input command, u_m. At this point, there are no restrictions placed on either the structure or size of the compensator. Note that $G_m H_{11}$ acts in parallel to S_m, and thus has the effect of changing the apparent sensitivity of the master robot. The master's apparent sensitivity can be increased by choosing a large gain for H_{11}. This is equivalent to reducing the master impedance.

The impedance of the slave robot is controlled in a similar manner to that of the master robot. The force imposed on the slave robot by the environment, f_s, is measured and used as an input command to the slave primary control loop. The environmental interaction force is modified by the compensator H_{22} which produces as its output the slave input command, u_s. This compensator generates compliance in the slave robot. Compliance is necessary for system stability, and it prevents the build up of large contact forces when the slave encounters a rigid surface (Kazerooni 1989).

The measured interaction forces f_m and f_s are also used as the communication signals between the master and the slave. The bilateral communication is regulated by the two compensators H_{12} and H_{21}. The master interaction force f_m is used to drive the slave robot after passing through the compensator H_{21}. This compensator transmits information in the forward direction from the master to the slave, and thus couples the motions of the two robots. The slave interaction force f_s is used to drive the master robot after passing through the compensator H_{12}. This compensator transmits information in the reverse direction from the slave to the master, and thus provides force reflection.

The compensators H_{11}, H_{12}, H_{21}, and H_{22} make up the elements of the matrix H. By proper selection of these four elements, the system designers can achieve desired performance characteristics. However, the designers do not have complete freedom in choosing the structure and magnitude of H. The closed-loop system of Figure 1.6 must remain stable for any chosen value of H.

1.4 Areas of Research

The research will be done in two phases. In the first phase, the theoretical basis for performance and stability will be developed. In the second phase, the predictions of theory will be experimentally verified on a multi-degree-of-freedom telemanipulator. The main areas of research are outlined in the following sections.

1.4.1 Performance

The ideal performance of a telerobotic system can be expressed in many ways. One way is to strive for a completely transparent interface between the human operator and the environment. If such a system could be attained, the operator would experience the same sensations as if she were actually present at the remote location. This may not always be desirable, however. For example, suppose that the telerobotic system is used to maneuver a large object through an arbitrary trajectory. Inertial, centrifugal, coriolis, and gravitational forces will be imposed on the slave. It seems reasonable to mask the dynamic behavior of the load through the design of appropriate controllers so that the human feels scaled-down values of these forces. In another example, suppose that the slave is holding a pneumatic jack hammer. The objective is not only to decrease the amount of force transferred to the human arm, but also to filter the forces so that the human feels only the low frequency components. These examples illustrate that in the most general case, it should be possible to specify any desired relationship between the master and slave forces.

In addition, it should be possible to specify a desired relationship between the master and slave positions. For example, the slave position could be a scaled-down version of the master position to allow greater precision in maneuvering. Thus, in general, it is necessary to shape the relationships between the forces and the positions at both ends of the system such that

$$f_s = R_f(f_m) \tag{1.5}$$

$$y_s = R_y(y_m) \tag{1.6}$$

where the functions R_f and R_y represent the desired relationships.

The performance of the telerobotic system can be characterized by four state variables. These are the forces f_m and f_s and the positions y_m and y_s. If any one of the state variables is chosen to be independent, then the remaining three variables become dependent.

This means that three independent relationships are required to relate the three dependent variables to the independent variable. This concept is illustrated in Figure 1.7, where lines connecting the state variables indicate possible relationships.

Three independent relationships are necessary to relate the four state variables. Two of these relationships are given by equations 1.5 and 1.6. A third relationship must be specified that relates either f_m and y_m, or f_s and y_s.[3] For the control architecture of Figure 1.6, it turns out that the relationship between the slave variables must be specified to insure system stability. Therefore, the necessary third equation is

$$f_s = Z_s(y_s) \tag{1.7}$$

where Z_s is the slave impedance.

The three parameters R_f, R_y, and Z_s completely describe the system performance. These parameters are independent, and thus can be arbitrarily specified by the designers to achieve desired performance characteristics. Other sets of three parameters can also be used to describe system performance, as long as the parameters are independent. For example, Z_m, Z_s, and R_f constitute such a set.

The performance parameters are fundamentally related to the elements in the H matrix. One of the primary objectives of the research is to design the compensators in H such that the desired performance characteristics are realized. First, the performance parameters will be expressed in terms of the system variables. The designers specify values for the performance parameters, and these expressions can then be solved for H_{11}, H_{12}, H_{21}, and H_{22}. This method will be used to determine the relative magnitudes of the compensators.

The structure of the compensators will be chosen to modulate the robot impedance. It will be shown that when a constant gain is used, a stiffness impedance results where the interaction force is proportional to position. When an integrator is used, the force is proportional to velocity, and a damping impedance is obtained. The impedance can be adjusted to suit the requirements of the task. For example, inserting a peg into a hole requires a large impedance along the axial direction, and a small impedance along the radial direction (Kazerooni *et al.* 1986). Various structures for the compensators will be investigated in the research program.

---

[3]Note that it is theoretically possible to specify a relationship between y_m and f_s, or between f_m and y_s. However, these relationships do not have any physical significance.

1.4.2 Stability

Another goal of the research effort is to determine the conditions which are sufficient to guarantee stability for the overall telerobotic system, including the human and the environment. The system designers select the performance parameters that dictate specific values for the H matrix. This implies that the performance criteria may conflict with the conditions for system stability. In other words, there is a trade-off between performance and stability. The goal is to arrive at a set of conditions on H such that closed-loop stability is guaranteed.

The stability analysis will be based on unstructured models of the system components. The advantage of this approach is that dynamic behavior of the system can be represented in a very general form. There is no need to model the rigid body and actuator dynamics of a particular manipulator with transfer functions. Thus, the resulting stability conditions are universally valid.

Two mathematical techniques will be used in the stability analysis. These are the Small Gain Theorem and the Multivariable Nyquist Criteria. The Small Gain Theorem will be used to arrive at a general stability condition that is equally valid for linear as well as nonlinear systems (Vidyasagar and Desoer 1975, Vidyasagar 1978). The Multivariable Nyquist Criteria will be used for the special case of linear systems with transfer function matrix operators (Lehtomaki *et al.* 1981). The linear theory best illustrates the roles of robot sensitivity and environment dynamics on overall system stability.

1.4.3 Robustness

The performance of the telerobotic system must be robust to uncertainties in the dynamic model used to design the H matrix. Modeling uncertainties fall into two broad classes. The first class consists of uncertainties that affect system performance at all frequencies. Variations in the robot inertia matrix and link geometry are examples of this type of uncertainty. The second class consists of unmodeled dynamics that affect performance only at high frequencies. The bending and torsional modes of the robot links are examples of this type of uncertainty (Kazerooni *et al.* 1986).

Performance is constant over a range of frequencies known as the bandwidth. The bandwidth determines the allowable frequency range for system operation, and consequently the speed of response. The maximum attainable bandwidth of the telerobotic system is limited by the dynamics of the human operator (Sheridan and Ferrell 1974). The unmodeled structural dynamics generally appear at frequencies greater than the maximum

attainable bandwidth, so their effect on overall system performance is usually negligible. Therefore, only modeling uncertainties of the first class will be investigated.

Robustness of the control architecture will be demonstrated by relating deviations in the specified performance characteristics to uncertainties in the dynamic model. The magnitude of acceptable modeling uncertainties will be determined from the measured frequency response of the performance parameters R_f, R_y, and Z_s. The ARX method of system identification will be used to derive the frequency response from observed input-output behavior (Ljung 1987).

1.4.4 Bond Graph Modeling

Other investigators have analyzed the theoretical performance of several telerobotic control architectures with two-port network models. Network models express the system dynamics in terms of analogous electrical circuit components. Most of this work has concentrated on two methods of control: the classical position error architecture and the forward flow architecture.

Raju *et al.* (1989) developed a two-port model of the classical position-error based teleoperator using an impedance matrix formulation. Hannaford (1989) used a hybrid parameter formulation to analyze both the classical and the forward flow architectures. Anderson (1989) used a passive Hilbert network approach in conjunction with transmission line theory to model communication time delay.

In order to relate the proposed research to previous work, the control architecture of Figure 1.6 will be described with a bond graph model. Bond graphs are a convenient notation for representing the flow of energy and information in any physical system. The bond graph of the telerobotic system will be used to illustrate how power is transformed, stored, and dissipated. In addition, the bond graph will be used to show why only three performance parameters can be specified simultaneously.

1.5 Experimental Verification

Much of the past work in telerobotic control has relied on simulation to verify the predictions of theory. The few experimental studies that have been done utilized one-degree-of-freedom manipulators because of their relative simplicity. Almost no attention has been given to the implementation of new control strategies on multi-degree-of-freedom telemanipulators. This is due to two factors: the additional complexity involved and the lack of available hardware. In order to fill this gap in experimental practice, the bilateral

impedance control architecture of Figure 1.6 will be implemented on a manipulator having seven degrees of freedom.

The theoretical predictions for performance and stability will be compared to experimental results. First, values will be determined for the system variables that govern the dynamic behavior of the human arm, the robots, and the environment. These values will be used in the design of the H matrix. Next, by tailoring the H matrix, the system performance characteristics will be arbitrarily specified. The force ratio, the position ratio, and the robot impedances will be measured and compared to their desired values. The frequency response of the performance parameters will be obtained to demonstrate robustness of the control architecture to modeling uncertainties. Finally, the stability conditions will be verified by establishing bounds on the robot impedances for which the system remains stable.

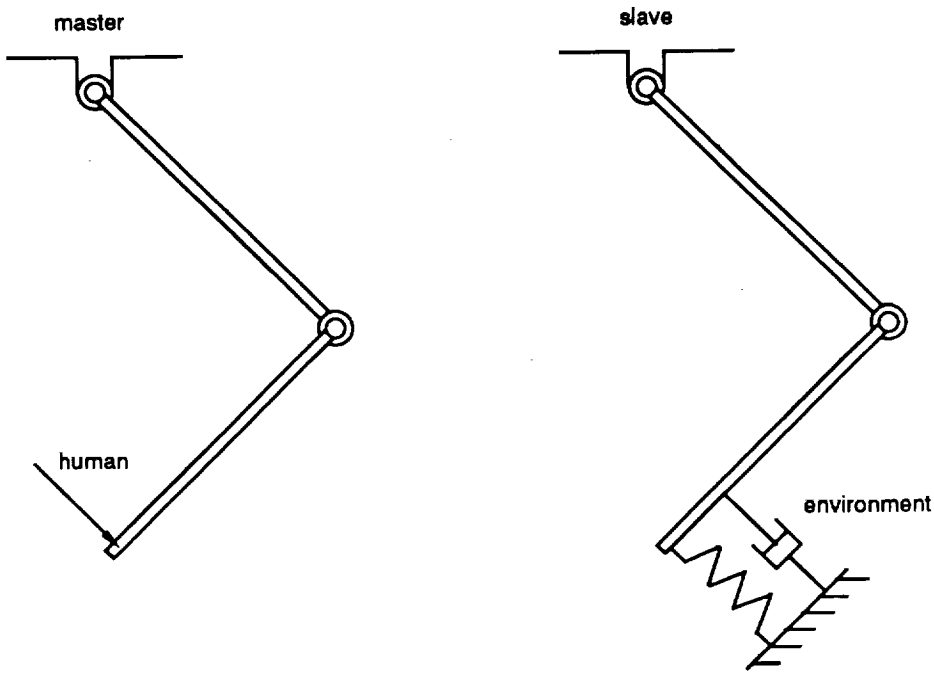

Figure 1.1: Elements of a Telerobotic System

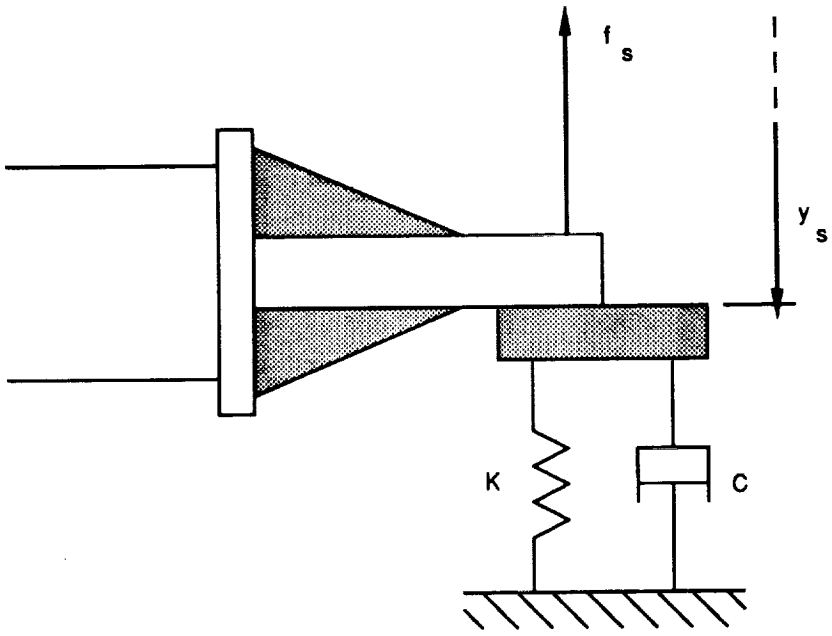

Figure 1.2: Interaction with a Compliant Environment

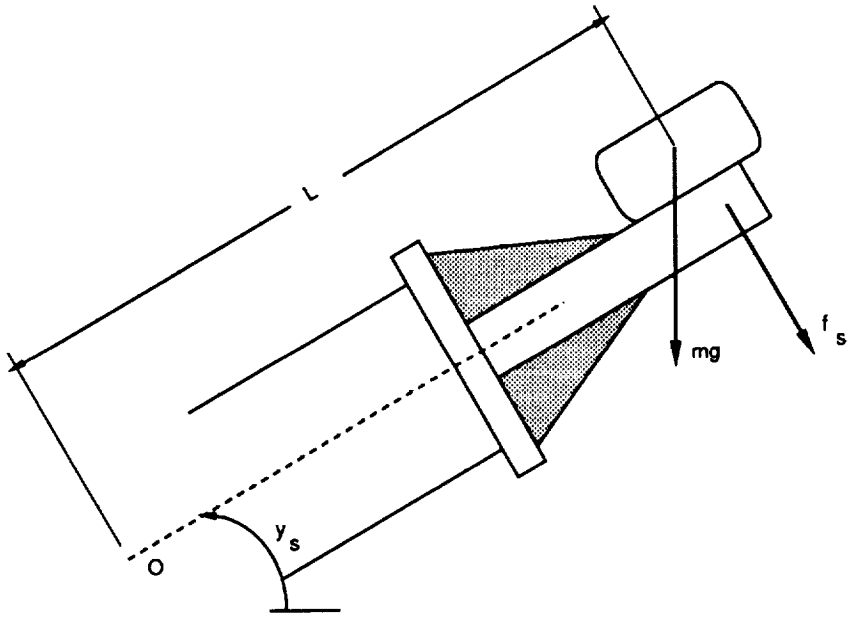

Figure 1.3: Interaction with an Inertial Environment

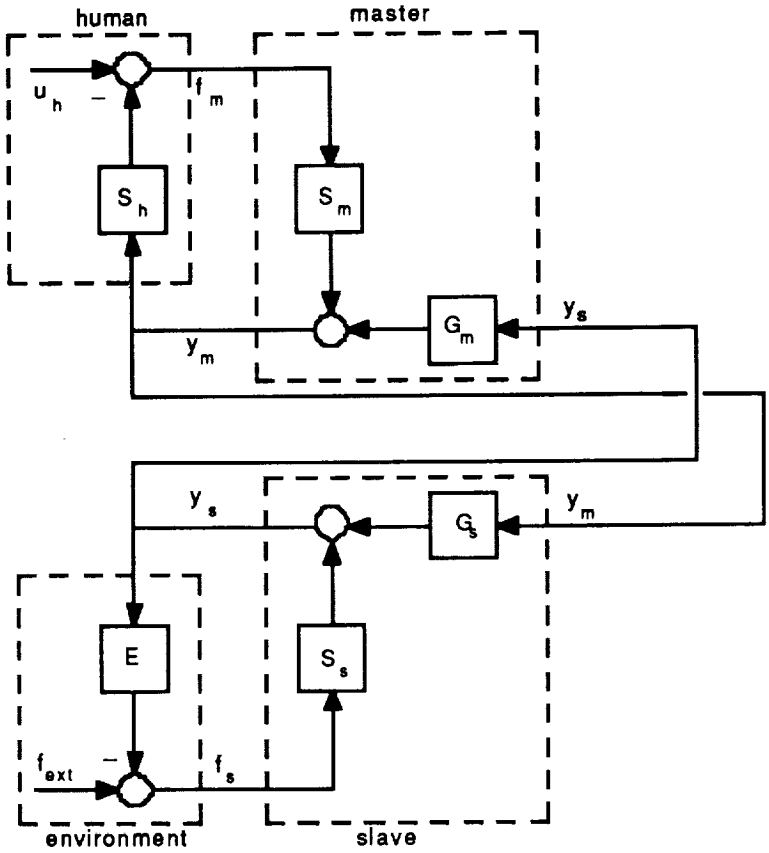

Figure 1.4: Position Error Control Architecture

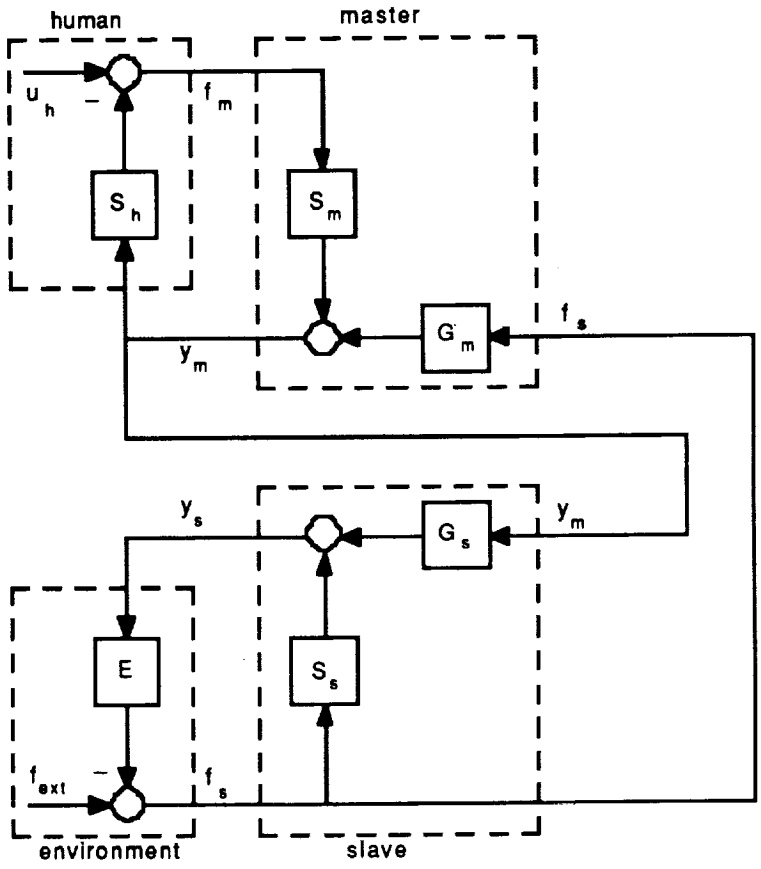

Figure 1.5: Forward Flow Control Architecture

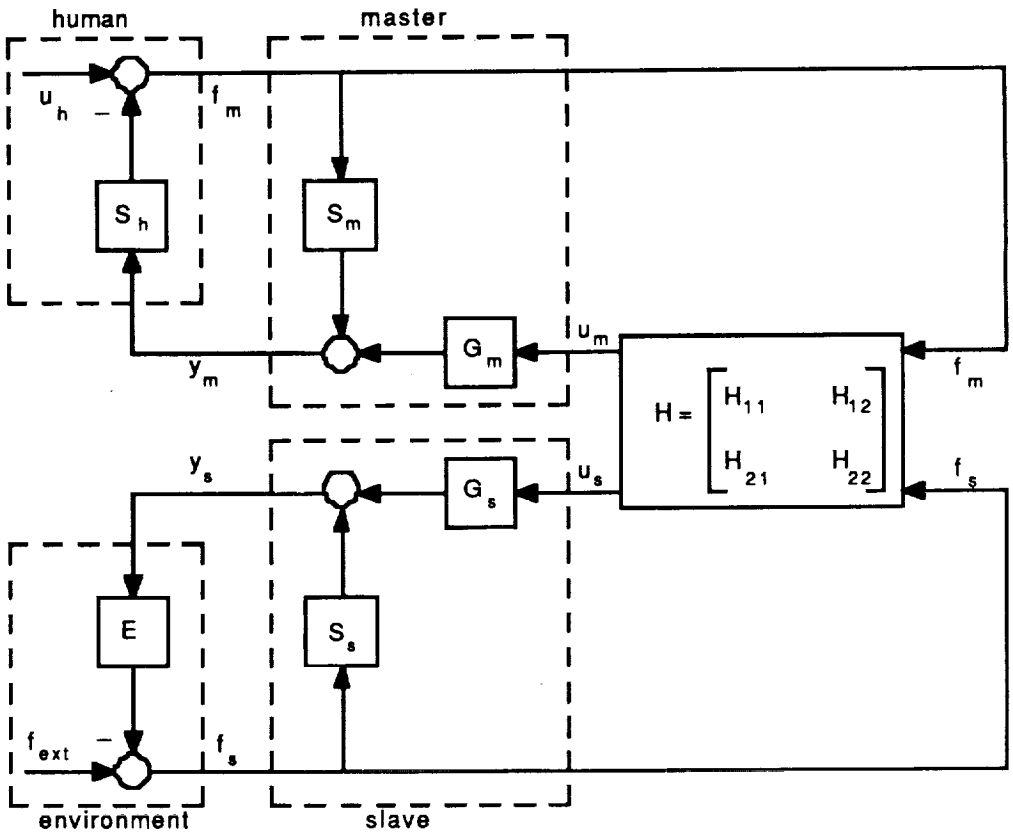

Figure 1.6: Bilateral Impedance Control Architecture

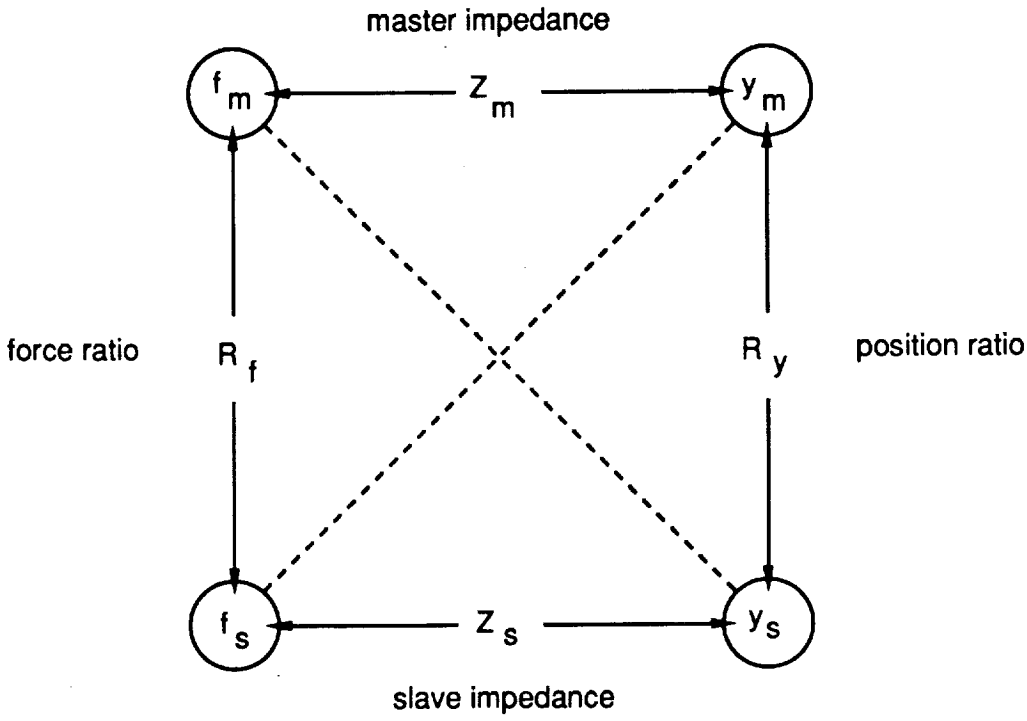

Figure 1.7: State Variable Relationships for a Telerobotic System

Chapter 2
PERFORMANCE PARAMETERS

2.1 Introduction

The performance of a telerobotic system can be completely described by a set of three independent parameters. In this chapter, the equations that express the performance parameters in terms of system variables will be derived for the bilateral impedance control architecture. It will be shown that the performance parameters are fundamentally related to the structure of the H matrix.

2.2 Force Ratio

The performance parameter that relates the forces acting on the master and slave robots is known as the force ratio. For a single degree-of-freedom, it is defined as

$$R_f = \frac{f_s}{f_m} \tag{2.1}$$

For many tasks, it is desirable to specify the force ratio. This enables the human operator to exert large forces with the slave robot by applying small forces to the master robot. The force ratio is specified by selecting the relative magnitudes of the elements in the H matrix. The expression that relates the force ratio to the H matrix and other system variables will be derived next.

The following equations can be obtained from the block diagram of Figure 1.6:

$$f_s = f_{ext} - Ey_s \tag{2.2}$$

$$y_s = G_s u_s + S_s f_s \tag{2.3}$$

$$u_s = H_{21} f_m + H_{22} f_s \tag{2.4}$$

Equation 2.2 is the dynamic model of the environment, equation 2.3 is the dynamic model of the slave robot, and equation 2.4 is the input command to the slave stabilizing control system.

Substituting equation 2.4 into equation 2.3 and collecting terms yields

$$y_s = (G_s H_{21}) f_m + (G_s H_{22} + S_s) f_s \tag{2.5}$$

Substituting equation 2.5 into equation 2.2 gives

$$f_s = f_{ext} - E[(G_s H_{21}) f_m + (G_s H_{22} + S_s) f_s]$$

Rearranging

$$[1 + (G_s H_{22} + S_s)E] f_s = f_{ext} - (G_s H_{21} E) f_m$$

Only an independent source of effort can impose external forces on the slave robot. All other forces acting on the slave result from the environmental dynamics, E. Thus, it is a reasonable assumption in most cases that $f_{ext} = 0$. Making this assumption in the previous equation yields

$$\frac{f_s}{f_m} = - \frac{G_s H_{21} E}{1 + (G_s H_{22} + S_s) E} \tag{2.6}$$

By defining the two admittances

$$P_{21} = G_s H_{21} \tag{2.7}$$

$$P_{22} = G_s H_{22} + S_s \tag{2.8}$$

equation 2.6 can be written as

$$\boxed{\frac{f_s}{f_m} = - \frac{P_{21} E}{1 + P_{22} E}} \tag{2.9}$$

The force ratio depends on the dynamics of the environment, and on the relationship between two elements in the H matrix. The compensator H_{21} filters the master force, while the compensator H_{22} filters the slave force. The outputs of both compensators are used to drive the slave robot. H_{21} couples the motion of the slave robot to that of the master robot. H_{22} determines the compliance of the slave robot to forces exerted on it by the environment.

The force ratio can be arbitrarily specified by selecting the relative magnitudes of H_{21} and H_{22}.

Note that the force ratio does not depend on H_{12}, the element in the H matrix that governs force reflection. This may seem surprising at first, until it is realized that force reflection increases the master impedance. As a result, the human must apply a greater force to move the robot, but the force ratio is unaffected.

2.3 Position Ratio

The performance parameter that relates the positions of the master and slave robots is known as the position ratio. For a single degree-of-freedom, it is defined as

$$R_y = \frac{y_s}{y_m} \tag{2.10}$$

Often it is desirable to specify a non-unity value for the position ratio so that the two robots move in the same direction, but have different amplitudes of motion. This enables the slave robot to perform small, precise motions in response to large, coarse motions of the master robot. The position ratio is specified by selecting the relative magnitudes of the elements in the H matrix. The expression that relates the position ratio to the H matrix and other system variables will be derived next.

The following equations can be obtained from the block diagram of Figure 1.6:

$$y_m = G_m u_m + S_m f_m \tag{2.11}$$

$$u_m = H_{11} f_m + H_{12} f_s \tag{2.12}$$

Equation 2.11 is the dynamic model of the master robot, and equation 2.12 is the input command to the master stabilizing control system.

Substituting equation 2.12 into equation 2.11 and collecting terms yields

$$y_m = (G_m H_{11} + S_m) f_m + (G_m H_{12}) f_s \tag{2.13}$$

Solving for f_m

$$f_m = \frac{y_m - (G_m H_{12}) f_s}{G_m H_{11} + S_m} \tag{2.14}$$

Substituting equation 2.14 into equation 2.5 gives

$$y_s = \frac{G_s H_{21}[y_m - (G_m H_{12})f_s]}{G_m H_{11} + S_m} + (G_s H_{22} + S_s)f_s \tag{2.15}$$

If there are no external forces imposed on the slave, then $f_{ext} = 0$ and equation 2.2 reduces to

$$f_s = -Ey_s \tag{2.16}$$

Substituting this expression into equation 2.15 and simplifying

$$\frac{y_s}{y_m} = \frac{G_s H_{21}}{(G_m H_{11}+S_m)+[(G_m H_{11}+S_m)(G_s H_{22}+S_s)-G_m G_s H_{12} H_{21}]E} \tag{2.17}$$

By defining the two admittances

$$P_{11} = G_m H_{11} + S_m \tag{2.18}$$

$$P_{12} = G_m H_{12} \tag{2.19}$$

and making use of equations 2.7 and 2.8, equation 2.17 can be written as

$$\boxed{\frac{y_s}{y_m} = \frac{P_{21}}{P_{11} + \Delta PE}} \tag{2.20}$$

where

$$\Delta P = P_{11}P_{22} - P_{12}P_{21} \tag{2.21}$$

In the general case where the slave robot is constrained by the environment, the position ratio depends on the relative magnitudes of all four elements in the H matrix. However, when the slave robot is moving freely through space, there are no forces exerted on it by the environment. In that case, E = 0 and the position ratio becomes

$$R_y = \frac{P_{21}}{P_{11}}$$

Thus, for unconstrained motion, the position ratio depends on the relationship between only two elements in the H matrix. The compensator H_{11} filters the master force, and its output is used to drive the master robot. H_{11} determines the motion of the master robot by controlling its impedance. The compensator H_{21} also filters the master force, and its output is used to drive the slave robot. H_{21} couples the motion of the slave robot to that of the master robot. For unconstrained motion, the position ratio can be arbitrarily specified by selecting the relative magnitudes of H_{11} and H_{21}.

2.4 Impedance

The performance parameter that relates force and position is known as impedance. An impedance may be defined at each end of the telerobotic system. For a single degree-of-freedom, the robot impedances are defined as

$$Z_m = \frac{f_m}{y_m} \tag{2.22}$$

$$Z_s = \frac{f_s}{y_s} \tag{2.23}$$

The master impedance Z_m is the impedance that the telerobotic system presents to the human. It is desirable to specify Z_m to reduce fatigue of the human operator. The slave impedance Z_s is the impedance that the telerobotic system presents to the environment. It is desirable to specify Z_s to insure system stability, and to suit the requirements of the task. The robot impedances are specified by selecting the relative magnitudes of the elements in the H matrix.

An expression for the master impedance will be derived first. Substituting equation 2.16 into equation 2.13 yields

$$y_m = (G_m H_{11} + S_m) f_m - (G_m H_{12}) E y_s \tag{2.24}$$

Substituting equation 2.16 into equation 2.5 gives

$$y_s = (G_s H_{21}) f_m - (G_s H_{22} + S_s) E y_s$$

Solving for y_s

$$y_s = \frac{G_s H_{21} f_m}{1 + (G_s H_{22} + S_s)E} \tag{2.25}$$

Substituting equation 2.25 into equation 2.24 and simplifying

$$\frac{f_m}{y_m} = \frac{1+(G_s H_{22}+S_s)E}{(G_m H_{11}+S_m)+[(G_m H_{11}+S_m)(G_s H_{22}+S_s)-G_m G_s H_{12} H_{21}]E} \tag{2.26}$$

Equation 2.26 can be written in terms of admittances as

$$\boxed{\frac{f_m}{y_m} = \frac{1 + P_{22}E}{P_{11} + \Delta P E}} \tag{2.27}$$

In the general case, Z_m depends not only on the internal dynamics of the telerobotic system, but also on the impedance of the environment. However, when the slave robot is moving freely through space, there are no forces exerted on it by the environment. In that case, $E = 0$ and equation 2.27 for the master impedance becomes

$$Z_m = \frac{1}{P_{11}}$$

For this special case, the master impedance is determined by a single element in the H matrix. The compensator H_{11} filters the master force, and its output is used to drive the master robot. Because H_{11} relates force to position, it governs the robot impedance. For unconstrained motion, the master impedance can be arbitrarily specified by adjusting H_{11}.

An expression for the slave impedance will be derived next. This requires an impedance model of the human arm. From the block diagram in Figure 1.6, the dynamic behavior of the human arm is given by

$$f_m = u_h - S_h y_m \tag{2.28}$$

The impedance of the human arm is actively modulated by the central nervous system. It is also a function of the arm orientation. However, it is assumed that the human arm presents a strictly passive impedance to the slave at each instant in time. This instantaneous impedance can be found by setting $u_h = 0$ in equation 2.28. This gives

$$f_m = - S_h y_m \tag{2.29}$$

where S_h is now a function of many variables such as central nervous system commands, muscle stiffness, and arm orientation. Substituting equation 2.29 into equation 2.5 yields

$$y_s = - (G_sH_{21})S_hy_m + (G_sH_{22} + S_s)f_s \tag{2.30}$$

Substituting equation 2.29 into equation 2.13 gives

$$y_m = - (G_mH_{11} + S_m)S_hy_m + (G_mH_{12})f_s$$

Solving for y_m

$$y_m = \frac{G_mH_{12}f_s}{1 + (G_mH_{11} + S_m)S_h} \tag{2.31}$$

Substituting equation 2.31 into equation 2.30 and simplifying

$$\frac{f_s}{y_s} = \frac{1+(G_mH_{11}+S_m)S_h}{(G_sH_{22}+S_s)+[(G_mH_{11}+S_m)(G_sH_{22}+S_s)-G_mG_sH_{12}H_{21}]S_h} \tag{2.32}$$

Equation 2.32 can be written in terms of admittances as

$$\boxed{\frac{f_s}{y_s} = \frac{1 + P_{11}S_h}{P_{22} + \Delta PS_h}} \tag{2.33}$$

In the general case, Z_s depends on the internal dynamics of the telerobotic system and the impedance of the human arm. It should be remembered that S_h is not a constant, but that it is a complex function of many variables. The value of S_h at any particular instant must be estimated from outside of the telerobotic system.

When there is no force reflection from the environment, the slave impedance does not depend on the human arm dynamics. Since there is no communication from the slave to the master, the gain of H_{12} is zero. Therefore, $P_{12} = 0$ and $\Delta P = P_{11}P_{22}$. Equation 2.33 for the slave impedance can then be simplified to

$$Z_s = \frac{1}{P_{22}}$$

For this special case, the slave impedance is determined by a single element in the H matrix. The compensator H_{22} filters the slave force, and its output is used to drive the slave robot.

Because H_{22} relates force to position, it governs the robot impedance. In the absence of force reflection, the slave impedance can be arbitrarily specified by adjusting H_{22}.

2.5 Independent Parameters

The expressions that relate the performance parameters to system variables are summarized below:

$$R_f = -\frac{P_{21}E}{1 + P_{22}E} \tag{2.9}$$

$$R_y = \frac{P_{21}}{P_{11} + \Delta PE} \tag{2.20}$$

$$Z_m = \frac{1 + P_{22}E}{P_{11} + \Delta PE} \tag{2.27}$$

$$Z_s = \frac{1 + P_{11}S_h}{P_{22} + \Delta PS_h} \qquad \text{when } u_h = 0 \tag{2.33}$$

where

$$P_{11} = G_m H_{11} + S_m \tag{2.18}$$

$$P_{12} = G_m H_{12} \tag{2.19}$$

$$P_{21} = G_s H_{21} \tag{2.7}$$

$$P_{22} = G_s H_{22} + S_s \tag{2.8}$$

$$\Delta P = P_{11}P_{22} - P_{12}P_{21} \tag{2.21}$$

It turns out that the first three performance parameters are not independent. This can be seen by dividing equation 2.20 by equation 2.9

$$\frac{R_y}{R_f} = -\frac{1 + P_{22}E}{E(P_{11} + \Delta PE)}$$

Comparing this expression to equation 2.27, it is apparent that

$$\frac{R_y}{R_f} = -\frac{Z_m}{E} \tag{2.34}$$

Thus, it is not possible to arbitrarily specify Z_m if R_y and R_f are also selected as performance parameters. For this reason, the set of three independent performance parameters must include Z_s as one of its members. The other two parameters can be chosen from the remaining variables R_y, R_f, and Z_m.

The slave impedance Z_s will always be an independent parameter because it describes the dynamic behavior of the telerobotic system from the perspective of the environment. Equation 2.33 was derived by assuming that $u_h = 0$. This assumption implies that the human arm appears to be a passive element. In contrast, the parameters R_f, R_y, and Z_m describe the dynamic behavior of the telerobotic system from the perspective of the human. Equations 2.9, 2.20, and 2.27 were derived by assuming that $f_{ext} = 0$. This assumption implies that the environment appears to be a passive element.

2.6 Structure of the H Matrix

The relationship between the performance parameters and the structure of the H matrix can be seen more clearly if several approximations are made in the governing equations. The closed-loop transfer functions of both the master and the slave have the form

$$G_{m,s} = \frac{G_p(s)K(s)}{1 + G_p(s)K(s)}$$

where $G_p(s)$ is the transfer function of the robot and $K(s)$ is the transfer function of the primary stabilizing compensator.

The sensitivity functions of both the master and the slave have the form

$$S_{m,s} = \frac{1}{1 + G_p(s)K(s)}$$

For good position control, the magnitude of $G_p(s)K(s) >> 1$. Thus, over the bandwidth $(0, \omega_o)$, the following approximations can be made:

$$G_{m,s} \approx 1$$
$$S_{m,s} \approx 0$$

That is, the closed-loop transfer functions have approximately unity gain, while the sensitivity functions are negligibly small. Above the frequency ω_o, the magnitude of the closed-loop transfer function begins to drop off, and the approximations are no longer valid. However, the system performance within the bandwidth is of primary interest. Using the approximations in equations 2.5 and 2.13 yields

$$y_m \approx H_{11} f_m + H_{12} f_s \tag{2.38}$$

$$y_s \approx H_{21} f_m + H_{22} f_s \tag{2.39}$$

These two equations can be written in matrix form as

$$\begin{Bmatrix} y_m \\ y_s \end{Bmatrix} = \begin{bmatrix} H_{11} & H_{12} \\ H_{21} & H_{22} \end{bmatrix} \begin{Bmatrix} f_m \\ f_s \end{Bmatrix} \tag{2.40}$$

Thus, the H matrix can be thought of as a set of relationships between force and position. The following relationships can be obtained from equation 2.40 by setting one of the force variables to zero:

$$H_{11} = \frac{y_m}{f_m}\bigg|_{f_s = 0}$$

$$H_{12} = \frac{y_m}{f_s}\bigg|_{f_m = 0}$$

$$H_{21} = \frac{y_s}{f_m}\bigg|_{f_s = 0}$$

$$H_{22} = \frac{y_s}{f_s}\bigg|_{f_m = 0}$$

By considering the elements as input-output relationships, the inherent structure of the H matrix is revealed. It can be seen that H_{11} controls the master impedance, while H_{22} controls the slave impedance. H_{12} and H_{21} regulate the communication between the robots.

H_{12} controls force reflection since it transmits information from the slave to the master. H_{21} controls motion coupling since it transmits information from the master to the slave. Therefore, the H matrix has the following characteristic structure:

$$H = \begin{bmatrix} 1/Z_m & \text{force reflection} \\ \text{motion coupling} & 1/Z_s \end{bmatrix}$$

2.7 Conclusions

The main advantage of the control architecture in Figure 1.6 is that it allows the arbitrary specification of desired performance characteristics. System performance can be described by a set of three independent parameters. To form an independent set, one of these parameters must be the slave impedance Z_s. The equations that relate the performance parameters to system variables were derived. It was shown that the performance parameters are fundamentally related to the structure of the H matrix. The H matrix can be designed to achieve specific values of the performance parameters. The process of H matrix design will be illustrated with numerous examples during experimental verification.

Chapter 3
STABILITY

3.1 Introduction

The arbitrary specification of desired performance characteristics may conflict with the requirements for system stability. In other words, there may be a trade-off between performance and stability. The conditions that are sufficient to guarantee closed-loop stability will be determined in this chapter. It will be shown that the stability conditions place limitations on possible structures for the H matrix.

The stability analysis will be based on unstructured models of the system components. The advantage of this approach is that the dynamic behavior of the system can be represented in a very general form. The resulting stability conditions are universally valid, and do not depend on the rigid-body dynamics of a particular manipulator.

The stability of a multivariable telerobotic system will be studied with two methods. The first method will use the Small Gain Theorem to arrive at a general set of stability conditions. These general conditions can be applied to linear as well as nonlinear systems. The second method will use the Multivariable Nyquist Criterion to analyze the stability of linear systems with transfer function matrix operators. It will be demonstrated that the stability conditions obtained with this method are a subset of the general conditions. Often nonlinear systems can be treated as linear systems when the robots move at slow speed. In addition, the linear theory best illustrates the roles of the human and the environment on overall system stability.

3.2 Small Gain Theorem

This section presents the mathematical background for the Small Gain Theorem (Vidyasagar 1978, Vidyasagar and Desoer 1975). This method is used to derive a general set of stability conditions which can be applied to nonlinear systems.

First, the concept of L_p stability is introduced. An operator $V[\cdot]$ is said to be L_p-stable if it satisfies the following conditions:

(1) $V[\cdot] : L_p^n \rightarrow L_p^n$ (3.1)

(2) there exist real constants $\alpha \geq 0$ and β such that
$\| V[e] \|_p < \alpha \| e \|_p + \beta$ (3.2)

The first condition states that the operator V[·] maps an input in the L_p^n space to an output in the L_p^n space. An n x 1 vector function f(t) exists in the L_p^n space if its L_p-norm is bounded. That is, if

$$\| f \|_p < \infty, \text{ then } f(t) \in L_p^n$$

where $\| f \|_p$ denotes the L_p-norm of f(t). The L_p-norm is defined as

$$\| f \|_p = \left[\int_{\infty}^{0} |f(t)|^p \, dt \right]^{1/p} \qquad \text{for all } p \in [1, \infty]$$

In cases where the L_p-norm is unbounded, a truncated function $f_T(t)$ can be defined such that

$$f_T(t) = \begin{cases} f(t) & 0 < t \leq T \\ 0 & t > T \end{cases}$$

where T is any finite time. If $\| f_T \|_p < \infty$, then f(t) belongs to the extended L_p^n space denoted by L_{pe}^n. This definition facilitates the analysis of systems in which the subsystems are unstable while the entire system may be stable.

The second condition for L_p-stability states that the norm of the output is no larger than α times the norm of the input plus the offset constant β. The smallest α such that inequality 3.2 is satisfied is called the gain of operator V[·].

The Small Gain Theorem states the stability condition for the closed-loop system of Figure 3.1. V is a nonlinear operator that represents the dynamics of the plant and the primary stabilizing compensator. H is a nonlinear operator that represents the compensation in the feedback path. It is assumed that the operators V and H are L_p-stable. That is,

$$V[e] : L_p^n \rightarrow L_p^n$$

$$\| V[e] \|_p < \alpha_1 \| e \|_p + \beta_1 \qquad (3.3)$$

$$H[f] : L_p^n \rightarrow L_p^n$$

$$\| H[f] \|_p < \alpha_2 \| f \|_p + \beta_2 \tag{3.4}$$

Since the output f = V[e], inequality 3.3 can be substituted into inequality 3.4. This gives

$$\| HV[e] \|_p < \alpha_2\alpha_1 \| e \|_p + \alpha_2\beta_1 + \beta_2 \tag{3.5}$$

which means that the loop mapping HV[e] is L_p-stable. From Figure 3.1, the error signal, e, results from the difference between the input command, r, and the feedback signal. Thus,

$$e = r - HV[e] \tag{3.6}$$

Taking the truncated L_p-norms of both sides of equation 3.6 yields

$$\| e_T \|_p = \| r_T \|_p + \| HV[e]_T \|_p \qquad \text{for all } t \in [0, T] \tag{3.7}$$

Since HV[e] is L_p-stable, inequality 3.5 can be substituted into equation 3.7

$$\| e_T \|_p < \| r_T \|_p + \alpha_2\alpha_1 \| e_T \|_p + \alpha_2\beta_1 + \beta_2 \qquad \text{for all } t \in [0, T] \tag{3.8}$$

If the gain $\alpha_2\alpha_1$ is less than unity, inequality 3.8 can be rearranged to give

$$\| e_T \|_p < \frac{\| r_T \|_p}{1 - \alpha_2\alpha_1} + \frac{\alpha_2\beta_1 + \beta_2}{1 - \alpha_2\alpha_1} \qquad \text{for all } t \in [0, T] \tag{3.9}$$

Note that the gain $\alpha_2\alpha_1$ is the gain of the loop mapping HV[e]. This fact will be important later.

Now assume that the input command r exists in the L_p^n space. Then $\| r \|_p < \infty$ for all $t \in [0, \infty]$. Because r is always bounded, inequality 3.9 shows that e must also be bounded for all t. Therefore

$$\| e \|_p < \infty \qquad \text{for all } t \in [0, \infty]$$

This implies that e belongs to the L_p^n space whenever r belongs to the L_p^n space. Thus, the closed-loop mapping $A : r \rightarrow e$ satisfies the first condition for L_p-stability

$$A[\cdot] : L_p^n \rightarrow L_p^n \tag{3.10}$$

Since e = A[r] and r is always bounded, inequality 3.9 can be written in the form of inequality 3.2

$$\| A[r] \|_p < \alpha \| r \|_p + \beta \qquad \text{for all } t \in [0, \infty] \tag{3.11}$$

where

$$\alpha = \frac{1}{1 - \alpha_2\alpha_1}$$

$$\beta = \frac{\alpha_2\beta_1 + \beta_2}{1 - \alpha_2\alpha_1}$$

Thus, the closed-loop mapping A[·] satisfies the second condition for L_p-stability as well. Therefore, the closed-loop system of Figure 3.1 is L_p-stable. This constitutes a proof of the Small Gain Theorem which can be summarized as follows:

> If operators V and H are L_p-stable, and the gain of the loop mapping HV[e] is less than unity, then the closed-loop system is L_p-stable.

The Small Gain Theorem implies that the nonlinear behavior of a stable system can be bounded by a linear function with a slope less than unity. This concept is illustrated in Figure 3.2.

Now the Small Gain Theorem will be used to find the general stability conditions for the telerobotic system of Figure 1.6. The output of the system is the slave position, y_s. From the block diagram

$$y_s = G_s u_s + S_s f_s$$

It is assumed that the operators G_s and S_s are L_p-stable. Thus

$$\| y_s \|_p < \alpha_{Gs} \| u_s \|_p + \alpha_{Ss} \| f_s \|_p + \beta_1 \tag{3.12}$$

The electronic input command to the slave is given by

$$u_s = H_{21}f_m + H_{22}f_s$$

It is also assumed that the operators H_{21} and H_{22} are L_p-stable. Thus

$$\| u_s \|_p < \alpha_{H21}\| f_m \|_p + \alpha_{H22}\| f_s \|_p + \beta_2 \tag{3.13}$$

Substituting inequality 3.13 into inequality 3.12

$$\| y_s \|_p < \alpha_{P21}\| f_m \|_p + \alpha_{P22}\| f_s \|_p + \beta_3 \tag{3.14}$$

where

$$\alpha_{P21} = \alpha_{Gs}\alpha_{H21} \tag{3.15}$$

$$\alpha_{P22} = \alpha_{Gs}\alpha_{H22} + \alpha_{Ss} \tag{3.16}$$

Similarly, from the block diagram

$$y_m = G_m u_m + S_m f_m$$

assuming that the operators G_m and S_m are L_p-stable

$$\| y_m \|_p < \alpha_{Gm}\| u_m \|_p + \alpha_{Sm}\| f_m \|_p + \beta_4 \tag{3.17}$$

The electronic input command to the master is given by

$$u_m = H_{11}f_m + H_{12}f_s$$

assuming that the operators H_{11} and H_{12} are L_p-stable

$$\| u_m \|_p < \alpha_{H11}\| f_m \|_p + \alpha_{H12}\| f_s \|_p + \beta_5 \tag{3.18}$$

Substituting inequality 3.18 into inequality 3.17

$$\| y_m \|_p < \alpha_{P11}\| f_m \|_p + \alpha_{P12}\| f_s \|_p + \beta_6 \tag{3.19}$$

where

$$\alpha_{P11} = \alpha_{Gm}\alpha_{H11} + \alpha_{Sm} \tag{3.20}$$

$$\alpha_{P12} = \alpha_{Gm}\alpha_{H12} \tag{3.21}$$

The dynamic behavior of the human arm is represented by

$$f_m = u_h - S_h y_m$$

Since the human arm is assumed to be stable

$$\| f_m \|_p < \| u_h \|_p + \alpha_{Sh} \| y_m \|_p + \beta_7 \tag{3.22}$$

Substituting inequality 3.19 into inequality 3.22

$$\| f_m \|_p < \| u_h \|_p + \alpha_{Sh}\alpha_{P11} \| f_m \|_p + \alpha_{Sh}\alpha_{P12} \| f_s \|_p + \beta_8 \tag{3.23}$$

If $\alpha_{Sh}\alpha_{P11} < 1$, then inequality 3.23 can be rearranged to give

$$\| f_m \|_p < \frac{\| u_h \|_p}{1 - \alpha_{Sh}\alpha_{P11}} + \frac{\alpha_{Sh}\alpha_{P12}}{1 - \alpha_{Sh}\alpha_{P11}} \| f_s \|_p + \beta_9 \tag{3.24}$$

Substituting inequality 3.24 into inequality 3.14

$$\| y_s \|_p < \frac{\alpha_{P21}}{1 - \alpha_{Sh}\alpha_{P11}} \| u_h \|_p + \left[\frac{\alpha_{Sh}\alpha_{P12}\alpha_{P21}}{1 - \alpha_{Sh}\alpha_{P11}} + \alpha_{P22} \right] \| f_s \|_p + \beta_{10} \tag{3.25}$$

The force acting on the slave is given by

$$f_s = f_{ext} - E y_s$$

It is not clear if the environment is a stable function of y_s. However, the nonlinear mapping $E[\cdot]$ is assumed to bounded within any finite interval T. Thus, taking the truncated L_p-norms of both sides of the previous equation

$$\| f_{s,T} \|_p < \| f_{ext,T} \|_p + \alpha_E \| y_{s,T} \|_p + \beta_{11} \quad \text{for all } t \in [0, T] \tag{3.26}$$

Substituting inequality 3.26 into inequality 3.25 and rearranging

$$\begin{aligned} \| y_{s,T} \|_p < \alpha_E \left[\frac{\alpha_{Sh}\alpha_{P12}\alpha_{P21}}{1 - \alpha_{Sh}\alpha_{P11}} + \alpha_{P22} \right] \| y_{s,T} \|_p \\ + \left[\frac{\alpha_{Sh}\alpha_{P12}\alpha_{P21}}{1 - \alpha_{Sh}\alpha_{P11}} + \alpha_{P22} \right] \| f_{ext,T} \|_p \\ + \frac{\alpha_{P21}}{1 - \alpha_{Sh}\alpha_{P11}} \| u_{h,T} \|_p + \beta_{12} \end{aligned} \tag{3.27}$$

In the previous inequality, $\| f_{ext,T} \|_p$ and $\| u_{h,T} \|_p$ are bounded inputs to the closed-loop system. The Small Gain Theorem states that for stability, the gain of the output $\| y_s \|_p$ must be less than unity. That is,

$$\alpha_E \left[\frac{\alpha_{Sh}\alpha_{P12}\alpha_{P21}}{1 - \alpha_{Sh}\alpha_{P11}} + \alpha_{P22} \right] < 1$$

Rearranging, the stability condition for the closed-loop system becomes

$$\boxed{\frac{1 - \alpha_{Sh}\alpha_{P11}}{\alpha_{P22} - \alpha_{Sh}(\alpha_{P11}\alpha_{P22} - \alpha_{P12}\alpha_{P21})} > \alpha_E} \tag{3.28}$$

This stability condition applies when the slave robot is constrained by the environment. A second stability condition is necessary when the slave robot is moving freely through space. The stability condition for unconstrained motion can be found from inequality 3.28 by setting α_E equal to zero. This gives

$$1 - \alpha_{Sh}\alpha_{P11} > 0$$

which implies that

$$\boxed{\alpha_{P11} < \frac{1}{\alpha_{Sh}}} \tag{3.29}$$

Note that this condition was assumed previously in the derivation of inequality 3.24.

Inequalities 3.28 and 3.29 are the general stability conditions for a nonlinear system. These conditions are related to the H matrix through equations 3.15 and 3.16 and equations

3.20 and 3.21. It will be shown in the next section that the stability conditions for a linear system are a subset of the general conditions.

3.3 Multivariable Nyquist Criterion

This section presents the mathematical background for the Multivariable Nyquist Criterion (Lehtomaki *et al.* 1981). This method is used to analyze the stability of linear systems with transfer function matrix operators.

Figure 3.3 shows a generic closed-loop control system. G(s) is a linear operator that represents dynamics of the plant and the primary stabilizing compensator. H(s) represents the compensation in the feedback path. In multivariable systems, the operators G(s) and H(s) are matrices of transfer functions. Tracing the signal flow path through the system yields

$$y = Ge$$

where it is understood that all operators are matrix functions of s. The error signal, e, is the difference between the command input, u, and the feedback signal, Hy. Thus, the previous equation becomes

$$y = G(u - Hy)$$

Rearranging

$$[I + GH]y = Gu$$

Premultiplying both sides by $[I + GH]^{-1}$

$$y = [I + GH]^{-1}Gu$$

Therefore, the closed-loop transfer function matrix which relates the output vector, y, to the input vector, u, is

$$G_{CL} = [I + GH]^{-1}G \tag{3.30}$$

The inverse of the matrix [I + GH] is given by

$$[I + GH]^{-1} = \frac{adj[I + GH]}{|I + GH|}$$

It follows that the characteristic equation of the system is

$$|I + GH| = 0 \tag{3.31}$$

The determinant $|I + GH|$ can be expressed as a ratio of polynomials in s

$$|I + GH| = \frac{f_{CL}(s)}{f_{OL}(s)} \tag{3.32}$$

where $f_{CL}(s)$ is a closed-loop characteristic polynomial, and $f_{OL}(s)$ is an open-loop characteristic polynomial. The roots of $f_{CL}(s)$ are the closed-loop poles of the system, while the roots of $f_{OL}(s)$ are the open-loop poles of the system. For the system to be stable, the closed-loop poles must lie in the left half of the s-plane. Roots of the characteristic polynomials that lie in the right half of the s-plane are unstable.

The Nyquist method uses conformal mapping to analyze system stability. For every point in the right half of the s-plane, there is a corresponding point z = F(s) in the z-plane. The function F(s) maps the right half of the s-plane into some region of the z-plane. The right half of the s-plane is bounded by the imaginary axis and a semicircle of infinite radius. As w ranges from $-\infty$ to $+\infty$, the boundary of the right half of the s-plane maps into a contour in the z-plane (see Figure 3.4).

The contour in the z-plane encircles the origin. The number of clockwise encirclements, N, is given by

$$N = Z - P \tag{3.33}$$

where Z and P are the number of zeros and the number of poles of F(s) in the right half of the s plane, respectively. Equation 3.33 is a property of the conformal mapping, and is stated without proof. A justification for using this equation is given in Ogata (1970).

Now let $F(s) = f_{CL}(s)$. Since $f_{CL}(s)$ is a polynomial, it has no denominator and consequently no poles. Therefore, P = 0 and equation 3.33 becomes

$$N(f_{CL}) = Z_{CL}$$

where Z_{CL} is number of unstable roots (zeros) of $f_{CL}(s)$. The roots of $f_{CL}(s)$ are the closed-loop poles of the system. Thus, the number of clockwise encirclements that $f_{CL}(s)$ makes of the origin is equal to the number of unstable closed-loop poles.

Similarly, let $F(s) = f_{OL}(s)$. Since $f_{OL}(s)$ is a polynomial, it has no denominator and consequently no poles. Therefore, $P = 0$ and equation 3.33 becomes

$$N(f_{OL}) = Z_{OL}$$

where Z_{OL} is number of unstable roots (zeros) of $f_{OL}(s)$. The roots of $f_{OL}(s)$ are the open-loop poles for the system. Thus, the number of clockwise encirclements that $f_{OL}(s)$ makes of the origin is equal to the number of unstable open-loop poles.

The polynomials in equation 3.32 are functions of the complex variable s. Therefore, their arguments (phase angles) can be subtracted to obtain

$$N\{\det[I + GH]\} = N(f_{CL}) - N(f_{OL}) \tag{3.34}$$

For stability, the number of unstable closed-loop poles must be zero. That is, $N(f_{CL}) = 0$. Since $N(f_{OL})$ equals the number of open-loop poles in the right half of the s-plane, equation 3.34 becomes

$$N\{\det[I + GH]\} = -\text{ (number of unstable open-loop poles)} \tag{3.35}$$

where the minus sign indicates encirclement in the counterclockwise direction. Equation 3.35 is the Multivariable Nyquist Stability Criterion, which can be stated as follows:

> If the loop transfer function matrix G(s)H(s) has m poles in the right-half of the s-plane, then for stability the locus $\det[I + G(j\omega)H(j\omega)]$ must encircle the origin m times in the counterclockwise direction, as ω varies from $-\infty$ to $+\infty$.

In analyzing the stability of the telerobotic system, two cases must be considered: constrained and unconstrained motion. Constrained motion occurs when the slave robot is interacting with the environment. Unconstrained motion occurs when the slave robot is moving freely through space. These two cases give rise to two different stability conditions. The case of constrained motion will be considered first.

The telerobotic control architecture must be reduced to an equivalent loop transfer function before the Multivariable Nyquist Criterion can be applied. Using matrix operators,

the block diagram in Figure 1.6 can be rearranged to obtain the simplified block diagram shown in Figure 3.5. A single control loop has been formed by merging the separate control loops of the master and slave robots. Further simplification is possible by combining the G, H, and S matrices in Figure 3.5 using the rules of block diagram algebra. The resulting block diagram is shown in Figure 3.6 where the admittance matrix P is defined as

$$P = GH + S \tag{3.36}$$

From the simplified block diagram, the equivalent loop transfer function is RP. It is a sufficient condition for stability that det[I + RP] does not pass through the origin. This condition guarantees that the contour in the z-plane will always encircle the origin in the counterclockwise direction. In other words, the origin cannot be encircled if the contour passes through it. Thus, the Multivariable Nyquist Criterion for the telerobotic system becomes

$$\det[I + RP] \neq 0 \quad \text{for all } \omega \in [0, \infty] \tag{3.37}$$

or using equation 3.36 for P

$$\det[I + RGH + RS] \neq 0 \quad \text{for all } \omega \in [0, \infty] \tag{3.38}$$

Substituting R, G, H, and S from Figure 3.5 into equation 3.38 for calculation of the determinant yields

$$S_h E \Delta P + S_h P_{11} + E P_{22} + 1 \neq 0 \quad \text{for all } \omega \in [0, \infty] \tag{3.39}$$

where the admittances are given by

$$P_{11} = G_m H_{11} + S_m \tag{3.40}$$

$$P_{12} = G_m H_{12} \tag{3.41}$$

$$P_{21} = G_s H_{21} \tag{3.42}$$

$$P_{22} = G_s H_{22} + S_s \tag{3.43}$$

$$\Delta P = P_{11}P_{22} - P_{12}P_{21} \tag{3.44}$$

For the system to be stable, the left hand side of equation 3.39 must not equal zero. If it is assumed that

$$S_h P_{11} + 1 \neq 0 \quad \text{for all } \omega \in [0, \infty] \tag{3.45}$$

equation 3.39 can be written as

$$1 + \frac{E[S_h \Delta P + P_{22}]}{S_h P_{11} + 1} \neq 0 \qquad \text{for all } \omega \in [0, \infty] \tag{3.46}$$

A sufficient condition to insure the validity of equation 3.46 is

$$\left| \frac{E[S_h \Delta P + P_{22}]}{S_h P_{11} + 1} \right| < 1 \tag{3.47}$$

Rearranging

$$\boxed{\left| \frac{1 + S_h P_{11}}{P_{22} + S_h \Delta P} \right| > |E|} \tag{3.48}$$

This is the stability condition for constrained motion. Comparing the left hand side of inequality 3.48 to equation 2.33, it can be seen that the stability condition is really a limitation on possible values of the slave impedance. That is, for stability

$$|Z_S| > |E| \tag{3.49}$$

The slave impedance must be greater than the impedance of the environment. Since Z_S is a performance parameter that can be arbitrarily specified, it is usually possible to stabilize the system by selecting a sufficiently large value for the slave impedance. There is no conflict between performance and stability in this case. However, if the slave robot is in contact with a rigid surface, the slave impedance must be very large to stabilize the system. As $E \rightarrow \infty$, it is impossible to specify Z_S large enough such that stability of the system is guaranteed. Thus, there must be some initial compliancy in the environment for the system to be stable.

Next, the case of unconstrained motion will be considered. In deriving equation 3.46, it was assumed that equation 3.45 must be true. A sufficient condition to insure the validity of equation 3.45 is

$$|S_h P_{11}| < 1 \tag{3.50}$$

which implies that

$$\boxed{|P_{11}| < \left|\frac{1}{S_h}\right|} \tag{3.51}$$

This is the stability condition for unconstrained motion. When the slave robot is moving freely through space, there are no forces exerted on it by the environment. In that case, $E = 0$ and equation 2.27 for the master impedance becomes

$$Z_m = \frac{1}{P_{11}}$$

Comparing the previous equation to the left hand side of inequality 3.51, it can be seen that the stability condition is really a limitation on possible values of the master impedance. That is, for stability

$$|Z_m| > |S_h| \qquad \text{when } E = 0 \tag{3.52}$$

The master impedance must be greater than the impedance of the human arm. Since Z_m is a performance parameter that can be arbitrarily specified, there is no conflict between performance and stability in most cases. However, if the human grips the master robot tightly, the master impedance must be very large to stabilize the system. As $S_h \rightarrow \infty$, it is impossible to specify Z_m large enough such that stability of the system is guaranteed. Thus, there must be some initial compliancy in the human arm for the system to be stable.

Inequalities 3.48 and 3.51 are the stability conditions for a linear system. Inequalities 3.28 and 3.29 are a general set of stability conditions expressed in terms of operator gains. Since no assumptions were made regarding the structure of the operators, the general stability conditions must be equally valid for linear as well as nonlinear systems. By replacing the nonlinear operator gains with the magnitudes of linear transfer functions, it

can be shown that inequalities 3.48 and 3.51 result from inequalities 3.28 and 3.29.[4] Thus, the linear stability conditions obtained with the Multivariable Nyquist Criterion are a subset of the general stability conditions obtained with the Small Gain Theorem.

The linear stability conditions are related to the H matrix through equations 3.40 to 3.44. By specifying the elements in the H matrix, it is possible to influence both the stability and performance of the telerobotic system.

3.4 Conclusions

It has been shown that the arbitrary specification of performance does not conflict with the requirements for stability. However, there must be some initial compliance in both the environment and the human arm for the system to be stable. Two stability conditions were derived that are equally valid for linear and nonlinear systems. The stability condition for constrained motion requires that the slave impedance Z_s must be greater than the environmental impedance E. The stability condition for unconstrained motion requires that the master impedance Z_m must be greater than the human arm impedance S_h. Like performance, the stability conditions are fundamentally related to the structure of the H matrix.

[4] It was assumed implicitly that $\| -S_h y_m \|_p < \alpha_{Sh} \| y_m \|_p + \beta$ in deriving inequality 3.22, so let $\alpha_{Sh} = |-S_h|$.

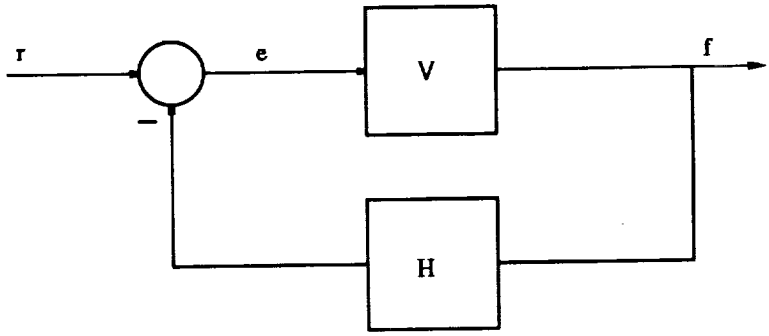

Figure 3.1: Nonlinear Closed-Loop System

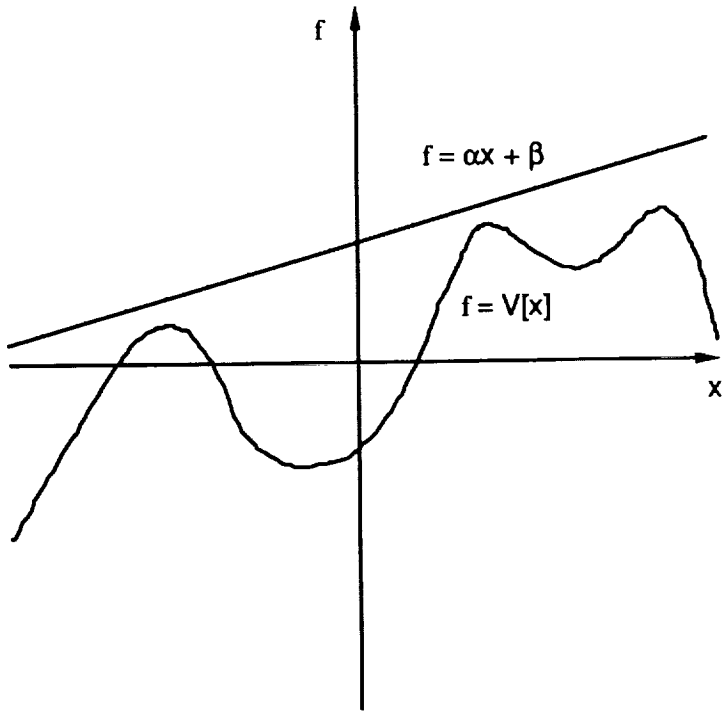

Figure 3.2: Geometric Interpretation of the Small Gain Theorem

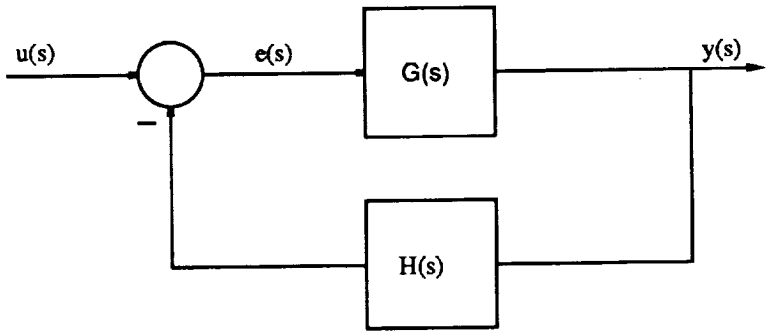

Figure 3.3: Linear Closed-Loop System

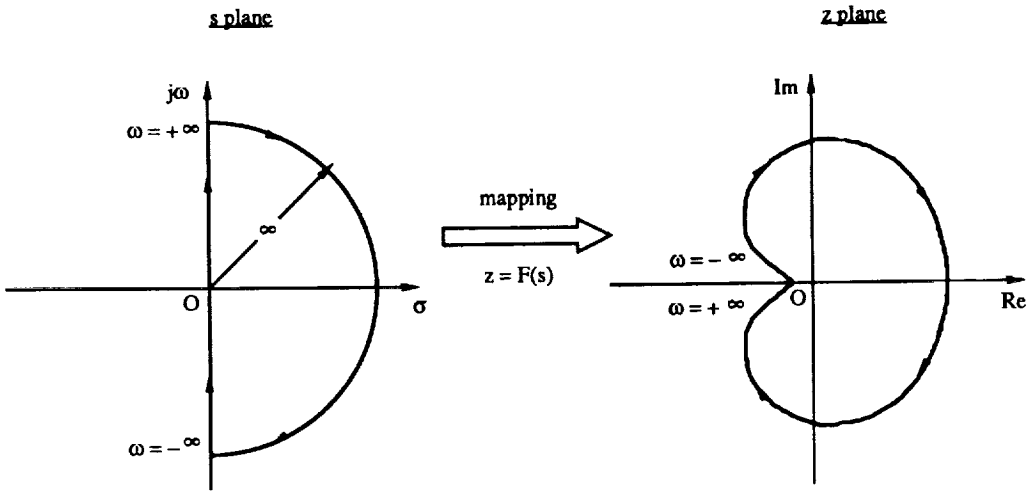

Figure 3.4: Nyquist Conformal Mapping

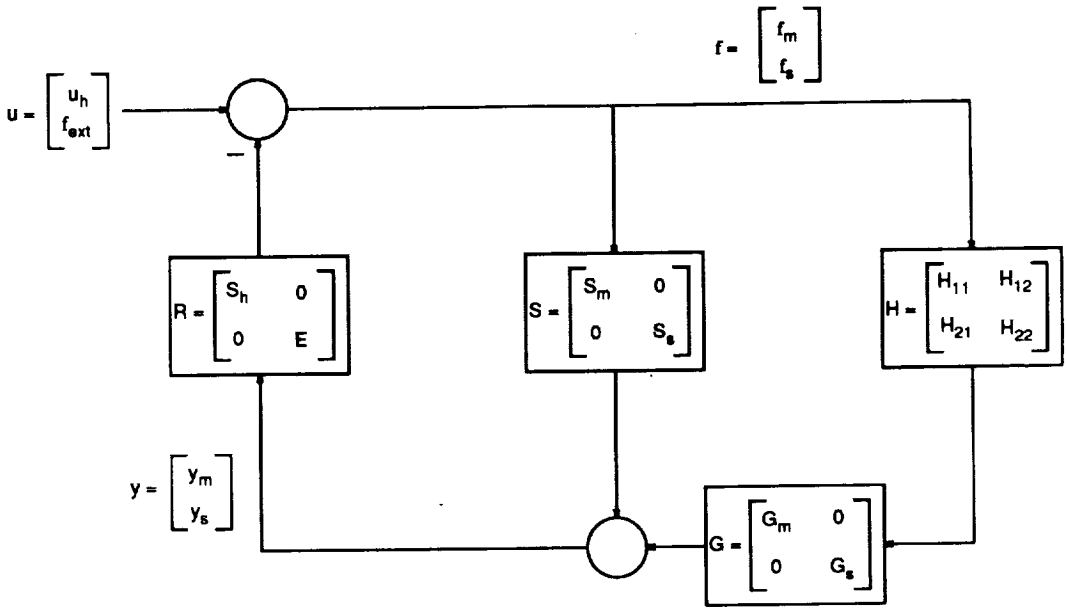

Figure 3.5: Block Diagram of Bilateral Impedance Control Architecture in Matrix Form

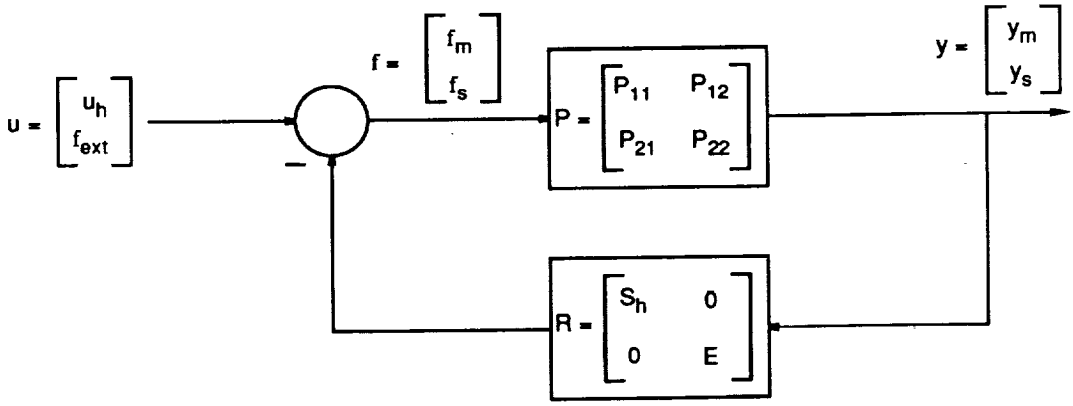

Figure 3.6: Simplified Block Diagram in Matrix Form

Chapter 4
BOND GRAPH ANALYSIS

4.1 Introduction

Bond graphs are a convenient notation for representing the flow of energy and information in any physical system. A bond graph model can be used to determine system state variables, and to formulate the differential equations that govern system dynamics. A bond graph of the telerobotic system will be constructed from basic elements. This bond graph will illustrate how power is transferred and dissipated within the system. It will also be used to show why only three performance parameters can be specified simultaneously. The theoretical background for bond graph analysis will be presented first. Additional information on this subject can be found in Karnopp and Rosenberg (1975).

A bond graph is a diagram constructed from a small set of ideal elements joined together by bonds. The elements represent subsystems or parts of the total system. The bonds represent the connections where power can flow between the subsystems. Figure 4.1 is the generalized bond graph of a system consisting of two subsystems. Power is flowing out of subsystem A and into subsystem B. The direction of power transfer is indicated by a half arrow on the bond. There are two power variables associated with each bond: an effort variable, e, and a flow variable, f. It is convention to place the effort variable above or to the left of the bond, and the flow variable below or to the right of the bond. The product of the effort variable and the flow variable is the power flowing between the two subsystems:

$$P(t) = e(t)\, f(t) \tag{4.1}$$

In mechanical systems, the effort is a force and the flow is a velocity. In electrical systems, the effort is a voltage and the flow is a current.

The two power variables always occur as an input-output pair. If one variable is an input, then the other must be an output. For subsystem A, the flow is an input signal and the effort is an output signal. Inputs and outputs are denoted on the bond graph by a causal stroke, which is a short perpendicular line at one end of the bond. The effort signal is always directed toward the causal stroke. Note that the causal stroke is independent of the direction of power transfer indicated by the half arrow.

Two other variables are important in describing the behavior of dynamic systems. These so-called energy variables are the momentum p and the displacement q. The momentum is defined as the time integral of an effort

$$p(t) = \int^t e(t)\, dt \tag{4.2}$$

Similarly, the displacement is defined as the time integral of a flow

$$q(t) = \int^t f(t)\, dt \tag{4.3}$$

The total energy E which has passed into or out of a subsystem in time t is given by the time integral of the instantaneous power. That is

$$E(t) = \int^t P(t)\, dt = \int^t e(t)\, f(t)\, dt \tag{4.4}$$

Alternate forms of the energy equation will be derived in the next section using the energy variables p and q.

In many cases, information signals are transmitted among the system components at zero power. For example, an ideal sensor extracts information about a system variable without disturbing the system to which it is attached. The transmission of information without the corresponding flow of power is indicated on the bond graph by a full arrow. Bonds that only transmit information are known as active bonds. Active bonds are useful in the modeling of automatic control systems in which sensors are essential devices.

Only a few basic types of elements are required to model the physical effects of complex systems. These elements will be defined next.

4.2 Basic Elements

The basic elements are idealized mathematical models of real components in the system. These elements are interconnected at one or more ports where power flows between subsystems. An element with one port or connection to the rest of the system is called a 1-port element. Similarly, an element with two ports or connections is called a 2-port element. There are also 3-port junction elements that interconnect the other elements to form systems and subsystems. Each of these basic element types will be discussed in turn, starting with the 1-ports.

The resistor is a 1-port element in which the effort and flow variables are related by a static function. If this function is linear, the resistance R is defined by the following constitutive equation:

$$e = R\,f \tag{4.5}$$

The resistor dissipates energy. It can be used to model such devices as a mechanical damper or an electrical resistor. The resistor has the following bond graph symbol:

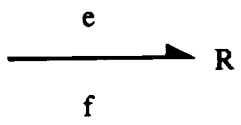

By convention, the half arrow on the bond graph points toward the resistor to indicate that power is flowing into the element.

The capacitor is a 1-port element in which an effort and a displacement are related by a static function. If this function is linear, the capacitance C is defined by the following constitutive equation:

$$q = C\,e \tag{4.6}$$

The capacitor stores energy, and this energy can be recovered without loss. An expression for the energy stored in the capacitor at any time t can be obtained by using the differential form of equation 4.3 ($dq = f\,dt$) in equation 4.4. This gives

$$E(t) = \int_0^t e(t)\,dq(t) + E_0 \tag{4.7}$$

where E_0 is the initial stored energy at $t = 0$. Since e is a function of q for the capacitor, the stored energy can also be written as

$$E(q) = \int_{q_0}^{q} e(q)\,dq + E_0 \tag{4.8}$$

Usually, it is convenient to define E_0 to be zero when $e = 0$ and $q = q_0$. The capacitor can be used to model such devices as a spring, an electrical capacitor, or a hydraulic accumulator. The capacitor has the following bond graph symbol:

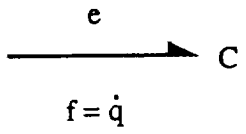

In the 1-port inertia element, a momentum and a flow are related by a static function. If this function is linear, the inertance I is defined by the following constitutive equation:

$$p = I\,f \tag{4.9}$$

Like the capacitor, the inertia stores energy which can be returned to the system. An expression for the energy stored in the inertia can be found by using the differential form of equation 4.2 (dp = e dt) in equation 4.4. This gives

$$E(t) = \int_0^t f(t)\,dp(t) + E_0 \tag{4.10}$$

Since f is a function of p for the inertia, the stored energy can also be written as

$$E(p) = \int_{p_0}^{p} f(p)\,dp + E_0 \tag{4.11}$$

Usually, it is convenient to define E_0 to be zero when f = 0 and p = p_0. The inertia can be used to model a mass or an electrical inductor. The inertia has the following bond graph symbol:

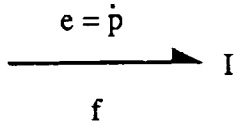

In mechanical systems, the energy associated with an inertia is called kinetic energy, while the energy associated with a capacitor is called potential energy. In an electrical system, these two forms of stored energy are called magnetic and electric energy, respectively.

The effort source and the flow source are 1-port elements that supply power. The effort source maintains a constant effort that is independent of the flow. The effort source can be used to model an electric battery or a mechanical actuator. Its bond graph symbol is

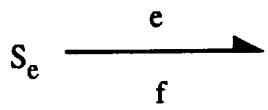

Note that the half arrow is directed away from the effort source to indicate that power is being supplied.

The flow source maintains a constant flow that is independent of the effort. A flow source can be used to model a pump or an electric motor. Its bond graph symbol is

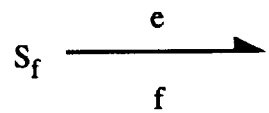

In modeling automatic control systems, it is often necessary to utilize sources whose output depends on some other variable in the system. In these cases, an effort or flow source is paired with an active bond that transmits the control signal. The resulting elements are known as controlled sources.

In the 2-port elements, the power flowing into one port must equal the power flowing out of the other port. Power is conserved such that

$$e_1 f_1 = e_2 f_2 \tag{4.12}$$

The transformer is a 2-port element whose constitutive equations are

$$\begin{aligned} e_1 &= m\, e_2 \\ m\, f_1 &= f_2 \end{aligned} \tag{4.13}$$

where the parameter m is known as the transformer modulus. The transformer can be used to model devices such as a gear train or a hydraulic ram. Its bond graph symbol is

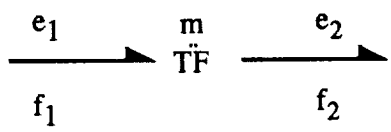

The power sign convention indicates that power flows through the transformer.

The gyrator is another 2-port element that satisfies the conservation of power dictated by equation 4.12. However, its constitutive equations relate an effort at one port to a flow at the other port:

$$e_1 = r\, f_2$$
$$r\, f_1 = e_2 \tag{4.14}$$

where r is called the gyrator modulus. A gyroscope is an example of a mechanical gyrator. Its speed of precession depends on the magnitude of the externally applied force. The bond graph symbol for a gyrator is

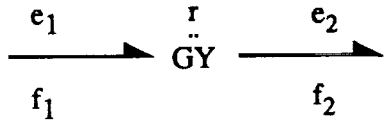

Like the transformer, a through power sign convention is established.

The 1 and 2-port elements are joined together by 3-port junction elements. There are two types of junction elements: a 0-junction and a 1-junction. The 0-junction connects elements having a common effort. Its bond graph symbol is

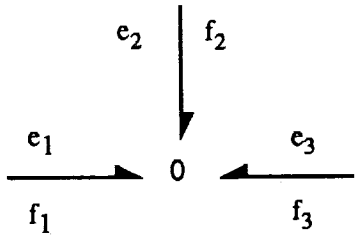

All power signs are directed inward by convention. The constitutive equations for the 0-junction are

$$e_1 = e_2 = e_3$$
$$f_1 + f_2 + f_3 = 0 \tag{4.15}$$

In other words, the effort on all bonds is identical, and the sum of all flows entering the junction is zero. Taken together, these two equations imply that the power on all bonds must sum to zero. That is

$$e_1 f_1 + e_2 f_2 + e_3 f_3 = 0 \tag{4.16}$$

This means that if power is flowing into the 0-junction on two of the ports, it must be flowing out at the third.

The 1-junction connects elements having a common flow. Its bond graph symbol is

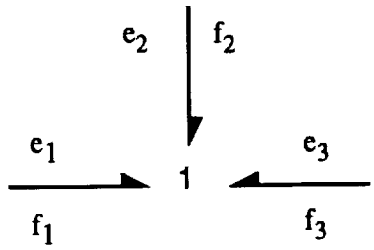

The power signs are directed inward by convention. The constitutive equations for the 1-junction are

$$e_1 + e_2 + e_3 = 0 \tag{4.17}$$
$$f_1 = f_2 = f_3$$

In other words, the efforts on all bonds must sum to zero, and the flow on all bonds is identical. Taken together, these two equations imply that the power on all bonds must sum to zero. This is the same condition stated in equation 4.16 for the 0-junction.

An electrical circuit provides a good analogy for the junction elements. The 0-junction can be thought of as a parallel connection in which all elements have a common voltage. Similarly, the 1-junction can be thought of as a series connection in which all elements have a common current.

The basic elements are summarized in Table 4.1. In addition, a pseudo-element called an impedance can be defined. An impedance is used to model the composite effect of a whole subsystem. The subsystem may consist of energy storage elements and energy dissipation elements. However, the exact structure of the subsystem is unknown. At a port, the impedance relates an effort and a flow such that

$$e = Z f \tag{4.18}$$

where Z is a complex function. The bond graph symbol for an impedance is

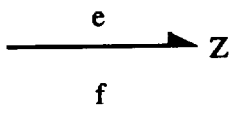

An impedance is not a basic element. Rather, it may incorporate several basic elements such as resistors, capacitors, and inertias. An impedance is merely a notational convenience for representing unstructured subsystems. It accurately models the input-output properties at a port, but it obscures the details of the subsystem's internal structure.

Table 4.1
Basic Elements

Element	*Type*	*Symbol*	*Constitutive Equation*
Resistor	1-port	R	$e = R\,f$
Capacitor	1-port	C	$q = C\,e$
Inertia	1-port	I	$p = I\,f$
Effort Source	1-port	S_e	
Flow Source	1-port	S_f	
Transformer	2-port	TF	$e_1 = m\,e_2$ $m\,f_1 = f_2$
Gyrator	2-port	GY	$e_1 = r\,f_2$ $r\,f_1 = e_2$
0-junction	3-port	0	$e_1 = e_2 = e_3$ $f_1 + f_2 + f_3 = 0$
1-junction	3-port	1	$e_1 + e_2 + e_3 = 0$ $f_1 = f_2 = f_3$

4.3 Causality

The concept of input-output causality was introduced previously. The causal stroke on the bond graph indicates the direction of the effort signal. The basic elements are constrained to have different causal properties. By applying these rules of causality to the bond graph, it is possible to predict fundamental properties of the system.

The allowable causalities of the effort and flow sources can be determined from their definitions. The effort source imposes an effort upon the system to which it is connected. Since the effort signal is always directed toward the causal stroke, the only permissible causality for the effort source is

Similarly, the flow source supplies the system with a flow. Since the effort signal must be directed in the opposite direction, the only possible causality for the flow source is

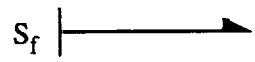

The resistor can accommodate two possible causalities, depending on whether the effort is an output or an input. If the effort is an output, the causality and the corresponding constitutive relationship are

$$e = R\,f$$

On the other hand, if the effort is an input, the causality and the constitutive relationship are

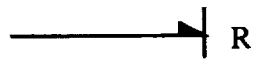

$$f = e/R$$

Note that the input is always on the right hand side of the constitutive equation, while the output is always on the left hand side. As long as the static function R and its inverse exist, the resistor does not prefer one causality over the other. Thus, the assignment of causality is arbitrary for the resistor.

The choice of causality for the capacitor has an important effect on the constitutive relationship. When the flow is the input to the capacitor, equation 4.6 can be written in

integral form as

$$e = 1/C \int f\,dt \tag{4.19}$$

In this case, the capacitor exhibits what is known as integral causality. On the bond graph, integral causality for the capacitor is indicated by

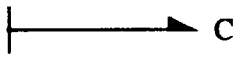

Similarly, when the effort is the input to the capacitor, the constitutive relationship can be written in derivative form as

$$f = \frac{d(C\,e)}{dt} \tag{4.20}$$

In this case, the capacitor exhibits derivative causality. On the bond graph, derivative causality for the capacitor is indicated by

The inertia element can also have either integral or derivative causality. Its constitutive relationship (equation 4.9) can be written in integral form as

$$f = 1/I \int e\,dt \tag{4.21}$$

or in derivative form as

$$e = \frac{d(I\,f)}{dt} \tag{4.22}$$

Integral causality exists when e is the input to the inertia, and derivative causality exists when f is the input. On the bond graph, integral causality for the inertia is indicated by

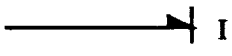

while derivative causality is indicated by

while derivative causality is indicated by

The distinction between integral and derivative causality is important in determining a fundamental characteristic of the system. The system's order is the number of state variables necessary to describe its dynamic behavior. It turns out that the number of independent state variables is equal to the number of energy storage elements with integral causality. If an energy storage element has derivative causality, it does not contribute any state variables.

The permissible causalities of the transformer can be determined from equation 4.13. As soon as one of the effort or flow variables has been assigned as the input, the other effort or flow is constrained to be an output. Thus, the only possible choices for causality are

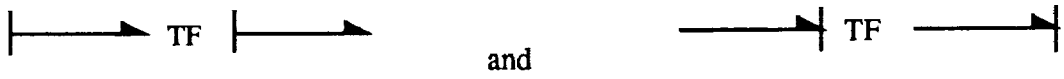

The gyrator also has only two possible causalities, which can be determined from equation 4.14. If the effort on one port is chosen to be an input, then the flow on the other port must be an output. Thus, the allowable causalities for the gyrator are

For the 0-junction, the efforts on all bonds are equal and the flows must sum to zero. If the effort on one of the bonds is an input to the junction, then the efforts on all the other bonds must be outputs. Conversely, if the flows on all bonds except one are inputs, the flow on the remaining bond must be an output. Thus, a typical permissible causality for the 0-junction is

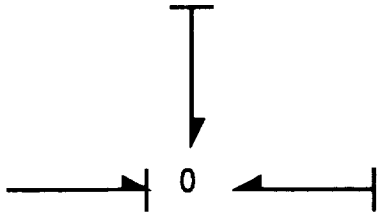

On one bond, the causal stroke is on the end nearest to the 0, while on all the other bonds, the causal strokes are on the ends away from the 0.

For the 1-junction, the causal considerations are the same as for the 0-junction, except that the roles of the efforts and flows are interchanged. The flows on all bonds in the 1-junction are equal and the efforts must sum to zero. If the flow on one of the bonds is an input to the junction, then the flows on all the other bonds must be outputs. Conversely, if the efforts on all bonds except one are inputs, the effort on the remaining bond must be an output. Thus, a typical permissible causality for the 1-junction is

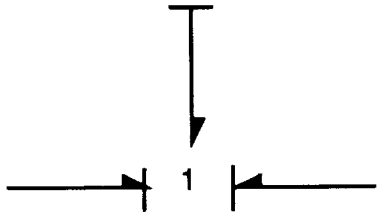

On one bond, the causal stroke is on the end away from the 1, while on all the other bonds, the causal strokes are on the ends nearest the 1.

Now that causal properties have been determined for each of the basic elements, this information can be applied to the bond graph. Assigning causality to one element in the bond graph usually implies a causality for several other elements as well. By extending these causal implications throughout the graph, it is possible to characterize the physical validity of the system. Violations of causality mean that there are inconsistencies in the physical model. The procedure for adding causal strokes to the bond graph will become apparent when a model of the telerobotic system is constructed.

4.4 Bond Graph of Telerobotic System

A bond graph of the telerobotic system will be assembled by joining smaller bond graphs of the major subsystems. The essential dynamic behavior of the subsystems will be modeled with basic elements. The telerobotic system can be divided into four subsystems: the human arm, the master robot, the slave robot, and the environment.

It is natural to think of the human arm as a source of effort because it supplies power to the rest of the system. However, some of the effort exerted by the muscles is expended in moving the arm. Thus, the force applied to the master robot is less than that commanded by the central nervous system. These ideas are embodied in the dynamic

equation for the human arm

$$f_m = u_h - S_h \dot{y}_m \tag{4.23}$$

This equation can be translated into the bond graph shown in Figure 4.2.

Bond 3 connects the human arm subsystem to the master robot subsystem. The two subsystems share common power variables. The effort variable is the force exerted on the master robot, f_m. The flow variable is the velocity of the master robot, $\dot{y}_m$. For a 1-junction, the flows on all bonds are equal. In this case, the flows are equal to $\dot{y}_m$.

The operator S_h maps the robot velocity into a force. In effect, S_h relates a flow to an effort. However, S_h is an unstructured representation of the human arm sensitivity function. It may contain energy storage elements in addition to energy dissipation elements. Therefore, S_h is modeled as a complex impedance. On the bond graph, the notation $Z : S_h$ means that the impedance of Z is S_h.

The efforts on all bonds of the 1-junction must sum to zero. Stated another way, there must be an equality between power inputs and outputs. The input to the 1-junction comes from the effort source used to model commands from the central nervous system, u_h. Equation 4.23 is satisfied if the efforts on bonds 2 and 3 are outputs. With these considerations in mind, the reference power directions are assigned to the bond graph. The input bond has its half arrow directed toward the 1-junction, while the two output bonds have their half arrows directed away from the junction. It is clear from the bond graph that power is transferred from the human arm to the master robot. Some of this power is dissipated or stored by the internal impedance of the arm.

The bond graph for the environment is identical in structure to the bond graph for the human arm. A 1-junction connects an effort source and an impedance as shown in Figure 4.3.

The bond graph represents the dynamic equation for the environment:

$$f_s = f_{ext} - E \dot{y}_s \tag{4.24}$$

This equation expresses the idea that the total force acting on the slave robot is a combination of external forces and reaction forces. The external forces are generated by a source of power that is outside the system. The reaction forces arise from the interaction between the slave robot and the environment. These forces are a function of the robot's velocity (or position).

Bond 3 connects the environment subsystem to the slave robot subsystem. The two subsystems share common power variables. The effort variable is the force exerted on the slave robot, f_S. The flow variable is the velocity of the slave robot, $\dot{y}_S$.

The environmental operator E maps the robot velocity into a reaction force. In effect, E relates a flow to an effort. However, the exact form of this relationship is unknown since E is an unstructured representation of the environmental dynamics. Therefore, E is modeled as a complex impedance. On the bond graph, the notation Z : E means that the impedance of Z is E. It is understood that the impedance may incorporate both energy storage and energy dissipation elements.

The 1-junction implies an equality between power inputs and outputs. The input to the junction comes from the effort source used to model the external forces, f_{ext}. Equation 4.24 is satisfied if the efforts on bonds 2 and 3 are outputs. The reference power directions are assigned accordingly.

The bond graph clearly illustrates how power is transferred from the external effort source to the slave robot. Some of the external power is dissipated or stored by the impedance of the environment. Usually, the external effort source is set to zero. In this case, the bond graph for the environment reduces to a passive impedance, with power flowing in from the slave robot.

Before the master robot can be modeled with a bond graph, it is necessary to determine its equation of motion. The dynamic equation of a robot manipulator has the general form

$$\tau = M(\theta)\ddot{\theta} + C(\theta,\dot{\theta})\dot{\theta} + G(\theta) \tag{4.25}$$

A derivation of this equation can be found in Craig (1988). $\ddot{\theta}$, $\dot{\theta}$, and θ are vectors of the joint accelerations, velocities, and positions. τ is the joint torque vector. $M(\theta)$ is the mass matrix, which is a function of θ. $C(\theta,\dot{\theta})$ is a matrix of Coriolis and centripetal force terms that are functions of both θ and $\dot{\theta}$. $G(\theta)$ is a matrix of gravitational force terms that depend only on θ.

The master robot is driven by two sources of power: the human arm and the control system actuators. The human arm exerts a force f_m on the end of the master robot. This force acts in the direction of motion, and produces a torque τ_m on each joint. The control system actuators stabilize the robot, and provide force reflection by backdriving the joints. In addition, the actuators enable the human to overcome the robot's friction and inertia. The actuator torque τ_a is assumed to act in the direction of motion, although at times it may oppose the robot's motion depending on commands received from the control system. The

total torque on each joint is the sum of the torque applied by the human arm, and the torque generated by the actuators. Therefore, the equation of motion for the master robot is

$$\tau_m + \tau_a = M(\theta)\ddot{\theta} + C(\theta,\dot{\theta})\dot{\theta} + G(\theta) \tag{4.26}$$

It is desirable to relate the force applied to end of the robot to the torque developed at the joints. However, f_m is defined in Cartesian space, while τ_m is defined in joint space. Thus, a transformation between spaces is required. The manipulator Jacobian is a matrix that maps joint velocities into Cartesian velocities. That is

$$\dot{y} = J(\theta)\,\dot{\theta} \tag{4.27}$$

where J is the Jacobian matrix, and $\dot{y}$ is the velocity of the robot end point. Note that J is a function of the joint angles. Thus, the Jacobian must be recalculated continuously as the robot moves.

The conservation of power requires that the product of efforts and flows be the same in joint space as it is in Cartesian space. That is

$$\tau^T \dot{\theta} = f^T \dot{y} \tag{4.28}$$

Substituting equation 4.27 into equation 4.28 gives

$$\tau^T \dot{\theta} = f^T J\,\dot{\theta} \tag{4.29}$$

Canceling $\dot{\theta}$ from both sides of the previous equation and transposing yields

$$\tau = J^T f \tag{4.30}$$

Therefore, the transpose of the Jacobian matrix J^T is the desired transformation between force and torque.

Equation 4.30 can be used to replace t_m in equation 4.26. The result is

$$J_m^T f_m + \tau_a = M(\theta)\ddot{\theta} + C(\theta,\dot{\theta})\dot{\theta} + G(\theta) \tag{4.31}$$

The right hand side of equation 4.31 represents the dynamics of the robot arm. The robot

dynamics are a function of θ and its derivatives. Therefore, it should be possible to model the dynamics with an operator that maps joint velocity (or position) into torque. Assuming that this is true, equation 4.31 can be rewritten as

$$J_m^T f_m + \tau_a = Z_{ma}\dot{\theta}_m \tag{4.32}$$

where the impedance Z_{ma} represents the dynamics of the robot arm.[5] It is apparent from equation 4.31 that Z_{ma} incorporates damping and inertial terms. The impedance may also include stiffness terms if the structure of the robot arm is flexible. Equation 4.32 is the basis for the bond graph model of the master robot.

The bond graph for the master robot is shown in Figure 4.4. Bond 1 connects the master robot subsystem to the human arm subsystem. The power variables on this bond are common to both subsystems. The effort is the force exerted on the master robot, f_m. The flow is the velocity of the master robot, $\dot{y}_m$.

The transformer changes power variables between Cartesian and joint space. The transformer modulus is J_m^{-1}, which is the inverse of the master Jacobian. The constitutive relationships for the transformer require that

$$\dot{\theta}_m = J_m^{-1}\dot{y}_m \tag{4.33}$$
$$(J_m^{-1})^T \tau_m = f_m$$

It can be shown that these equations are identical to equations 4.27 and 4.30.

The 1-junction implies an equality between power inputs and outputs. Power is flowing into the junction on bond 2 from the human arm, and on bond 4 from the actuator. To satisfy equation 4.32, power must be flowing out on bond 3. The reference power directions are assigned accordingly. The joint velocity $\dot{\theta}_m$ is the flow on all bonds of the 1-junction. The impedance Z_{ma} relates the joint velocity to the effort on bond 3. Since all efforts on the 1-junction must sum to zero, the effort on bond 3 is the total torque $\tau_m + \tau_a$. The actuator is modeled as a dependent effort source. Its output is regulated by the control system.

The bond graph illustrates how power is transferred and transformed in the master robot. Power originating from the human arm is transformed into joint space by the

[5] Note that Z_{ma} is not the same as Z_m, which is the overall impedance that the telerobotic system presents to the human on the master end.

manipulator Jacobian. There it adds to the power supplied by the control system actuator. The combined power is dissipated or stored in the impedance of the robot arm.

The dynamic equation of the slave robot can be expressed in the same form as equation 4.32. However, the sign of the applied torque is reversed because the robot's motion is constrained by the environment. The control system actuators drive the slave robot in response to commands from the master robot. The actuator torque τ_a acts in the direction of motion. The environment exerts a reaction force f_s on the end of the slave robot. This force opposes the robot motion, and produces a torque τ_s on each joint. The net torque on each joint is the difference between the torque exerted by the actuators, and the torque generated by interaction with the environment. Again, it will be assumed that the dynamics of the robot arm can be represented by an impedance. The dynamic equation of the slave robot is found by equating the net torque acting on the joints to the robot dynamics. That is

$$\tau_a - J_s^T f_s = Z_{sa} \dot{\theta}_s \tag{4.34}$$

where Z_{sa} is the impedance of the robot arm.[6] The transpose of the slave Jacobian J_s^T maps the end-point force f_s into the joint torque τ_s. Equation 4.34 is the basis for the bond graph model of the slave robot.

The bond graph for the slave robot is shown in Figure 4.5. Bond 1 connects the slave robot subsystem to the environmental subsystem. The power variables on this bond are common to both subsystems. The effort is the interaction force f_s, while the flow is the robot velocity $\dot{y}_s$. If there are no external forces acting on the slave robot, power flows from the robot into the environment. The transformer changes power variables between Cartesian and joint space. The transformer modulus is J_s, which is the slave Jacobian. Since the direction of power flow through the transformer is reversed, the modulus for the master robot is the inverse of the modulus for the slave robot. It can be shown that the transformer equations are identical for both robots.

For the 1-junction, the power inputs must equal the power outputs. Power from the actuator is flowing into the junction on bond 4. To satisfy equation 4.34, power must be flowing out on bonds 2 and 3. The reference power directions are assigned accordingly. The joint velocity $\dot{\theta}_s$ is the flow on all bonds of the 1-junction. The impedance Z_{sa} relates the joint velocity to the effort on bond 3. Since all efforts on the 1-junction must sum to

[6] Note that Z_{sa} is not the same as Z_s, which is the overall impedance that the telerobotic system presents to the environment on the slave end.

zero, the effort on bond 3 is the net torque $\tau_a - \tau_s$. The actuator is modeled as a dependent effort source. Its output is regulated by the control system.

The bond graph illustrates how power is transferred from the slave robot to the environment. Power is generated by the control system actuator. Some of this power is dissipated or stored by the robot impedance. The remainder is available at the robot end point where it is used to manipulate the environment.

Now the bond graph for the telerobotic system can be assembled by connecting the bond graphs of the individual subsystems (Figures 4.2 - 4.5). This has been done in Figure 4.6. Assuming that no external forces are acting on the slave robot, the bond graph for the environment reduces to a passive impedance. Power flows into the environment from the slave. If external forces were present, the direction of power flow would be reversed, and the bond graph of the slave robot would be identical to that of the master robot. The telerobotic system modeled in Figure 4.6 is uncontrolled. That is, no control law has been implemented that couples the two robots together. This will be done next.

For both robots, the control system actuators have been modeled as dependent effort sources. The variable output of these sources is determined by a control law. The robots are stabilized by position controllers that keep them stationary when the human is not interacting with the system. A position control law is implemented such that the actuator torque is given by

$$\tau_a = k_p(\theta_{ref} - \theta) + k_v(\dot{\theta}_{ref} - \dot{\theta}) \tag{4.35}$$

The position error is the difference between the commanded position θ_{ref} and the actual position θ. The position gain k_p multiplies the position error, and its value determines the controller stiffness. Similarly, the velocity error is the difference between the commanded velocity $\dot{\theta}_{ref}$ and the actual velocity $\dot{\theta}$. The velocity gain k_v multiplies the velocity error, and its value determines the controller damping. The controller governed by equation 4.35 is often called a proportional-derivative or PD controller.

The PD control law can be modeled with the bond graph shown in Figure 4.7. The input command to the control system is $\dot{\theta}_{ref}$. It is represented by a dependent flow source. The output of the control system is the actuator torque τ_a, which is the effort on all bonds of the 0-junction. The actuator drives the robot at the joint velocity $\dot{\theta}$, which is the flow on bond 2. The flows on all bonds of the 0-junction must sum to zero. Therefore, the flow on bond 3 is the velocity error $\dot{\theta}_{ref} - \dot{\theta}$. The velocity error is also the flow on all bonds of the 1-junction. The effort on bond 4 is determined by a resistor. If the resistance is k_v, the constitutive relationship for the resistor implies that

$$e_4 = k_v (\dot{\theta}_{ref} - \dot{\theta}) \tag{4.36}$$

The effort on bond 5 is determined by a capacitor. If the capacitance is $1/k_p$, the constitutive relationship for the capacitor implies that

$$e_5 = k_p (\theta_{ref} - \theta) \tag{4.37}$$

In effect, the capacitor integrates the velocity error to obtain the position error. The 1-junction implies that the effort on bond 3 is the sum of the efforts on bonds 4 and 5. Since the effort on bond 3 is also equal to τ_a, equation 4.35 is satisfied.

The bond graph illustrates how actuator power is stored and dissipated within the control system. The position gain k_p causes the controller to act like an energy storage element, while the velocity gain k_v causes the controller to act like an energy dissipating element.

The input commands to the control system have not yet been specified. They depend on the control architecture that is implemented in the computer. For the bilateral impedance control architecture, the input commands to the robots are governed by the H matrix. The input command to the master robot u_m is given by

$$u_m = J_m^T({}^b_h T_m \, H_{11} \, f_m + {}^b_h T_s \, H_{12} \, f_s) \tag{4.38}$$

while the input command to the slave robot u_s is given by

$$u_s = J_s^T({}^b_h T_m \, H_{21} \, f_m + {}^b_h T_s \, H_{22} \, f_s) \tag{4.39}$$

The interaction forces f_m and f_s are measured by force sensors located on the end of each robot. The H matrix filters the interaction forces in the hand coordinate frame. Since the slave robot may have a different orientation than the master robot, it is necessary to transform the robot forces into a common coordinate frame before they can be added. The transformation matrix ${}^b_h T$ maps the filtered force from each robot into the base coordinate frame. The base frame is always fixed, and is identical for both robots. The base frame forces are added in Cartesian space. The transpose of the robot Jacobian J^T maps the combined forces into joint space.

There is no transfer of mechanical power between the master and slave robots. The robots are driven by the electronic input commands to their control systems. The input commands are calculated in the computer from force sensor measurements. Thus, the robots are coupled only by information signals that can be represented on the bond graph with active bonds.

The bond graph of the PD controller can be used to replace the dependent effort sources in Figure 4.6. The resulting bond graph is shown in Figure 4.8, where the bilateral impedance control architecture has also been implemented. The active bonds, which have a full arrow, convey the force signals to the controllers' dependent flow sources. The input commands to the flow sources are determined from equations 4.38 and 4.39. This is indicated on the bond graph by the notation $S_f : \dot{\theta}_{ref} = u_m$ which means that the reference input velocity to the master robot is u_m.

The physical validity of the telerobotic system model can be determined by assigning causality to the bond graph. The assignment of causality follows several basic rules. First, causal strokes are assigned to all of the effort and flow sources. The causal implications are then extended through the bond graph as far as possible, using the causal constraints of the other basic elements. Second, integral causality is assigned to any one of the energy storage elements. Again the causal implications are extended through the bond graph. This process is repeated until all of the energy storage elements have been assigned a causality. Finally, an arbitrary causality is selected for any unassigned resistor element. The causal implications of this choice are extended as before. The process is repeated until all resistors have been assigned a causality. If any bonds are left unassigned at this point, an arbitrary causality is assigned to them.

The bond graph of the telerobotic system has been augmented with causal strokes in Figure 4.9. Since no causal constraints are violated, the bond graph must be a physically consistent model of the telerobotic system. The system's order can be determined by examining the causality of the energy storage elements. In the human arm, the energy storage elements have not been modeled explicitly. However, it will be assumed that the impedance S_h incorporates a capacitor which stores potential energy, and an inertia which stores kinetic energy. If the impedance is replaced by a capacitor, the causal stroke on bond 2 indicates that this element will have integral causality. Similarly, if the impedance is replaced by an inertia, the causal stroke indicates that this element will have derivative causality. Only energy storage elements with integral causality can contribute to the system's order. Therefore, the capacitor is an independent energy storage element, but not the inertia. The capacitor represents the stiffness of the human arm.

In the master robot, the impedance Z_{ma} is assumed to incorporate an inertia that

represents the robot's mass matrix $M(\theta)$. There is no stiffness associated with the impedance because the robot is modeled as a rigid structure. The causal stroke on bond 5 indicates that the inertia has integral causality. Thus, it is an independent energy storage element. In contrast, the inertia of the human arm is a dependent element. This means that the kinetic energy of the human arm depends on some other element in the system. That element must be the master robot since its inertia is independent. This reasoning makes sense intuitively because the human arm is in intimate contact with the master robot. It is not possible to change the kinetic energy of the robot without changing the kinetic energy of the human arm.

Energy can also be stored in the control system. The causal stroke on bond 8 indicates that the capacitor has integral causality. Thus, the control system acts like an independent energy storage element. Potential energy is stored in the stiffness of the PD controller.

In the slave robot, the impedance Z_{sa} is assumed to incorporate an inertia that represents the robot's mass matrix. The causal stroke on bond 16 indicates that the inertia has integral causality. Thus, it is an independent energy storage element. The environmental impedance E is assumed to incorporate a capacitor and an inertia. The capacitor corresponds to the stiffness of the environment, while the inertia represents the environment's mass. If E is replaced by a capacitor, the causal stroke on bond 18 indicates that it will have integral causality. If E is replaced by an inertia, it will have derivative causality. Therefore, the potential energy stored in the stiffness is independent, but the kinetic energy stored in the inertia depends on some other element in the system. That element must the slave robot since its inertia is independent. This reasoning makes sense intuitively because the slave robot and the environment are in contact. It is not possible to change the energy of one subsystem without affecting the energy of the other.

The order of the telerobotic system is the number of state variables required to describe its dynamic behavior. The energy variables associated with the independent storage elements are selected as state variables. The energy variable for a capacitor is the displacement q, while the energy variable for an inertia is the momentum p. From the bond graph, the state variables are

$$X = \begin{Bmatrix} y_m \\ M_m\dot{\theta}_m \\ \Delta\theta_m \\ \Delta\theta_s \\ M_s\dot{\theta}_s \\ y_s \end{Bmatrix} \tag{4.40}$$

where $\Delta\theta$ is the position error θ_{ref} - θ, and M is the robot mass matrix. There are six independent energy storage elements. Therefore, the order of the telerobotic system is six.

Finally, bond graph analysis will be used to prove that only three performance parameters can be specified simultaneously. A simplified bond graph of the telerobotic system is shown in Figure 4.10. The human arm is modeled as an independent effort source that exerts a force f_m on the master robot. From the perspective of the human, the telerobotic system acts like an impedance Z_m. This impedance relates the applied force f_m to the position of the master robot y_m. An active bond transmits force information from the master robot to the slave robot. The slave robot is modeled as a dependent effort source. The output of this dependent source is the slave force f_s, and it is regulated by the force ratio R_f. The force ratio depends on the dynamics of the environment. From the perspective of the environment, the telerobotic system acts like an impedance Z_s. This impedance is a performance parameter that relates the slave force f_s to the slave position y_s. If Z_s is connected to the dependent effort source, the flow on bond 2 is specified to be y_s. At this point, the efforts and flows on all bonds have been determined by specifying three performance parameters: Z_m, R_f, and Z_s.

The physical validity of the model can be tested by assigning causality to the bond graph. The causal strokes indicate that effort signals are directed away from the effort sources. This is consistent with the definitions of the sources. Since no causal constraints have been violated, it is possible to specify three performance parameters simultaneously.

Now a fourth performance parameter will be specified to see how causality is affected. The position ratio R_y relates the positions of the master and slave robots. In Figure 4.11, a second active bond transmits position information from the master robot to the slave robot. A dependent flow source has been added to the slave side of the telerobotic system. The output of this dependent source is the slave position y_s, and it is regulated by the position ratio R_y.

Causality is assigned to the flow source consistent with its definition. The causal stroke indicates that the effort signal is directed toward the flow source. Since f_s is the output of the dependent effort source on bond 2, y_s must be the input. However, causality indicates that y_s is also the output from the dependent flow source on bond 3. It is not possible for y_s to be both an input and an output at the same time. Therefore, causality is violated, and too many performance parameters have been specified.

4.5 Conclusions

A bond graph model of the telerobotic system was constructed from basic elements. This model illustrates how power is transferred and dissipated within the system. Power is generated by the human arm and the control system actuators. The human arm is an independent source of effort, while the actuators are dependent sources of effort. There is no transfer of power between master and slave robots. Force signals are exchanged through active bonds that only transmit information. The power supplied from the effort sources is dissipated by damping impedances in the human arm, the robots and their stabilizing controllers, and the environment.

The bond graph also shows how the total system energy is distributed. Potential energy is stored in the human arm, the environment, and the robot control systems. Kinetic energy is associated with the motion of the robots. The independent energy storage elements were used to determine the system's order. It was found that the telerobotic system has an order of six.

Causality was assigned to the bond graph to check the physical validity of the control architecture. The implications of causality were also used to prove that no more than three performance parameters can be specified simultaneously.

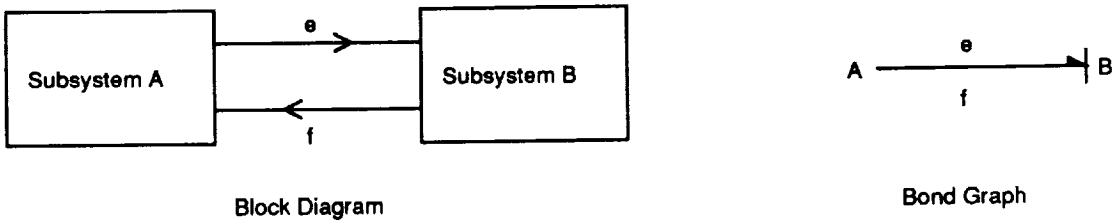

Figure 4.1: Generalized Bond Graph of a 2-Element System

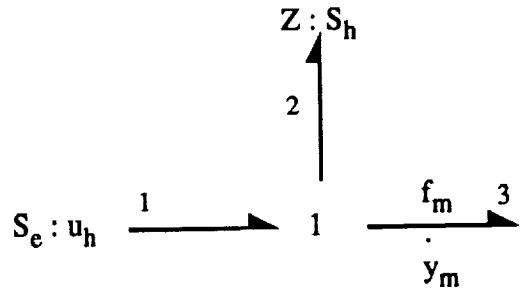

Figure 4.2: Bond Graph of the Human Arm

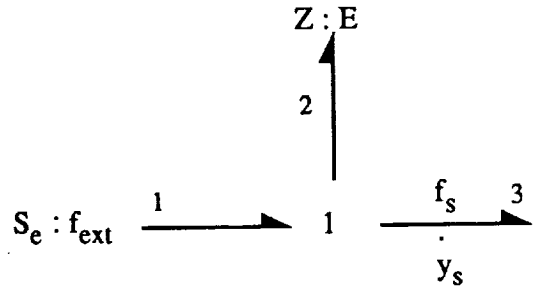

Figure 4.3: Bond Graph of the Environment

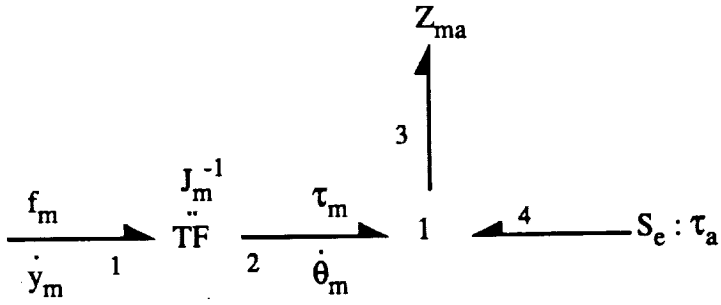

Figure 4.4: Bond Graph of Master Robot

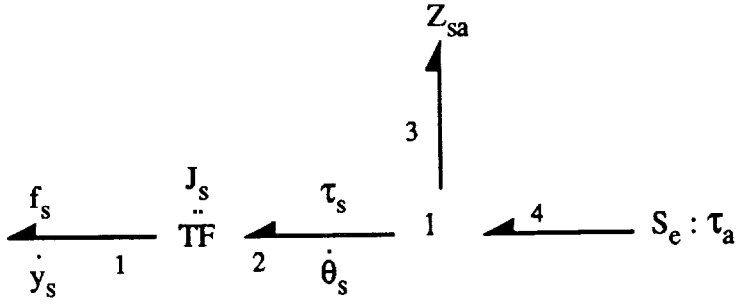

Figure 4.5: Bond Graph of the Slave Robot

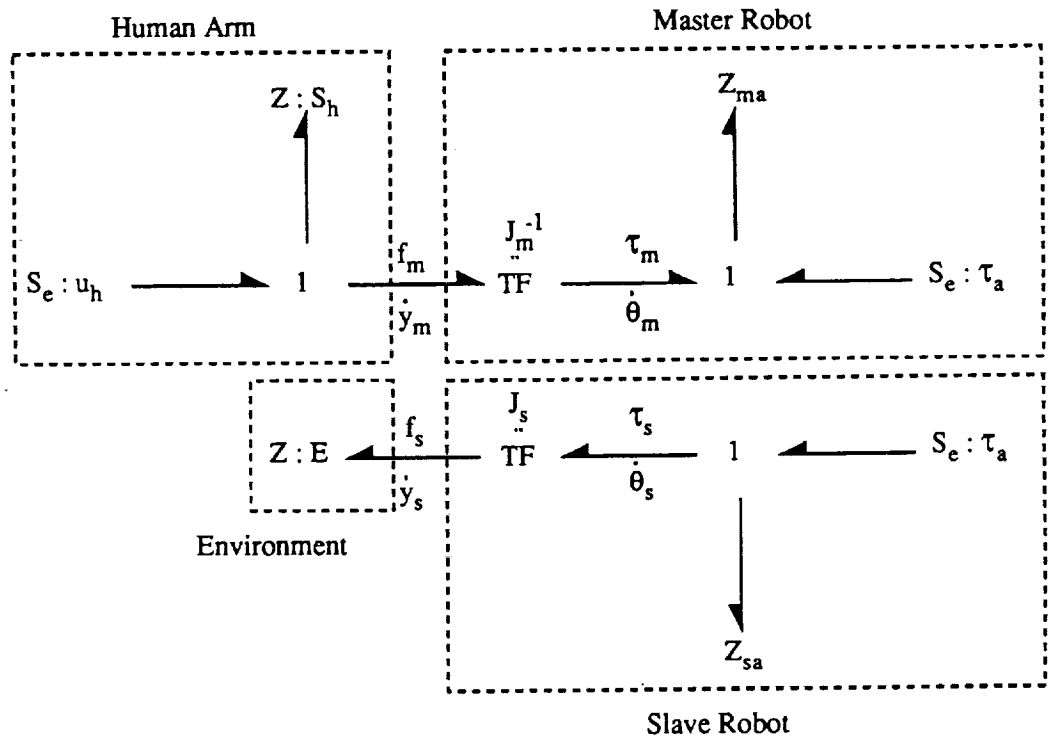

Figure 4.6: Bond Graph of the Telerobotic System (Uncontrolled)

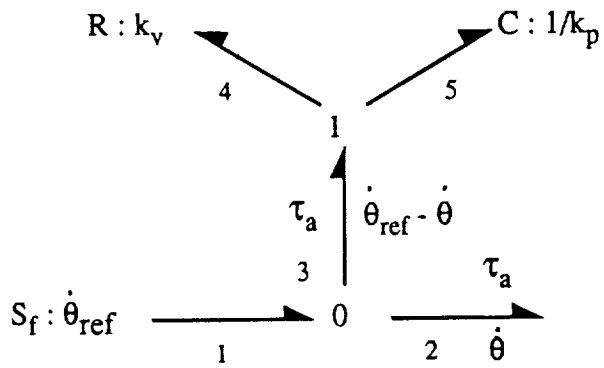

Figure 4.7: Bond Graph of PD Controller

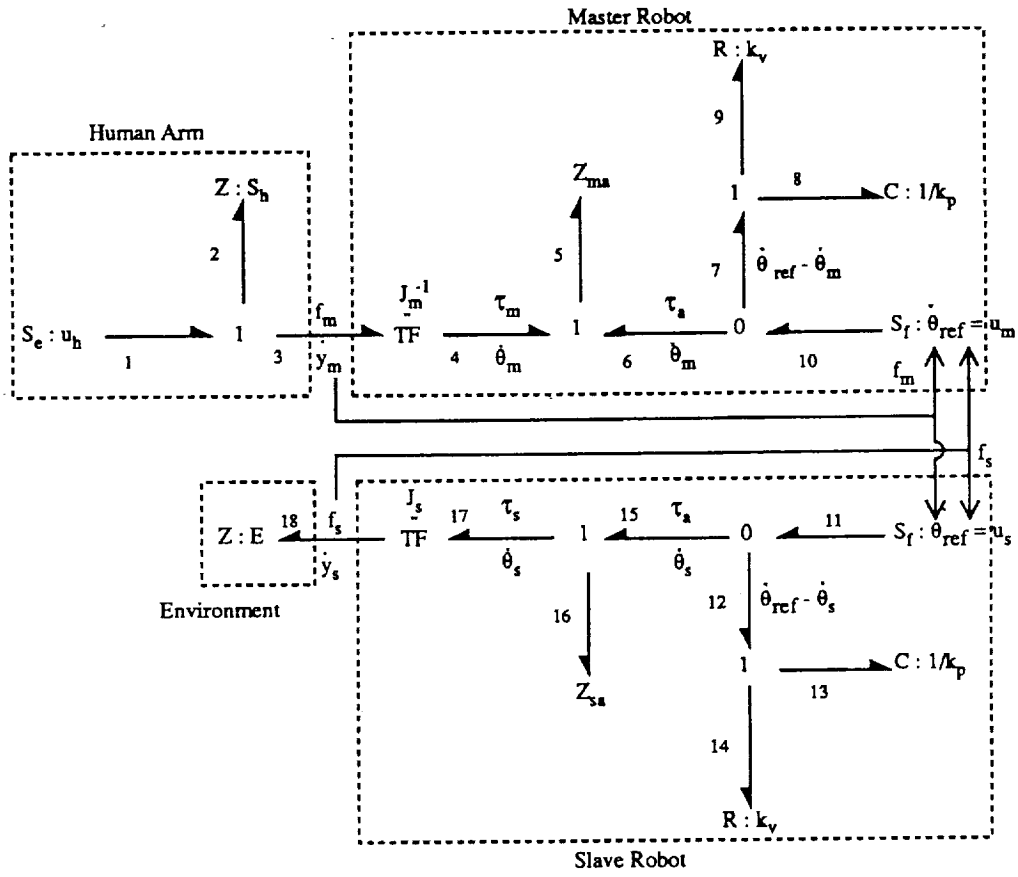

Figure 4.8: Bond Graph of the Telerobotic System (Controlled)

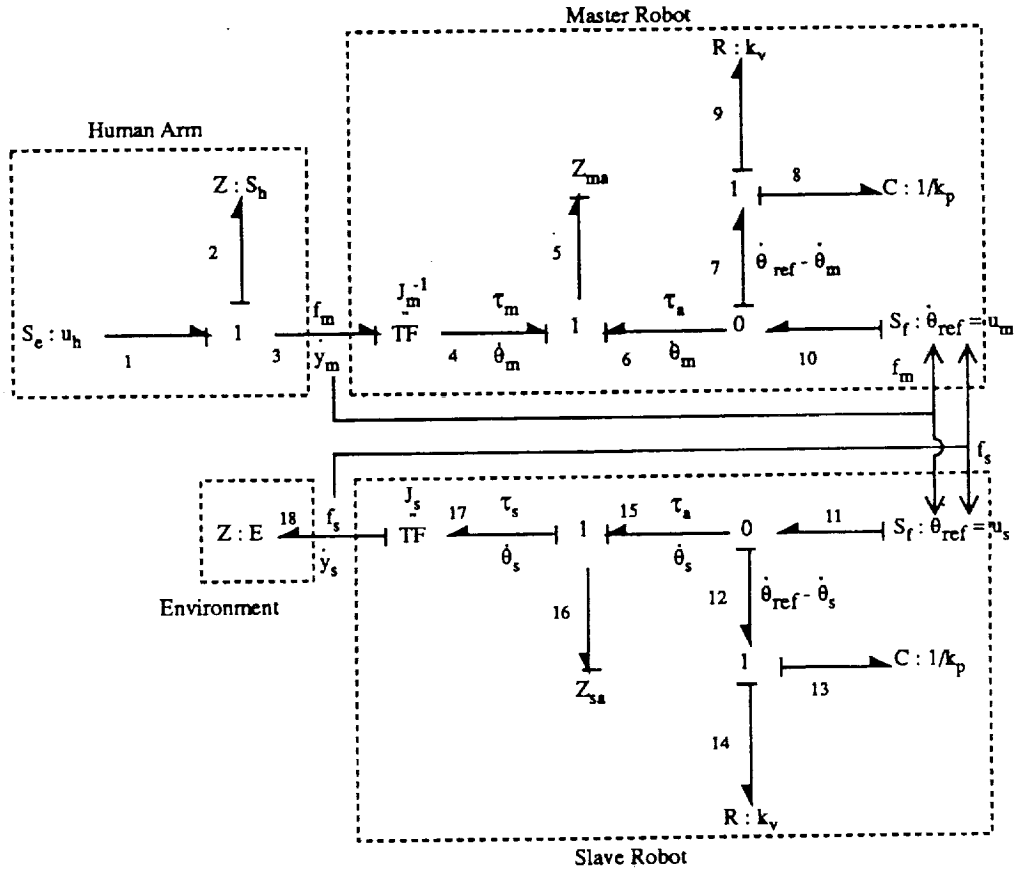

Figure 4.9: Causal Bond Graph of the Telerobotic System

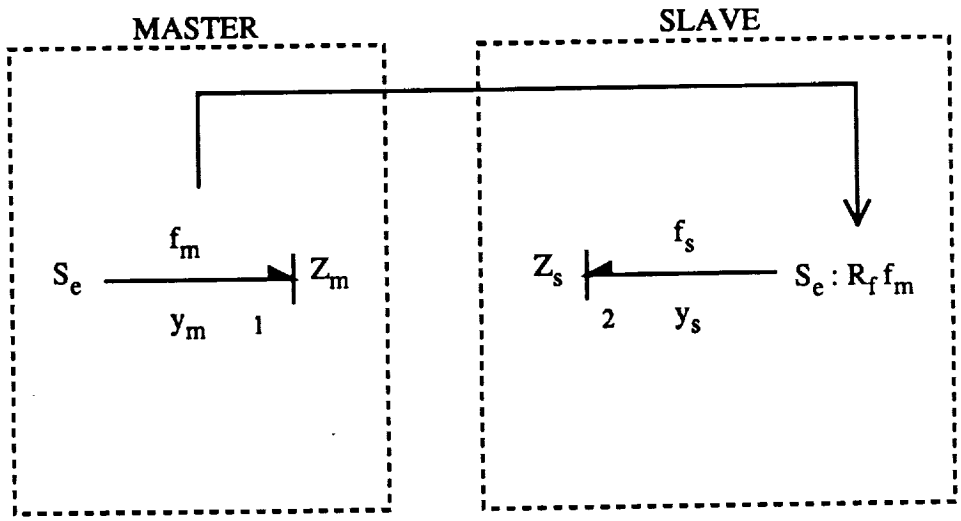

Figure 4.10: Bond Graph of 3 Performance Parameters

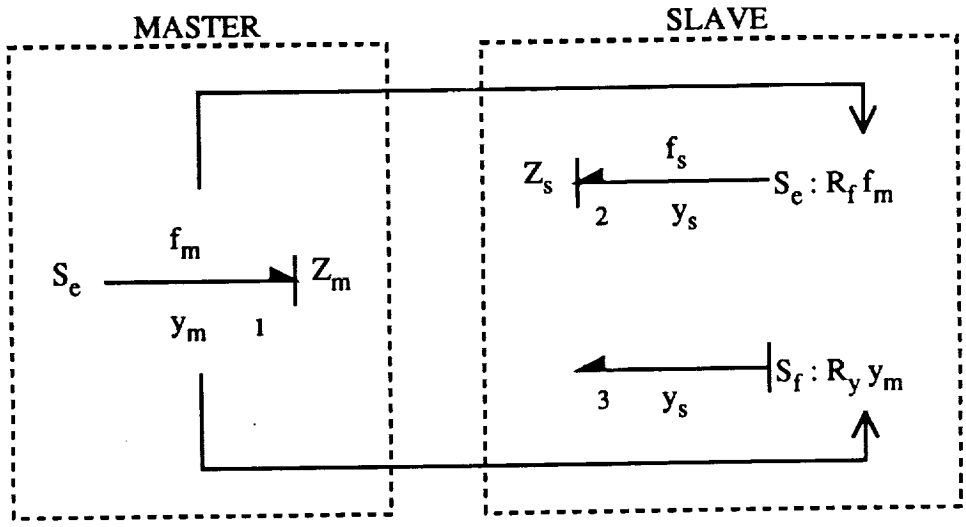

Figure 4.11: Bond Graph of 4 Performance Parameters

Chapter 5
EXPERIMENTAL VERIFICATION

5.1 Introduction

The theoretical predictions for performance and stability will be experimentally verified by implementing the bilateral impedance control architecture on a multi-degree-of-freedom telemanipulator. Experiments will be performed in four main areas.

First, static values will be determined for the system variables that govern the dynamic behavior of the robots, the human arm, and the environment. These values will be used in later experiments to design the H matrix.

Second, by tailoring the H matrix, the system performance characteristics will be arbitrarily specified. The performance parameters will be measured and compared with their desired values. The master robot impedance will be modulated to produce stiffness and damping. The position ratio will be varied in two degrees-of-freedom. The force ratio will be adjusted for interactions with a compliant environment. It will be shown that three performance parameters can be specified simultaneously.

Third, the frequency response of the performance parameters will be obtained to demonstrate robustness of the control architecture to modeling uncertainties. The frequency response will be calculated from an ARX dynamic model found through system identification.

Finally, the stability conditions will be verified by establishing lower bounds on the robot impedances for which the system remains stable. All of these experiments will be carried out on the NASA Laboratory Telerobotic Manipulator which is described below.

5.2 NASA Laboratory Telerobotic Manipulator

The NASA Laboratory Telerobotic Manipulator (LTM) was designed for ground-based research on the future application of telerobotic systems in space. The LTM is a bilateral, non-direct drive telemanipulator that has two pairs of master and slave arms. The robot arms are arranged in an anthropomorphic configuration as shown in Figure 5.1. Each arm has a shoulder, an elbow, and a wrist with common joint assemblies. All joints are capable of moving in both pitch and yaw. The wrist joint has an additional degree of freedom in roll. Altogether, each arm of the LTM has seven degrees of freedom.

The master and slave robots are kinematically identical. However, the slave robot has larger joint assemblies that can supply a greater output torque. The human operator

stands between the arms of the master robot. She grips a control handle attached to the end of the robot's wrist. The slave robot has a parallel-jaw end-effector for grasping remote objects. Both robots are mechanically counterbalanced to offset the force of gravity.

The pitch-yaw joint assembly consists of a differential traction drive mechanism powered by two DC servomotors. When the motors rotate in the same direction, the joint rotates in yaw. When the motors rotate in opposite directions, the joint rotates in pitch. Each motor is equipped with an antibacklash gear reducer, a permanent magnet brake, an optical encoder, a tachometer, and a torque sensor. Resolvers are mounted on both joint axes to measure absolute position (Herndon *et al.* 1988).

The LTM is controlled by multiple processors operating in parallel. Figure 5.2 is a schematic diagram of the computer hardware. A joint processor controls the acquistion of sensor data from each joint. The joint processors are imbedded in the robot arms, and they communicate with the main rack through fiber optics. The main rack contains three Motorola 68020 single-board computers on a VME bus. A link processor in the main rack receives information from the joint processors and passes it on to the arm processor. The arm processor performs the control algorithm calculations for each arm. It also sends commands to the pulse-width modulated (PWM) amplifiers that drive the motors. A communications processor handles the transfer of data between the master and slave racks. The two racks are connected by a high-speed fiber optic link. A system control processor on each rack coordinates the activities of the other processors. A Macintosh II personal computer provides a graphics-based interface with the master rack for system operation. This interface allows the system operator to set gains, change operating modes, and record experimental data while the system is running (Herndon *et al.* 1989).

The bilateral impedance control architecture was implemented on one arm pair of the LTM. The control software was written in the programming language "C" (Kernighan and Ritchie 1988). A six-component force-torque sensor manufactured by JR3, Inc. was mounted on the wrist of the master robot. An identical sensor was mounted to the end of the slave robot. These sensors measured forces and torques in the hand reference frame. The force data was transmitted to the control processors asynchronously via parallel communication.

5.3 Force Transformation

The H matrix for a multi-degree-of-freedom telemanipulator includes force transformation terms. These terms appear because the interaction forces f_m and f_s are measured in Cartesian space, while the robots are controlled in joint space.

The H matrix compensators filter the interaction forces in the hand reference frame. This facilitates the specification of impedance to suit the requirements of the task. Since the master robot may have a different orientation than the slave robot, the robot forces must be related to a common reference frame before they can be added. The transformation ${}^{b}_{h}T$ maps the filtered force from each robot into the base reference frame. The base frame is always fixed, and it is identical for both robots. The base frame forces are added in Cartesian space. To control the robots at the joint level, the combined force is mapped into joint space by J^T, which is the transpose of the robot Jacobian (Craig 1988). Thus, the H matrix for a manipulator with n degrees-of-freedom becomes

$$H = \begin{bmatrix} J_m^T \, {}^{b}_{h}T_m H_{11} & J_m^T \, {}^{b}_{h}T_s H_{12} \\ J_s^T \, {}^{b}_{h}T_m H_{21} & J_s^T \, {}^{b}_{h}T_s H_{22} \end{bmatrix} \tag{5.1}$$

where the elements of H are n x 6 matrices. The transformations J^T and ${}^{b}_{h}T$ are functions of the joint angles. The LTM transformations are derived from geometric parameters in Barker and McKinney (1989).

The flow of force signals through the various transformations is illustrated schematically in Figure 5.3. Note that only transformed base frame forces are passed between the robots. The transformations for each robot are calculated on the respective robot's arm processor. This eliminates the need to exchange joint angles between robots. The input command to the stabilizing control system is formed by adding the robot's initial position to the output of the H matrix. This insures that the position controller will return the robot to its original position in the absence of interaction forces. The bilateral impedance control algorithm runs at a loop rate of 200 Hz.

5.4 Stabilizing Control System

The robots are stabilized by closed-loop position controllers. The position controllers keep the robots stationary when there are no forces acting on them. In addition, the position controllers minimize small disturbances in the robot motion caused by joint friction and changing inertia.

Figure 5.4 is a block diagram of the stabilizing control system for a single joint. The reference input commands to the control system are generated by the H matrix. Each joint can move in both pitch and yaw. The pitch and yaw positions are measured by

resolvers mounted on both joint axes. The pitch error is obtained by subtracting the pitch position, P_m, from the pitch reference command, P_{ref}. Similarly, the yaw error is obtained by subtracting the yaw position, Y_m, from the yaw reference command, Y_{ref}. To drive the motors in the proper directions, it is necessary to decouple the pitch and yaw errors. The drive command to motor A is obtained by subtracting the pitch error from the yaw error, while the drive command to motor B is obtained by adding the pitch and yaw errors. This causes the motors to rotate in opposite directions for pitch commands, and in the same direction for yaw commands.

Next, the decoupled errors are filtered by two identical stabilizing compensators. The form of these compensators depends on the joint being controlled. The compensators are implemented in the computer algorithm by difference equations. The digital output of the compensators is changed into a corresponding analog voltage by the D/A converter. This voltage is sent to the PWM amplifers that supply current to the motors. The motor current is directly proportional to the amplifier input voltage. The combined torque of motors A and B drive the robot arm.

The closed-loop system consists of the robots, the stabilizing compensators, and the internal gains given in Figure 5.4. To simplify the equations governing the performance parameters, the force transformation terms in the H matrix will be included as a gain on the input to the stabilizing control system. This allows the transformations and the closed-loop system to be represented by a single gain. For the master robot, the overall closed-loop gain is represented by G_m. Similarly, G_s represents the overall closed-loop gain for the slave robot. The values of G_m and G_s will be determined in the next section.

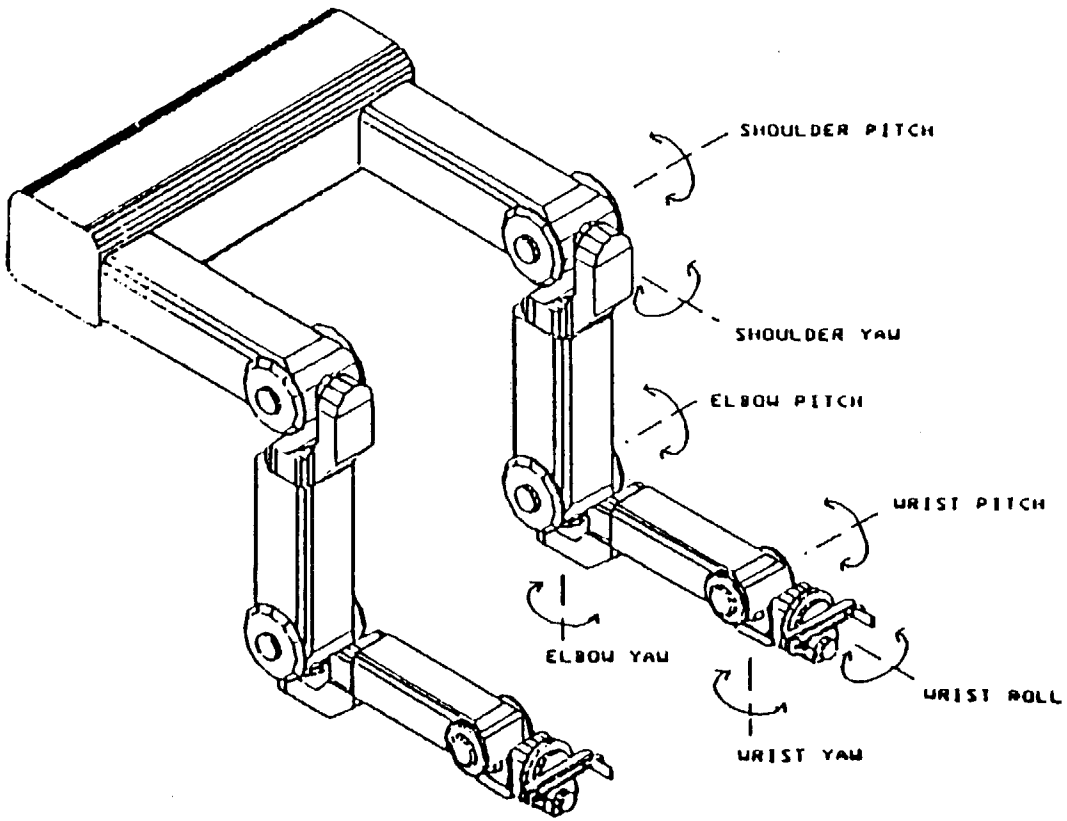

Figure 5.1: LTM Configuration (Slave Robot)

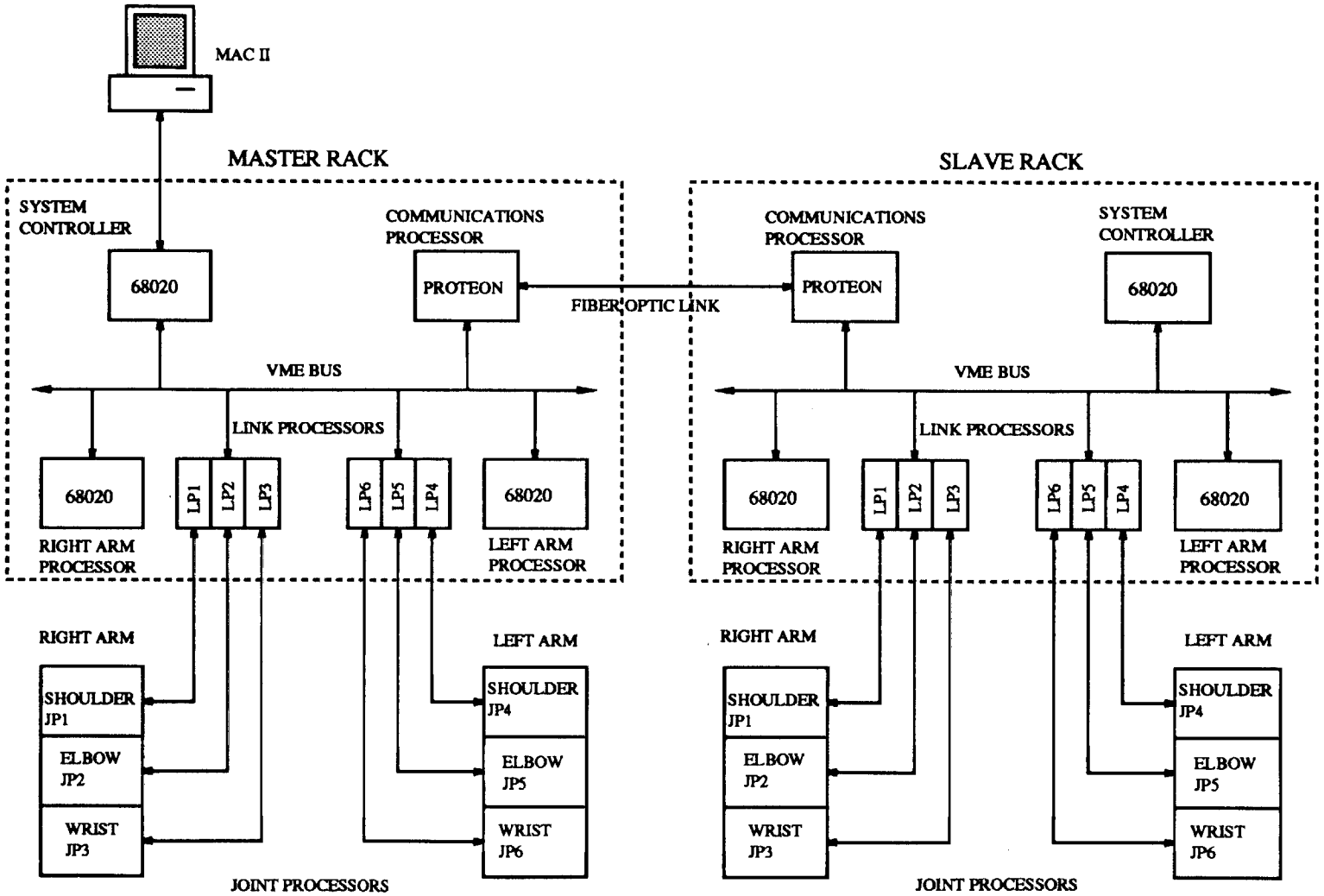

Figure 5.2: LTM Computer Hardware

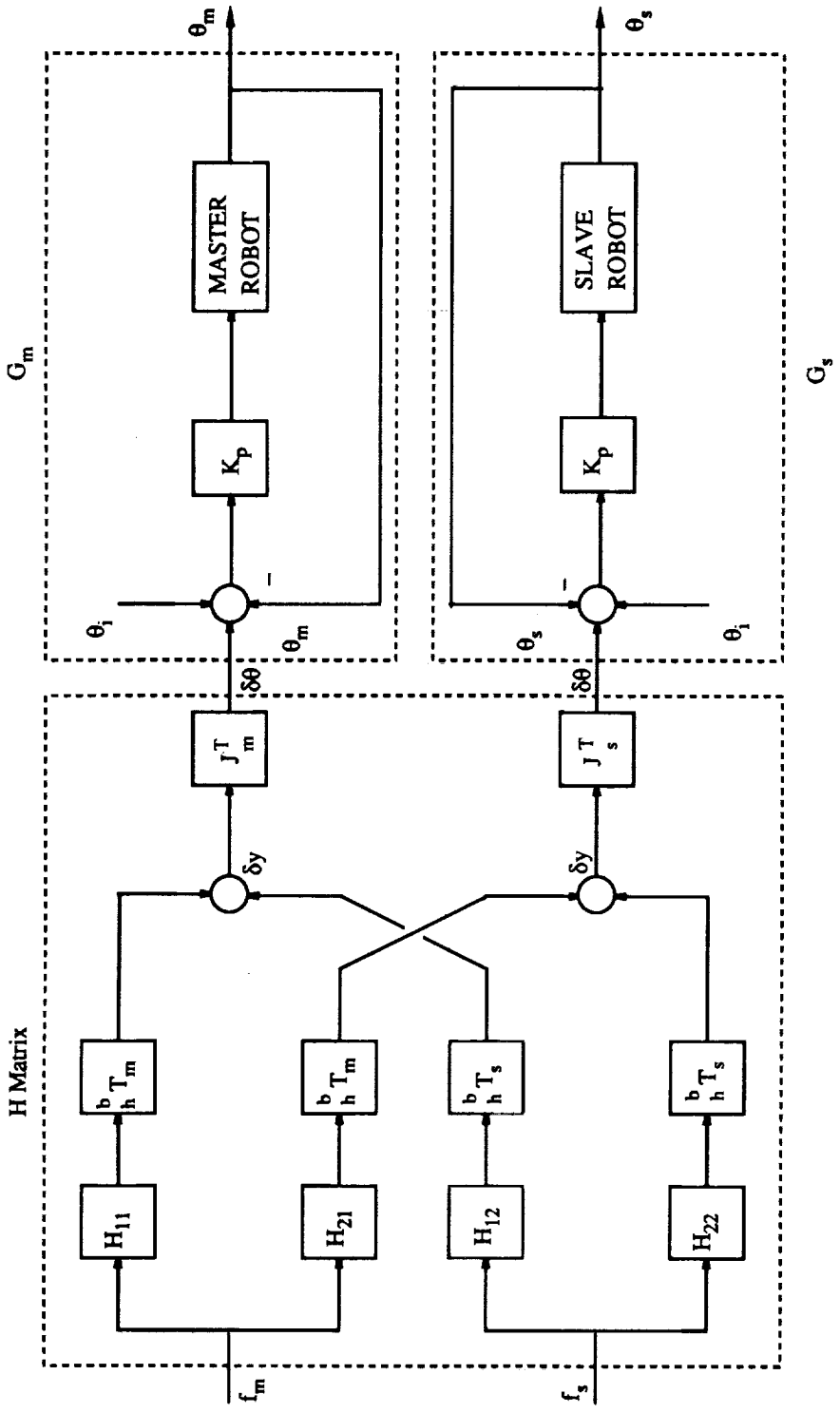

Figure 5.3: Force Transformation

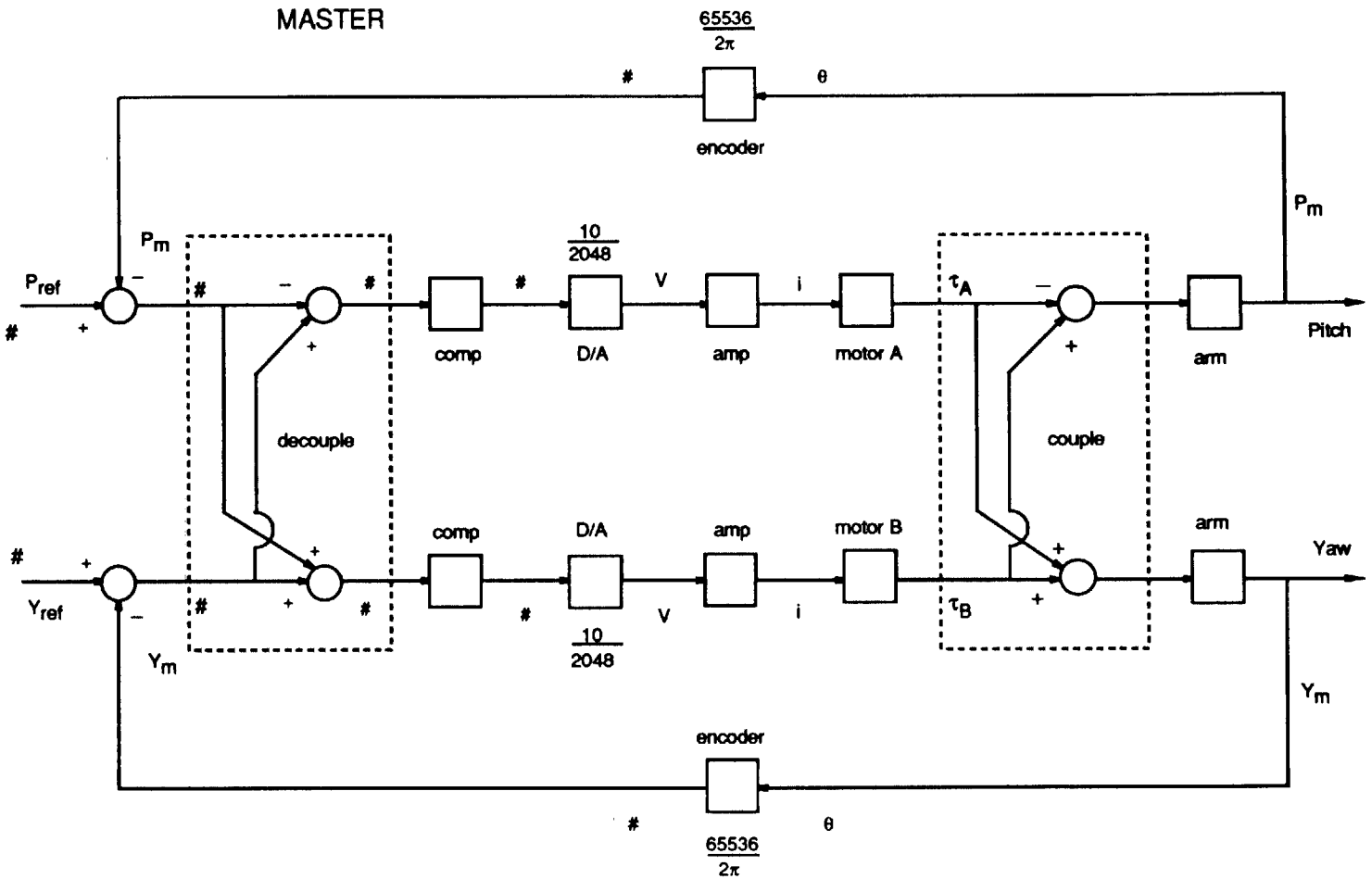

Figure 5.4: Stabilizing Control System

5.5 Determination of System Variables

The design of the H matrix to achieve desired performance characteristics depends on accurate knowledge of the system variables G_m, S_m, G_s, S_s, S_h, and E. The first four variables govern the dynamic behavior of the robots. These variables do not change as the telerobotic system performs different tasks. In contrast, the variables S_h and E are continually changing with the configuration of the human arm and the environment. In this section, static values for the system variables will be experimentally determined for later use. Static values can be used to design the H matrix as long as the robot motions are relatively slow .

For the master robot, the gain of the primary closed-loop system is G_m. The closed-loop system consists of the robot and the stabilizing controller. The input to the closed-loop system is the electronic command u_m that results from the operation of the H matrix on the robot forces

$$u_m = H_{11} f_m + H_{12} f_s \tag{5.2}$$

The output of the closed-loop system is the position of the master robot, y_m. The force exerted on the master robot by the human arm causes a position disturbance. The sensitivity of the master robot to the applied force is S_m. The sensitivity is mainly a function of the stiffness of the stabilizing control system, but the robot's friction and inertia are also significant contributors. The master robot's motion results from the action of the control system and the interaction between the robot and the human arm. The dynamic equation of the master robot is

$$y_m = G_m u_m + S_m f_m \tag{5.3}$$

Substituting equation 5.2 into equation 5.3 yields

$$y_m = G_m (H_{11} f_m + H_{12} f_s) + S_m f_m \tag{5.4}$$

Now suppose that all gains in the H matrix except H_{11} are zero. Then equation 5.4 becomes

$$y_m = (G_m H_{11} + S_m) f_m \tag{5.5}$$

The master impedance Z_m is the impedance that the telerobotic system presents to the human. It is defined as

$$Z_m = \frac{f_m}{y_m} \tag{5.6}$$

Using the definition of the master impedance, equation 5.5 can be written as

$$1/Z_m = G_m H_{11} + S_m \tag{5.7}$$

Equation 5.7 implies that there is a linear relationship between the inverse master impedance and the gain of H_{11}. Thus, if $1/Z_m$ is plotted as a function of H_{11}, the slope of the resulting curve will be G_m, and the Y-axis intercept will be S_m.

In the first experiment, the values of G_m and S_m were determined from measurements of the master impedance. All of the gains in the H matrix except H_{11} were set to zero. The gain of H_{11} was varied from 0 to 1.00 in increments of 0.10. An increasing vertical force was applied to the master robot so that its elbow executed a downward pitch motion. For each data set, the master force and position were recorded for 5 seconds. The master impedance was obtained by plotting the master force versus the master position. A typical plot is shown in Figure 5.5. The initial position of the master robot has been referenced to zero radians. The slope of this curve is Z_m. A least squares curve fit was used to calculate the slope for each data set, and the results are listed in Table 5.1.

The inverse master impedance is plotted as a function of H_{11} in Figure 5.6. A least squares curve fit was used to find the equation of the line that best represents the trend of the experimental data. The slope of this line is $G_m = 0.0117$ rad/lbf, and the Y-axis intercept is $S_m = 0.0033$ rad/lbf.

The motion of the slave robot results from the action of its control system and the interaction of the robot with the environment. The dynamic equation for the slave robot is

$$y_s = G_s u_s + S_s f_s \tag{5.8}$$

The gain of the primary closed-loop system is G_s. The input command to the closed-loop system is u_s. The H matrix filters the robot forces such that

$$u_s = H_{21} f_m + H_{22} f_s \tag{5.9}$$

Substituting equation 5.9 into equation 5.8 yields

$$y_s = G_s (H_{21} f_m + H_{22} f_s) + S_s f_s \tag{5.10}$$

Now suppose that all gains in the H matrix except H_{22} are zero. Then equation 5.10 becomes

$$y_s = (G_s H_{22} + S_s) f_s \tag{5.11}$$

The slave impedance Z_s is the impedance that the telerobotic system presents to the environment. It is defined as

$$Z_s = \frac{f_s}{y_s} \tag{5.12}$$

Using the definition of the slave impedance, equation 5.11 can be written as

$$1/Z_s = G_s H_{22} + S_s \tag{5.13}$$

Equation 5.13 implies that there is a linear relationship between the inverse slave impedance and the gain of H_{22}. Thus, if $1/Z_s$ is plotted as a function of H_{22}, the slope of the resulting curve will be G_s, and the Y-axis intercept will be S_s.

In the second experiment, the values of G_s and S_s were determined from measurements of the slave impedance. All of the gains in the H matrix except H_{22} were set to zero. The gain of H_{22} was varied from 0 to 0.60 in increments of 0.05. An increasing vertical force was applied to the slave robot so that its elbow executed an upward pitch motion. For each data set, the slave force and position were recorded for 5 seconds. The slave impedance was obtained by plotting the slave force versus the slave position. A typical plot is shown in Figure 5.7. The slope of this curve is Z_s. A least squares curve fit was used to calculate the slope for each data set, and the results are listed in Table 5.2.

It was found that Z_s could not be measured directly when the gain of H_{22} was small because there was a significant amount of backlash in the wrist joint. The wrist joint was locked to prevent rotation. However, when force was applied to the end of the robot, the wrist joint would move slightly before the locking mechanism engaged. As a result, the slave impedance was nonlinear in the region $H_{22} < 0.10$. This problem did not occur in the

master robot because its wrist joint was firmly locked.

The inverse slave impedance is plotted as a function of H_{22} in Figure 5.8. A least squares curve fit was used to find the equation of the line that best represents the trend of the experimental data. The slope of this line is $G_S = 0.0117$ rad/lbf, and the Y-axis intercept is $S_S = 0.0012$ rad/lbf.

The closed-loop gain of the master robot, G_m, is equal to the closed-loop gain of the slave robot, G_S. This is expected because the two robots are nearly identical, and they are stabilized by the same type of compensator. The measured slave sensitivity, S_S, is considerably lower than expected. The slave sensitivity should be approximately equal to the master sensitivity, S_m. However, the backlash of the wrist joint introduces flexibility into the slave robot. The force applied on the end of the robot causes deformation of the arm in addition to rotation of the elbow. Consequently, the sensitivity measured at the elbow is greatly reduced. To overcome the flexibility problem, an effective sensitivity was calculated for the slave robot when it was compressing a compliant environment. Before this could be done, it was necessary to determine the environmental impedance.

The environmental impedance can be obtained from the equation that governs the interaction force on the slave robot

$$f_S = f_{ext} - E\, y_S \tag{5.14}$$

If there are no external forces acting on the slave robot, the environment behaves like a passive impedance E such that

$$E = -\frac{f_S}{y_S} \qquad \text{when } f_{ext} = 0 \tag{5.15}$$

Thus, E can be determined by measuring the ratio between the slave force and position.

The magnitude of E was measured with the experimental setup shown in Figure 5.9. The environment was simulated by a spring scale that was attached at its base to a table. In this case, the environmental impedance can be approximated as a linear stiffness. For the third experiment, the H matrix had the following structure:

$$H = \begin{bmatrix} H_{11}=0 & H_{12}=0 \\ H_{21}=1 & H_{22}=0 \end{bmatrix}$$

Since H_{22} is zero, the slave robot has no electronically generated compliance to forces exerted on it by the environment. Therefore, all of the compliance in the system must result

from either the structural flexibility of the robot arm or the impedance of the environment. The combined stiffness of the robot arm and the environment is measured in the experiment. Thus, the value obtained for E is the effective impedance presented to the telerobotic system if the slave robot's structural flexibility is transferred to the environment.

The slave robot pushed down against the spring scale in response to an increasing vertical force exerted on the master robot. The end-point forces and elbow pitch positions of both robots were recorded for 5 seconds. Ten sets of data were acquired. For each data set, the slave force was plotted versus the slave position. A typical plot is shown in Figure 5.10. The slope of this curve is E, and it was calculated with a least-squares curve fit. The effective environmental impedance for each data set is listed in Table 5.3. The average value was E = 217.0 lbf/rad.

The calibrated stiffness of the spring scale was k = 22.9 lbf/in. When the elbow joint rotates through one radian, the end of the slave robot moves through an arc length equal to the distance from the elbow to the end effector. This distance is 34.5 inches. Therefore, for small displacements, the angular stiffness of the spring scale is

$$k = (22.9 \text{ lbf/in})\ (34.5 \text{ in/rad}) = 790.0 \text{ lbf/rad}$$

This is the actual environmental impedance. The effective environmental impedance is much lower because it includes the structural flexibility of the slave robot.

Once a value has been obtained for E, it is possible to calculate S_S. If the H matrix is designed so that $H_{21} = 1$ and $H_{22} = 0$, equation 5.10 becomes

$$y_S = G_S f_m + S_S f_S \tag{5.16}$$

Dividing both sides of the previous equation by f_S gives

$$\frac{y_S}{f_S} = G_S \frac{f_m}{f_S} + S_S \tag{5.17}$$

Making use of equation 5.15 and the definition of the force ratio yields

$$S_S = -\left(\frac{G_S}{R_f} + \frac{1}{E}\right) \tag{5.18}$$

Since G_S and E have already been determined, this equation can be used to calculate an effective value for S_S from measurements of the the force ratio. Using the data collected in

the third experiment, the force ratio was obtained by plotting the slave force versus the master force. A typical plot is shown in Figure 5.11. The slope was calculated with a least squares curve fit. The force ratio for each data set is listed in Table 5.4. The average value was $R_f = 1.48$. Substituting the average values given above for G_s, E, and R_f into equation 5.20, it was found that $S_s = 0.0033$ rad/lbf. This is the effective sensitivity of the slave robot. Note that it is equal to the measured sensitivity of the master robot. Both robots should have nearly the same sensitivity because they are almost identical.

From measurements of the slave impedance, it was previously determined that $S_s = 0.0012$ rad/lbf. The effective sensitivity is larger than the measured sensitivity because the flexibility of the slave robot has been transferred to the environment. The effective sensitivity is the sensitivity that the slave robot would have if it had a completely rigid structure. For this reason, the effective values for S_s and E will be used in the design of the H matrix.

Finally, the impedance of the human arm will be determined. The dynamic equation for the human arm is

$$f_m = u_h - S_h y_m \tag{5.19}$$

If the human is not actively controlling the tension of her muscles, there are no commands originating from the central nervous system. Therefore, $u_h = 0$ and the human arm behaves like a passive impedance S_h such that

$$S_h = -\frac{f_m}{y_m} \qquad \text{when } u_h = 0 \tag{5.20}$$

Thus, S_h can be determined by measuring the ratio between the master force and position. In general, S_h is a nonlinear function of the human arm's configuration. Therefore, the value obtained by this method is only valid for small deviations from the measurement configuration.

To determine the magnitude of S_h, a virtual force was generated in the computer. The virtual force simulated a steadily increasing external force acting on the slave robot's force sensor. Force reflection from the slave robot caused the master robot to push up against the human arm. To maximize its sensitivity, the human arm was kept as rigid as possible with the forearm nearly horizontal. The end-point force and elbow pitch position of the master robot were recorded for 5 seconds. Ten sets of data were acquired.

The H matrix had the following structure:

$$H = \begin{bmatrix} H_{11}=0 & H_{12}=1 \\ H_{21}=0 & H_{22}=0 \end{bmatrix}$$

Since H_{11} is zero, there is no electronically generated compliance in the master robot. Therefore, all the compliance on the master side of the telerobotic system must result from the sensitivity of the human arm. The master robot is driven by reflection of the virtual force from the slave robot. The force reflection is provided by H_{12}.

For each data set, the master force was plotted as a function of the master position. A typical plot is shown in Figure 5.12. The slope of this curve is the human arm sensitivity, S_h. The slope was calculated with a least-squares curve fit. The sensitivity for each data set is listed in Table 5.5. The average value was S_h = 115.5 lbf/rad.

A general method for determining the static values of system variables has been described in this section. First, each variable is expressed as a simple relationship between force and position. Next, a known force input is applied to the telerobotic system, and the resulting position output is measured. Finally, the static value is calculated by plotting the force and position variables on the same graph. With this method, the gains applied within the computer by the force sensor, the position encoders, and the coordinate frame transformations are included implicitly. The H matrix can then be designed without concern for units.

Table 5.1
Measured Values of Z_m

Data Set	H_{11}	Z_m *(lbf/rad)*
1	0	297.6
2	0.10	219.8
3	0.20	180.6
4	0.30	151.5
5	0.40	125.8
6	0.50	111.2
7	0.60	98.1
8	0.70	86.1
9	0.80	79.1
10	0.90	71.7
11	1.00	66.8

Table 5.2
Measured Values of Z_S

Data Set	H_{22}	Z_S *(lbf/rad)*
1	0	---
2	0.05	---
3	0.10	426.1
4	0.15	342.6
5	0.20	276.9
6	0.25	238.8
7	0.30	212.3
8	0.35	187.7
9	0.40	169.5
10	0.45	154.0
11	0.50	142.1
12	0.55	130.4
13	0.60	121.6

Table 5.3
Measured Values of E

Data Set	*E (lbf/rad)*	*Deviation*
1	218.0	1.0
2	212.8	-4.2
3	217.9	0.9
4	218.3	1.3
5	216.8	-0.2
6	217.0	0.0
7	213.0	-4.0
8	216.9	-0.1
9	219.1	2.1
10	220.3	3.3
mean =	217.0	*std. dev.* = 2.3

Table 5.4
Measured Values of R_f

Data Set	*R_f*		*Deviation*
1	1.52		0.04
2	1.46		-0.02
3	1.48		0.00
4	1.46		-0.02
5	1.51		0.03
6	1.50		0.02
7	1.45		-0.03
8	1.48		0.00
9	1.47		-0.01
10	1.46		-0.02
mean =	1.48	*std. dev.* =	0.02

Table 5.5
Measured Values of S_h

Data Set	*S_h (lbf/rad)*	*Deviation*
1	119.2	3.7
2	116.2	0.7
3	106.7	-8.8
4	115.8	0.3
5	114.5	-1.0
6	119.1	3.6
7	123.0	7.5
8	113.2	-2.3
9	115.6	0.1
10	111.3	-4.2
mean =	115.5	*std. dev. =* 4.3

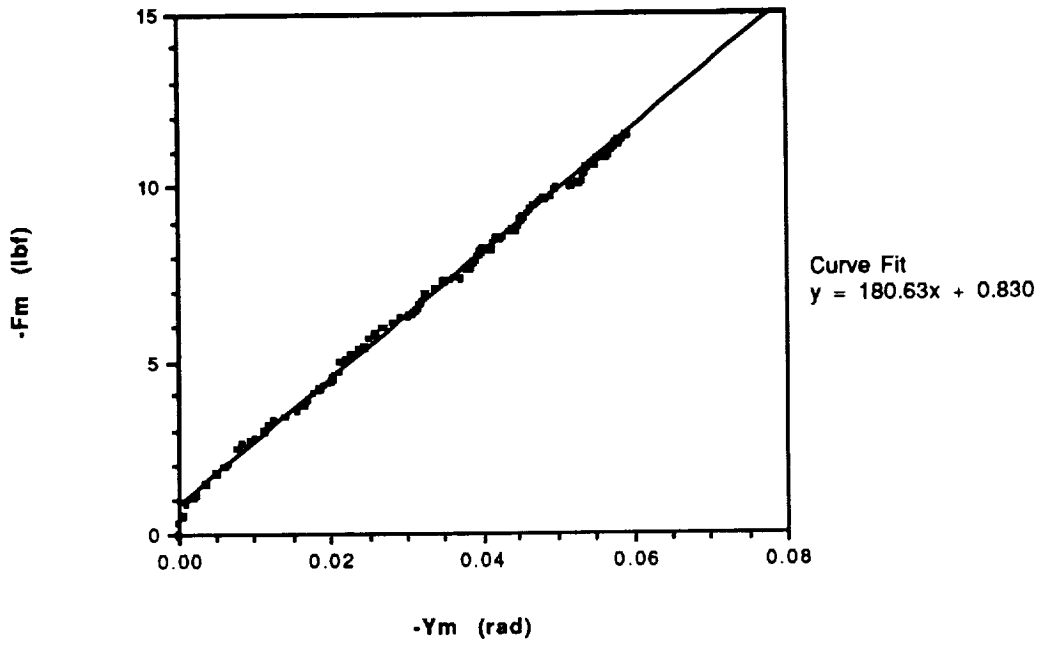

Figure 5.5: Master Impedance;
$H_{11} = 0.20$

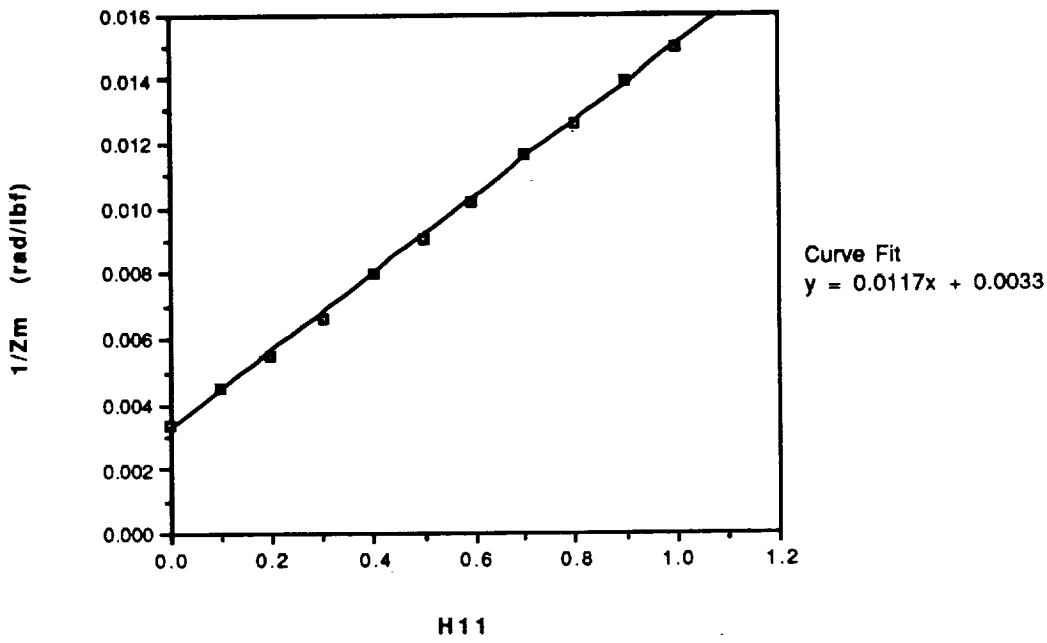

Figure 5.6: $1/Z_m$ vs. H_{11}

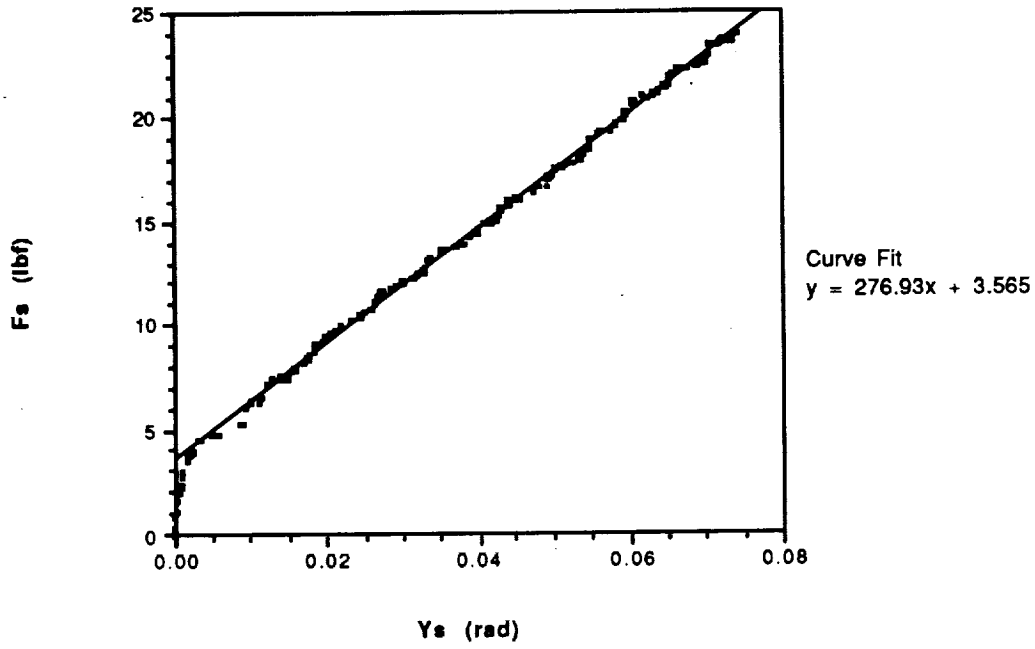

Figure 5.7: Slave Impedance;
$H_{22} = 0.20$

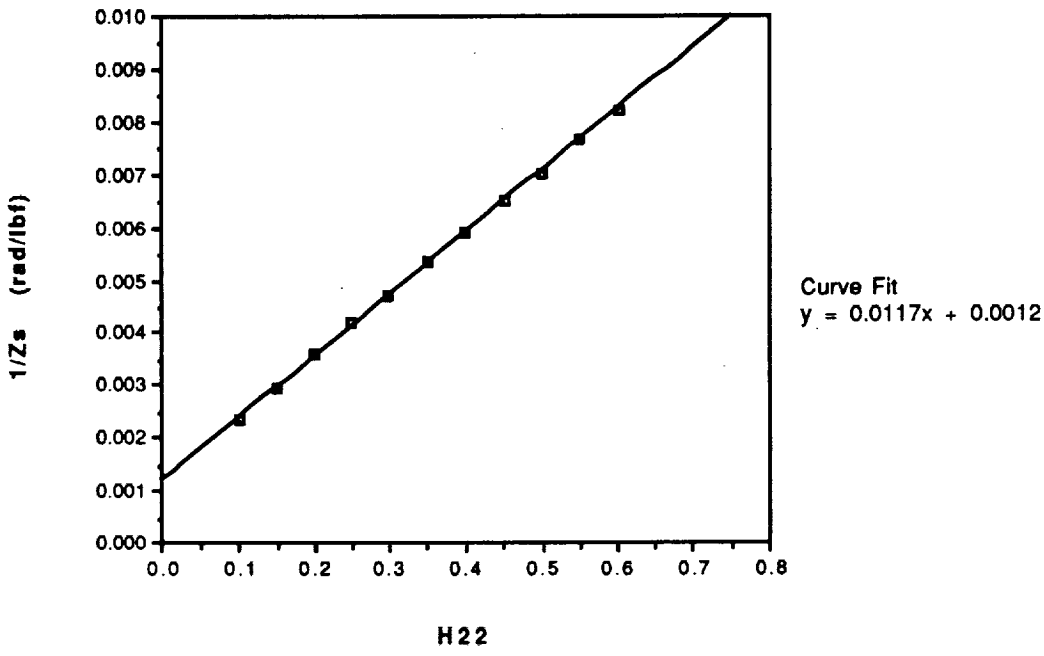

Figure 5.8: $1/Z_s$ vs. H_{22}

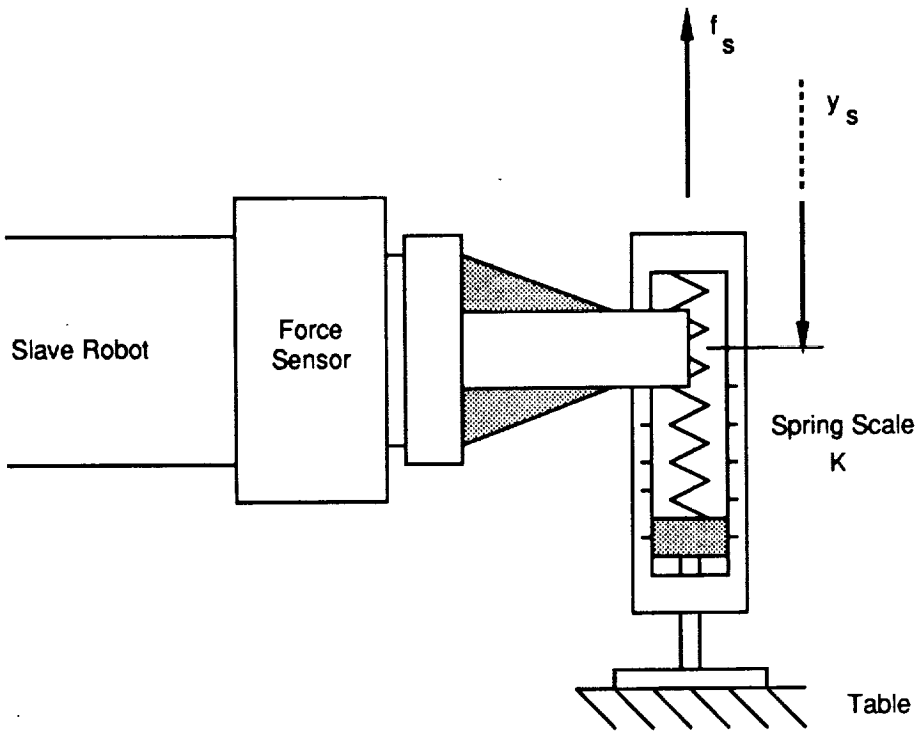

Figure 5.9: Experimental Setup for Determination of E

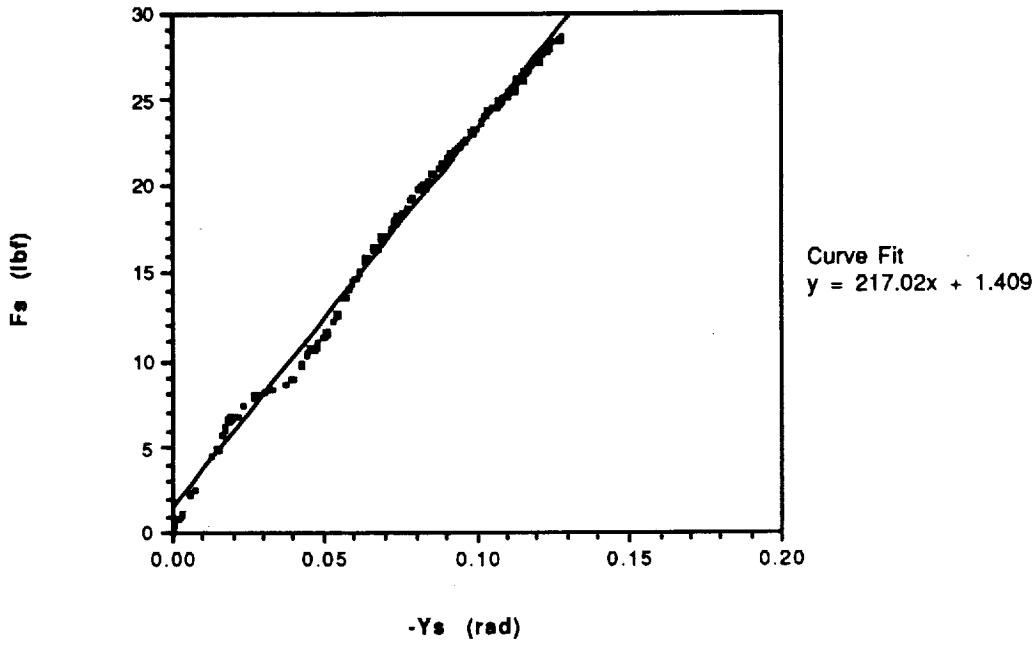

Figure 5.10: Determination of E;
Slave Force vs. Slave Position

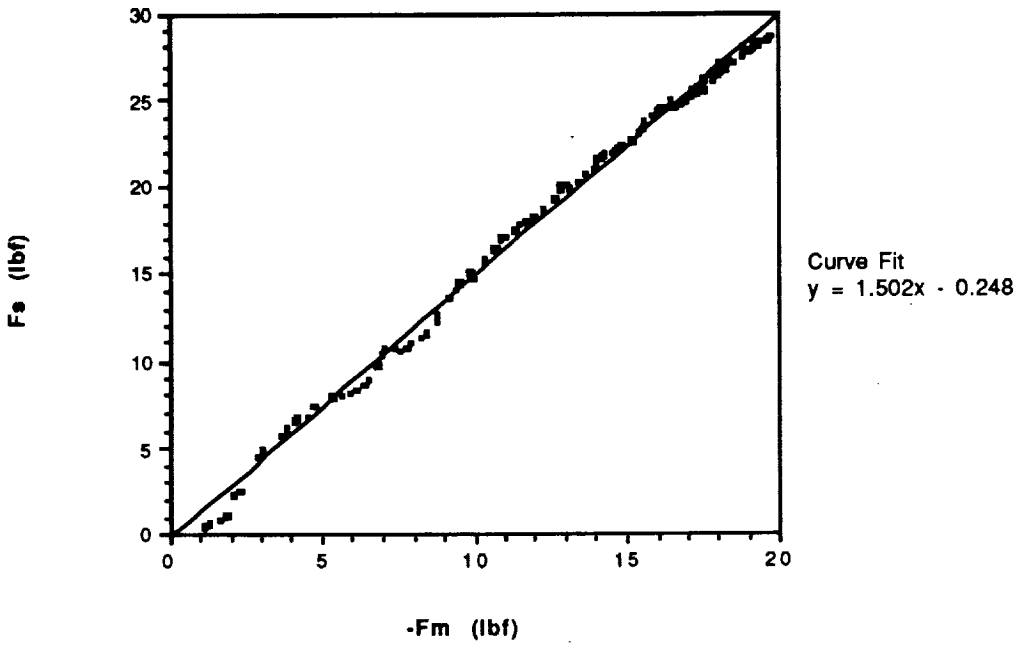

Figure 5.11: Determination of R_f ;
Slave Force vs. Master Force

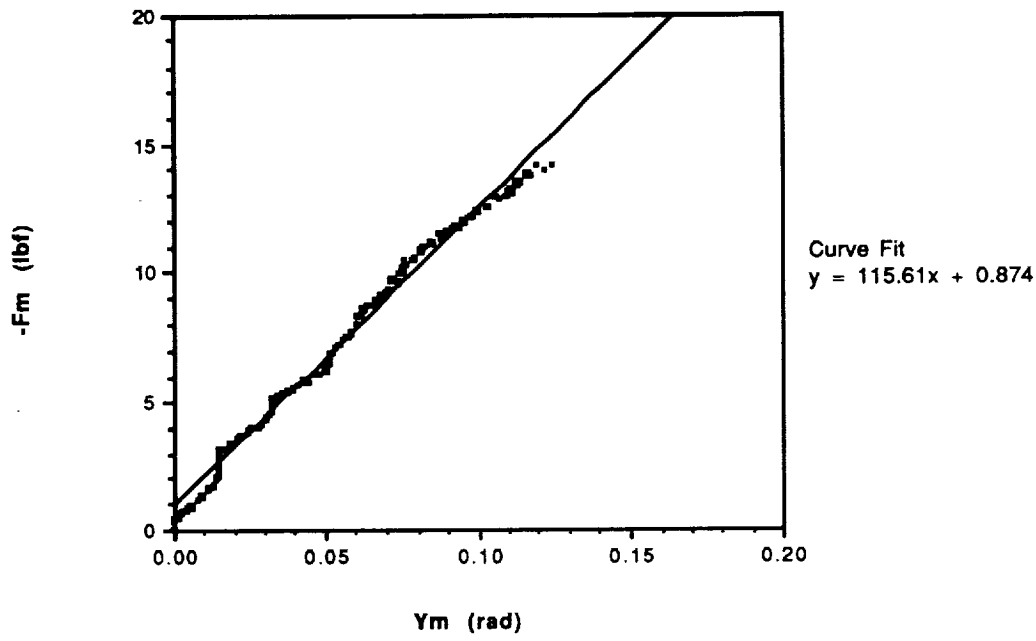

Figure 5.12: Determination of S_h;
Master Force vs. Master Position

5.6 Performance Parameters

Now that static values have been found for the system variables, the H matrix can be designed to specify desired performance characteristics. To illustrate their relationship to the H matrix more clearly, the performance parameters will be specified one at a time. Several values will be selected for each parameter, and the resulting performance of the telerobotic system will be measured. By comparing the actual performance to the desired performance, the validity of the theoretical performance equations will be confirmed. After the parameters have been specified individually, it will be demonstrated that three performance parameters can be specified simultaneously. The robot impedances, the position ratio, and the force ratio will be discussed.

5.6.1 Impedance

The performance parameter that relates force and position is known as impedance. An impedance may be defined at each end of the telerobotic system. For a single degree-of-freedom, the robot impedances are defined as

$$Z_m = \frac{f_m}{y_m} \tag{5.21}$$

$$Z_s = \frac{f_s}{y_s} \tag{5.22}$$

The master impedance Z_m is the impedance that the telerobotic system presents to the human. It is desirable to specify Z_m to reduce fatigue of the human operator. Z_m depends not only on the internal dynamics of the telerobotic system, but also on the impedance of the environment. The master impedance can be expressed in terms of system variables as

$$Z_m = \frac{1 + P_{22}E}{P_{11} + \Delta PE} \tag{5.23}$$

The slave impedance Z_s is the impedance that the telerobotic system presents to the environment. It is desirable to specify Z_s to insure system stability, and to suit the requirements of the task. Z_s depends on the internal dynamics of the telerobotic system and the impedance of the human arm. The slave impedance can be expressed in terms of system variables as

$$Z_s = \frac{1 + P_{11}S_h}{P_{22} + \Delta P S_h} \tag{5.24}$$

When there is no force reflection from the environment, the gain of H_{12} is zero. Therefore, $P_{12} = 0$ and $\Delta P = P_{11}P_{22}$. Equation 5.23 for the master impedance can then be simplified to

$$Z_m = \frac{1}{P_{11}} = \frac{1}{G_m H_{11} + S_m} \tag{5.25}$$

Similarly, when there is no force reflection, equation 5.24 for the slave impedance becomes

$$Z_s = \frac{1}{P_{22}} = \frac{1}{G_s H_{22} + S_s} \tag{5.26}$$

For this special case, the robot impedances are determined by a single element in the H matrix.

The purpose of the first experiment was to demonstrate that the magnitude of the impedance can be arbitrarily specified. It was not possible to measure the impedances of both robots at the same time, so only the master impedance was assigned a specific value. The gain of H_{11} necessary to achieve any desired master impedance Z_m is given by

$$H_{11} = \frac{1/Z_m - S_m}{G_m} \tag{5.27}$$

Equation 5.27 can be used to design the H matrix. The static values of the system variables have been experimentally determined. It was found that $G_m = 0.0117$ rad/lbf and $S_m = 0.0033$ rad/lbf for small elbow pitch motions. The master impedance was chosen to be $Z_m = 100$ lbf/rad. The H matrix had the following structure:

$$H = \begin{bmatrix} H_{11}=0.57 & H_{12}=0 \\ H_{21}=0 & H_{22}=0 \end{bmatrix}$$

The magnitude of H_{11} was calculated from equation 5.27 using the values given above for the system variables. An increasing vertical force was exerted on the end of the master robot. The end-point force and the elbow pitch position of the robot were recorded for 5 seconds.

Figure 5.13 is a plot of master force versus master position. The slope of this curve is Z_m. It was calculated with a least-squares curve fit. The measured impedance was Z_m = 101.2 lbf/rad. The experimental result agrees well with the theoretical prediction.

In addition to specifying the magnitude of the impedance, it is possible to shape its frequency response. This is done by choosing an appropriate structure for the compensators in the H matrix. If a constant gain is used, the robot's position is directly proportional to the applied force, and the impedance can be modeled as a spring stiffness. An impedance of this type was illustrated in the previous experiment. It causes the robot to return to its initial position after force is removed. However, the human must always work against the restoring force of the spring.

If a pure integrator is used, the H matrix relates force and position such that

$$\{y\} = \frac{[H]}{s}\{f\} \tag{5.28}$$

where s is the Laplace operator. In the time domain, this equation can be rewritten as

$$\{f\} = [C]\{\dot{y}\} \tag{5.29}$$

where the damping matrix $[C] = [H]^{-1}$. Thus, for an integrator, the force is directly proportional to velocity, and the impedance can be modeled as a viscous damper. After force is removed, the robot will remain in its last position. Since there are no restoring forces acting on the human arm, a damping impedance is the most natural mode of motion for teleoperation.

The purpose of the second experiment was to demonstrate a damping impedance for the master robot. The H matrix had the following structure:

$$H = \begin{bmatrix} H_{11}=1/s & H_{12}=0 \\ H_{21}=0 & H_{22}=0 \end{bmatrix}$$

The compensator H_{11} integrates the master force. The integration was implemented in the computer algorithm by difference equation of the form

$$y_{n+1} = y_n + H f_m \tag{5.30}$$

where H is the gain of the compensator, f_m is the force input, y_n is the position output at step n, and y_{n+1} is the position output at step n+1.

The elbow of the master robot was moved at a constant yaw velocity. The robot force and position were recorded for 5 seconds. Figure 5.14 is a plot of the master force versus master position. There is an initial transient where the force builds up enough to overcome the robot's inertia. Then the curve is fairly flat, indicating that a constant damping force is acting on the robot.

By tailoring the structure of the compensators in the H matrix, it is possible to modulate the robot impedances. It was shown that the master robot exhibits a stiffness impedance when the H matrix elements have constant gain. When the force input is integrated, the master robot exhibits a damping impedance. A combination of stiffness and damping could be attained by using a first-order filter in the H matrix. A second-order filter would add an inertial impedance where the interaction force is proportional to the robot's acceleration. It will be demonstrated in a later section that the robot impedance can be arbitrarily specified in conjunction with other performance parameters.

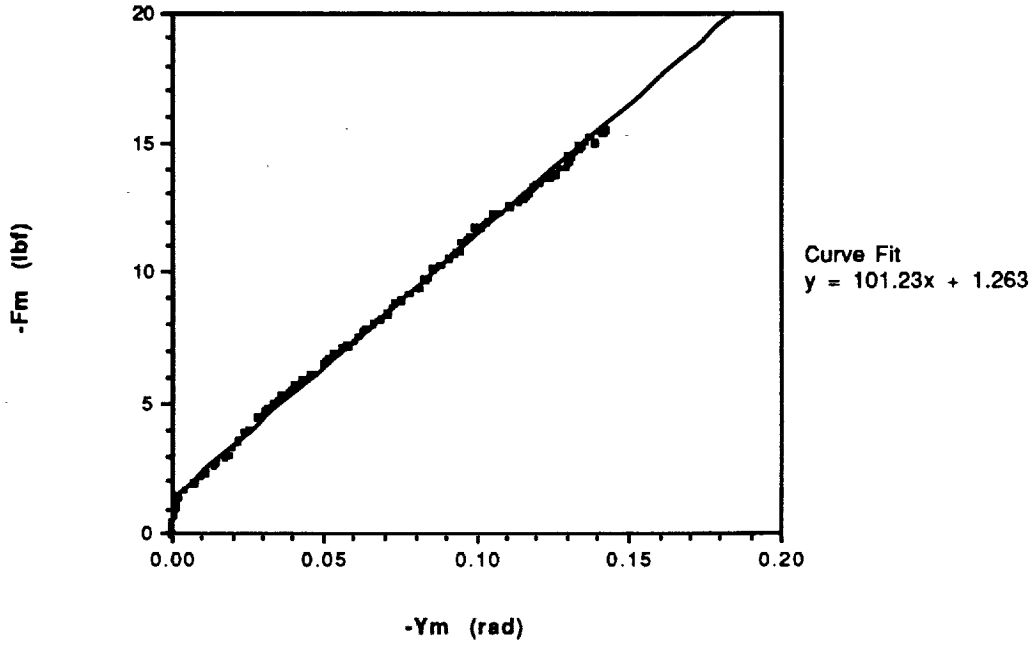

Figure 5.13: Master Force vs. Master Position;
Stiffness Impedance (Z_m = 100 lbf/rad)

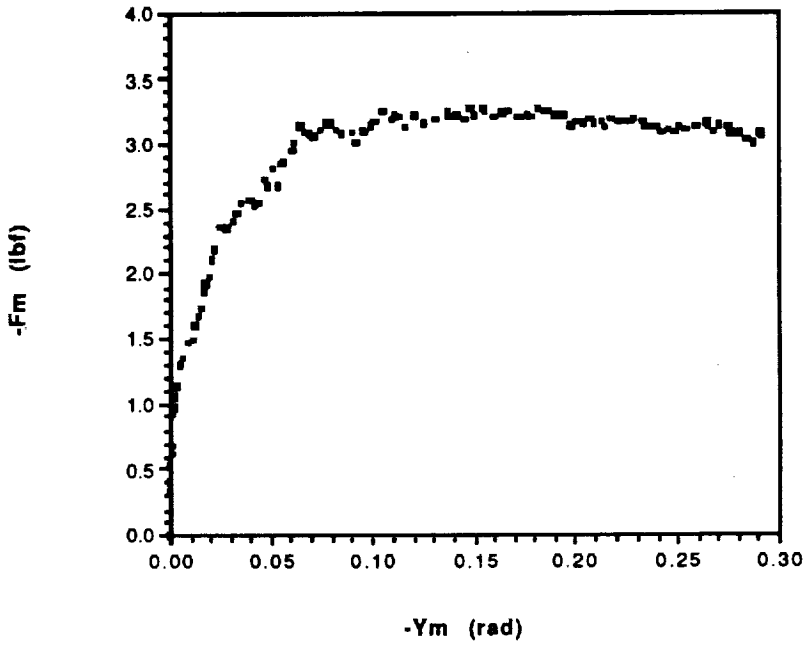

Figure 5.14: Master Force vs. Master Position;
Damping Impedance

5.6.2 Position Ratio

The performance parameter that relates the positions of the master and slave robots is known as the position ratio. For a single degree-of-freedom, it is defined as

$$R_y = \frac{y_s}{y_m} \tag{5.31}$$

Often it is desirable to specify a non-unity value for the position ratio so that the two robots move in the same direction, but have different amplitudes of motion. This enables the slave robot to perform small, precise motions in response to large, coarse motions of the master robot. The position ratio can be expressed in terms of system variables as

$$R_y = \frac{P_{21}}{P_{11} + \Delta PE} \tag{5.32}$$

When the slave robot is moving freely through space, there are no forces exerted on it by the environment. In this case, E = 0 and the position ratio becomes

$$R_y = \frac{P_{21}}{P_{11}} = \frac{G_s H_{21}}{G_m H_{11} + S_m} \tag{5.33}$$

Thus, for unconstrained motion, the position ratio depends on the relationship between two elements in the H matrix. The compensator H_{11} filters the master force, and its output is used to drive the master robot. H_{11} determines the motion of the master robot by controlling its impedance. The compensator H_{21} also filters the master force, and its output is used to drive the slave robot. H_{21} couples the motion of the slave robot to that of the master robot. The position ratio can be arbitrarily specified by selecting the relative magnitudes of H_{11} and H_{21}.

Now suppose that both compensators in the first column of the H matrix integrate the master robot force. This results in a damping impedance for the master robot. A damping impedance allows the human to move the robot to any position in space without a restoring force trying to return the robot to its initial position. When integrators are substituted into equation 5.33 for H_{11} and H_{21}, the position ratio becomes

$$R_y = \frac{G_s(H_{21}/s)}{G_m(H_{11}/s) + S_m} \tag{5.34}$$

where s is the Laplace operator. If the gains of G_m and G_s are approximately the same magnitude, equation 5.34 can be written as

$$R_y = \frac{H_{21}}{(S_m/G_m)s + H_{11}} \tag{5.35}$$

The sensitivity S_m is generally much smaller than the closed-loop gain G_m. Therefore, when the cyclic frequency of robot motion is small, equation 5.35 can be approximated as

$$R_y \approx \frac{H_{21}}{H_{11}} \tag{5.36}$$

This simple relationship will be used to design the H matrix in the next three experiments.

For the first experiment, the ratio of slave position to master position was specified to be R_y = 1:1. In this case, the slave robot should track the master robot exactly. The H matrix was designed to have the following structure:

$$H = \begin{bmatrix} H_{11}=1/s & H_{12}=0 \\ H_{21}=1/s & H_{22}=0 \end{bmatrix}$$

The compensators in the first column of the H matrix integrate the master force. The integration was implemented in the computer algorithm by a difference equation.

The elbow of the master robot was moved through a series of pitch and yaw motions. The motion of the slave robot was unconstrained. The joint angles of both robots were recorded over a 30-second period. Figure 5.15 is a plot of robot pitch position versus time. P_m is the pitch position of the master robot, and P_s is the pitch position of the slave robot. The robots had different initial positions. The initial position of each robot was referenced to zero radians so that their trajectories could be compared. Figure 5.16 is a plot of robot yaw position versus time. Y_m is the yaw position of the master robot, and Y_s is the yaw position of the slave robot. It can be seen that the slave robot tracks the master robot in both degrees-of-freedom.

The magnitude of the position ratio can be determined by plotting the slave position versus the master position. The slope of the resulting curve is the position ratio. Slave pitch position is plotted versus master pitch position in Figure 5.17. A least-squares curve fit yields an experimental value of R_y = 0.96 for elbow pitch. Figure 5.18 is a plot of slave yaw position versus master yaw position. The experimentally determined position ratio for elbow yaw is R_y = 1.01.

For the second experiment, the position ratio was specified to be R_y = 2:1. In this case, the slave robot should move twice as much as the master robot. The H matrix had the following structure:

$$H = \begin{bmatrix} H_{11}=1/s & H_{12}=0 \\ H_{21}=2/s & H_{22}=0 \end{bmatrix}$$

Figure 5.19 is a plot of robot pitch position versus time, while Figure 5.20 is a plot of robot yaw position versus time. Notice that for both degrees-of-freedom, the slave robot moves in phase with the master robot. However, the change in position of the slave robot is twice as large as the change in position of the master robot. Slave position is plotted versus master position in Figures 5.21 and 5.22. The experimentally determined position ratios are R_y = 2.00 for elbow pitch, and R_y = 2.01 for elbow yaw.

For the third experiment, the position ratio was specified to be R_y = 1:3. In this case, the slave robot should move a third as less as the master robot. The H matrix had the following structure:

$$H = \begin{bmatrix} H_{11}=1.5/s & H_{12}=0 \\ H_{21}=0.5/s & H_{22}=0 \end{bmatrix}$$

The pitch and yaw positions of the robots are plotted versus time in Figures 5.23 and 5.24. The slave robot moves in phase with the master robot for both degrees-of-freedom. Slave position is plotted versus master position in Figures 5.25 and 5.26. The measured position ratios are R_y = 0.30 for elbow pitch, and R_y = 0.31 for elbow yaw. The measured position ratios are slightly lower than predicted. This is probably due to small errors being amplified as the difference in robot positions increases.

Three position ratios have now been demonstrated: R_y = 1:1, R_y = 2:1, and R_y = 1:3. The position ratios were arbitrarily specified by selecting the relative magnitudes of the compensators in the first column of the H matrix. The slave robot tracks the master robot in two degrees-of-freedom. The measured position ratios agree well with theoretical predictions. To simplify the experiments, only the special case of unconstrained motion was investigated here. This restriction allowed only one performance parameter, the position ratio, to be specified at a time. The general case where three performance parameters are specified simultaneously will be demonstrated in a later section.

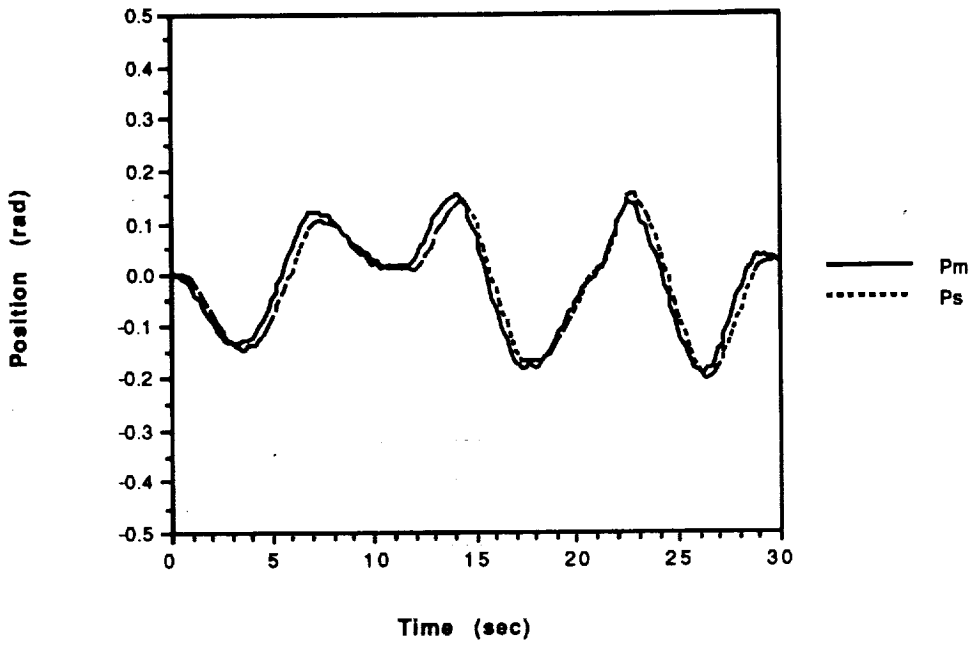

Figure 5.15: Position vs. Time
Elbow Pitch; R_y = 1:1

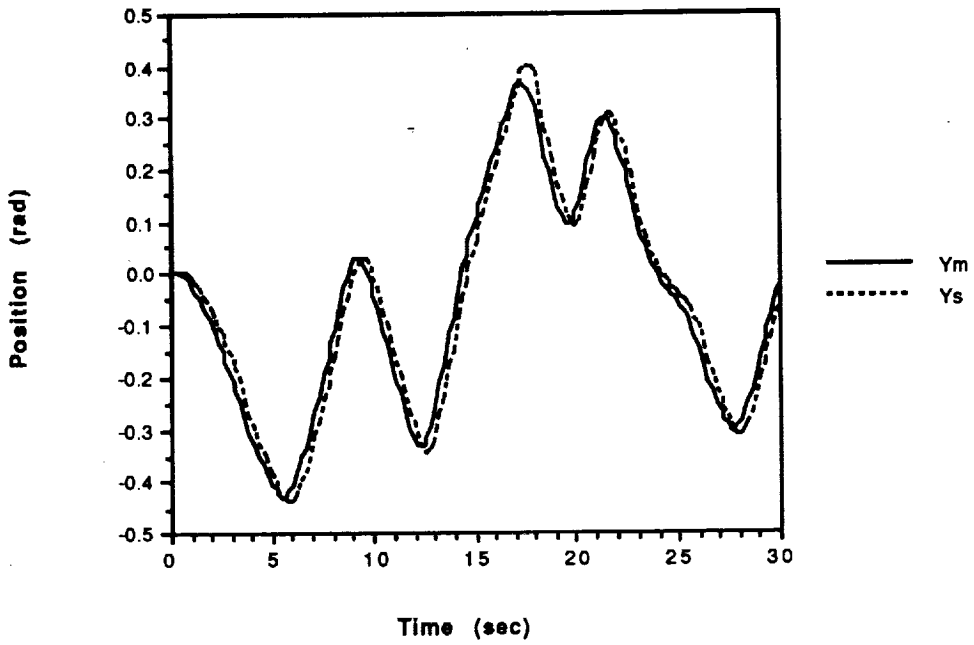

Figure 5.16: Position vs. Time
Elbow Yaw; R_y = 1:1

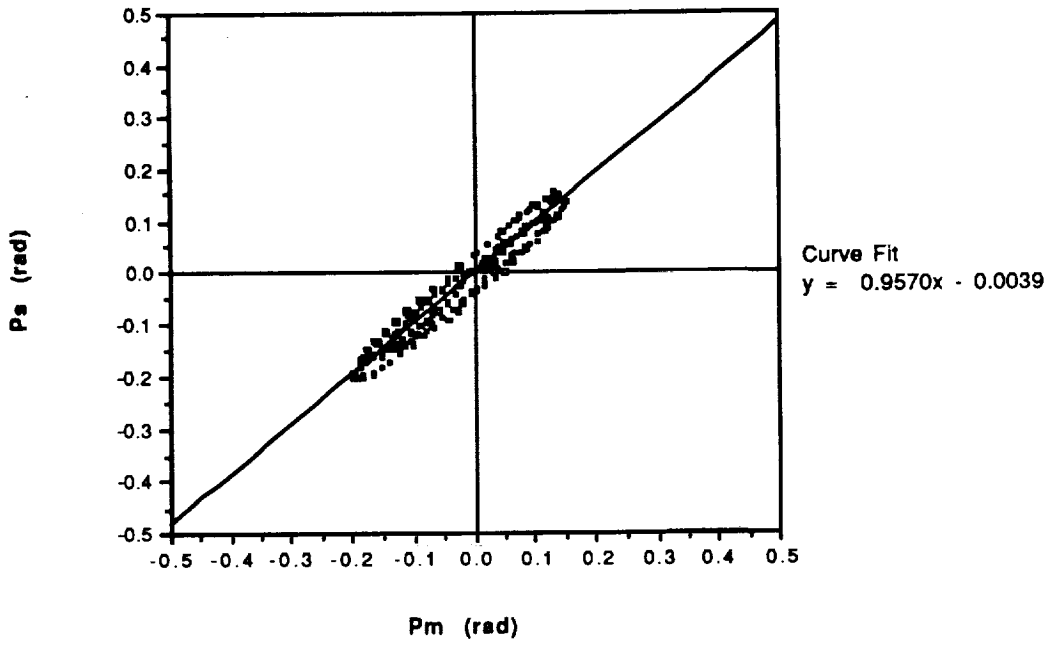

Figure 5.17: Slave Position vs. Master Position
Elbow Pitch; R_y = 1:1

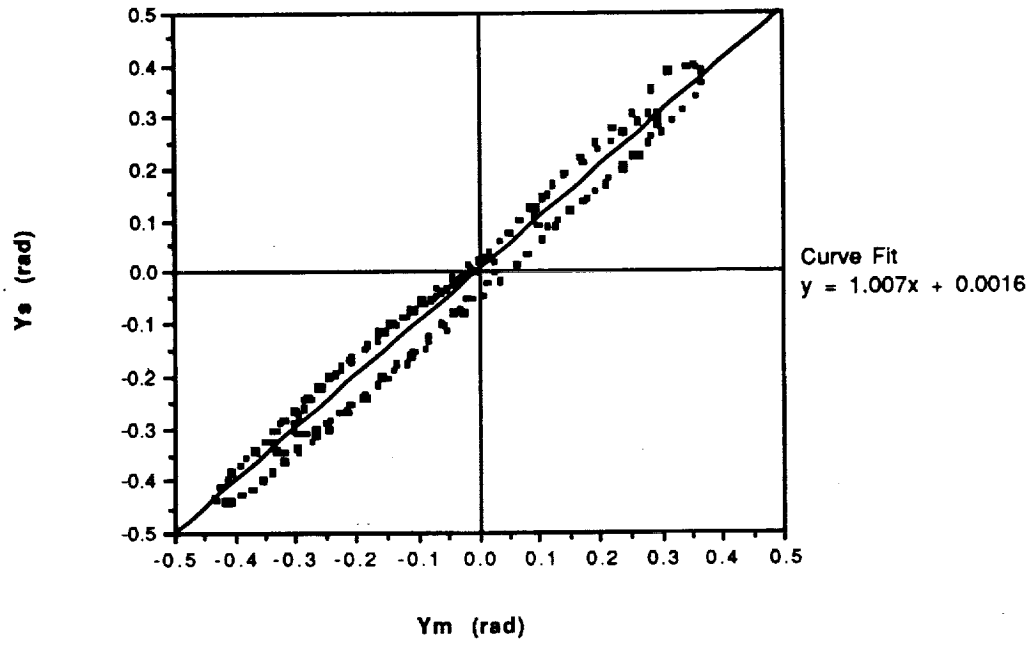

Figure 5.18: Slave Position vs. Master Position
Elbow Yaw; R_y = 1:1

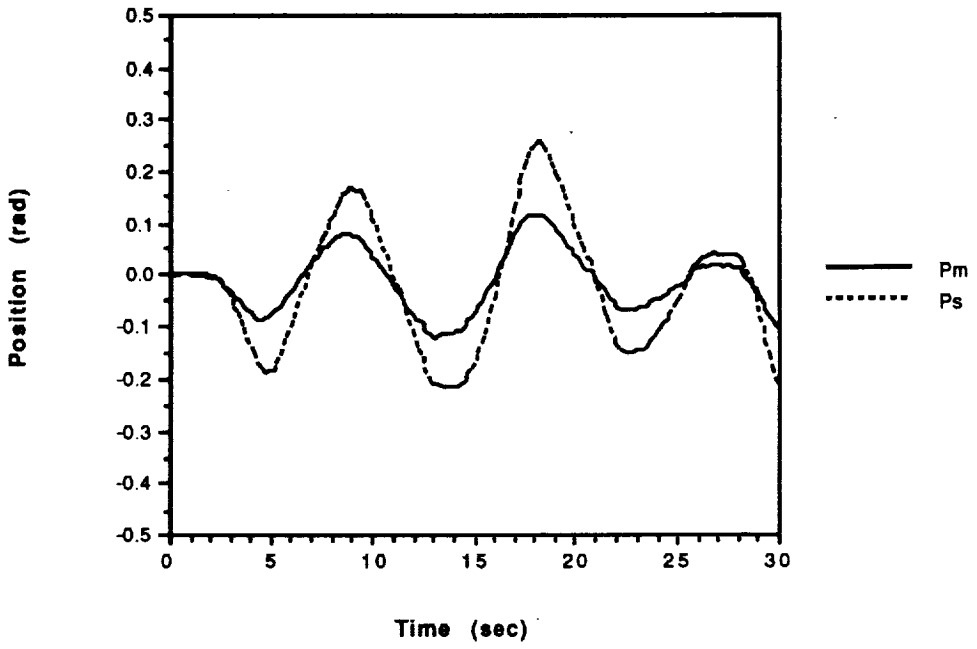

Figure 5.19: Position vs. Time
Elbow Pitch; $R_y = 2{:}1$

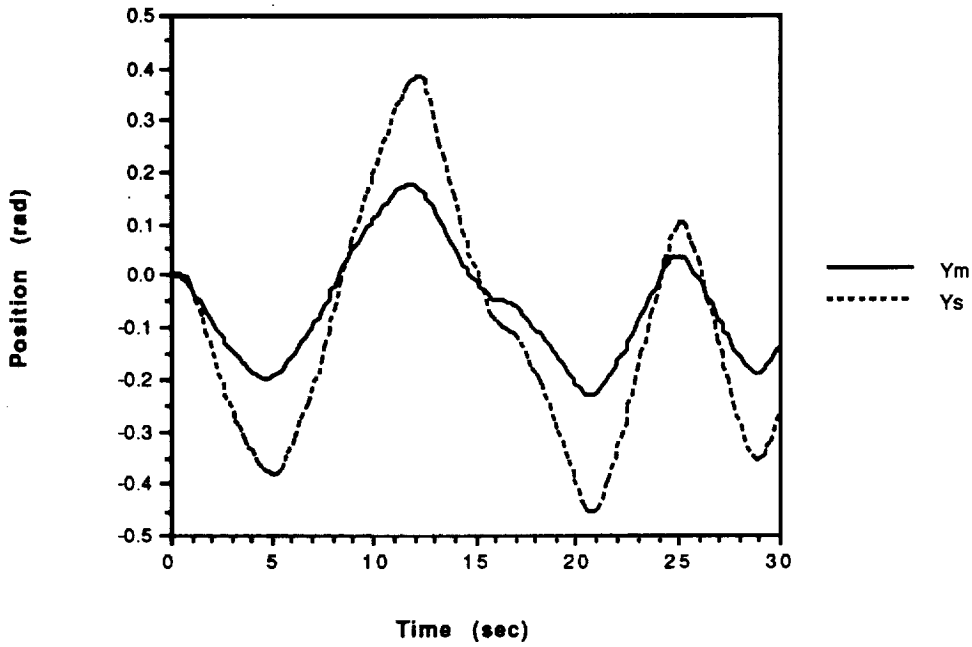

Figure 5.20: Position vs. Time
Elbow Yaw; $R_y = 2{:}1$

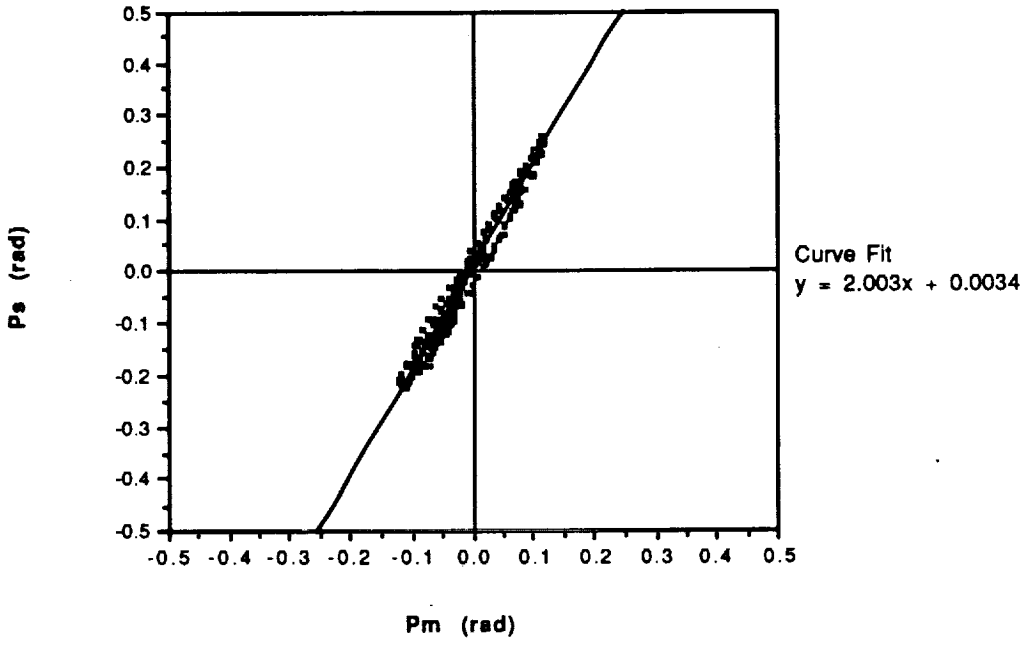

Figure 5.21: Slave Position vs. Master Position
Elbow Pitch; R_y = 2:1

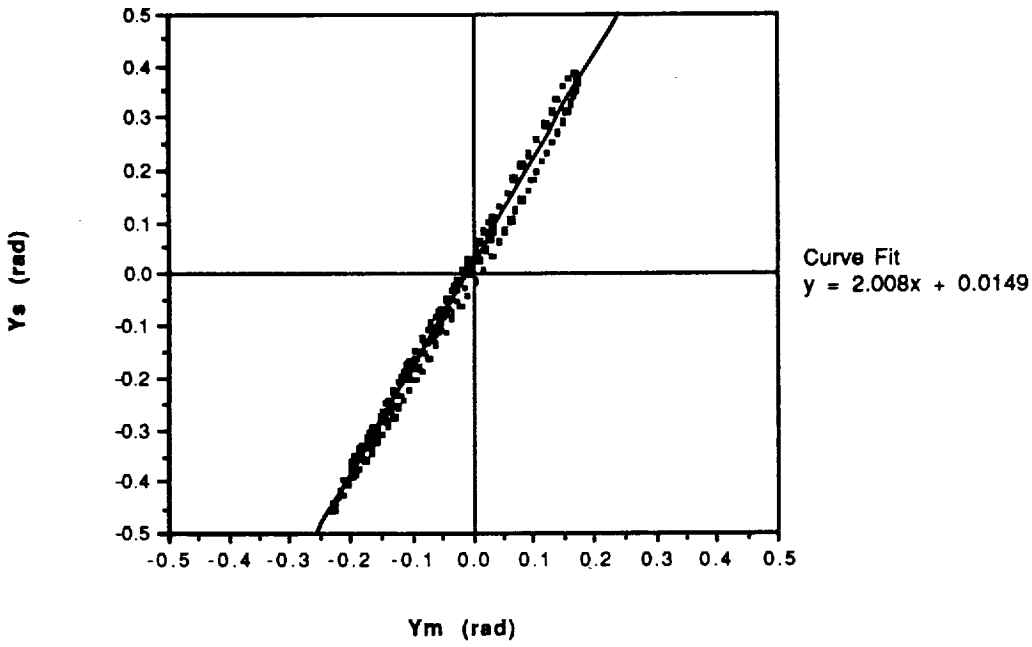

Figure 5.22: Slave Position vs. Master Position
Elbow Yaw; $R_Y = 2:1$

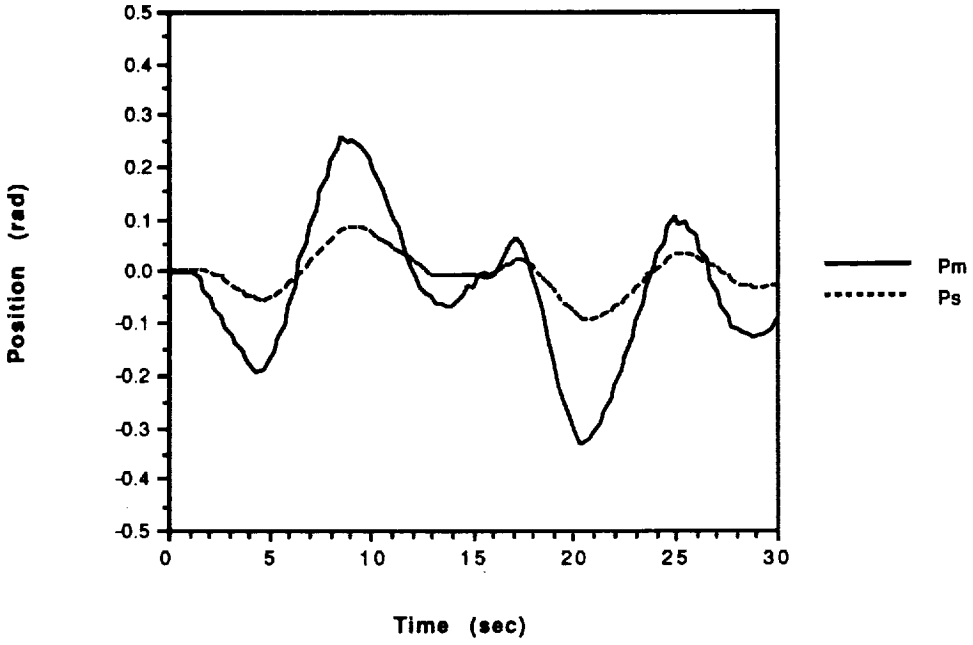

Figure 5.23: Position vs. Time
Elbow Pitch; R_y = 1:3

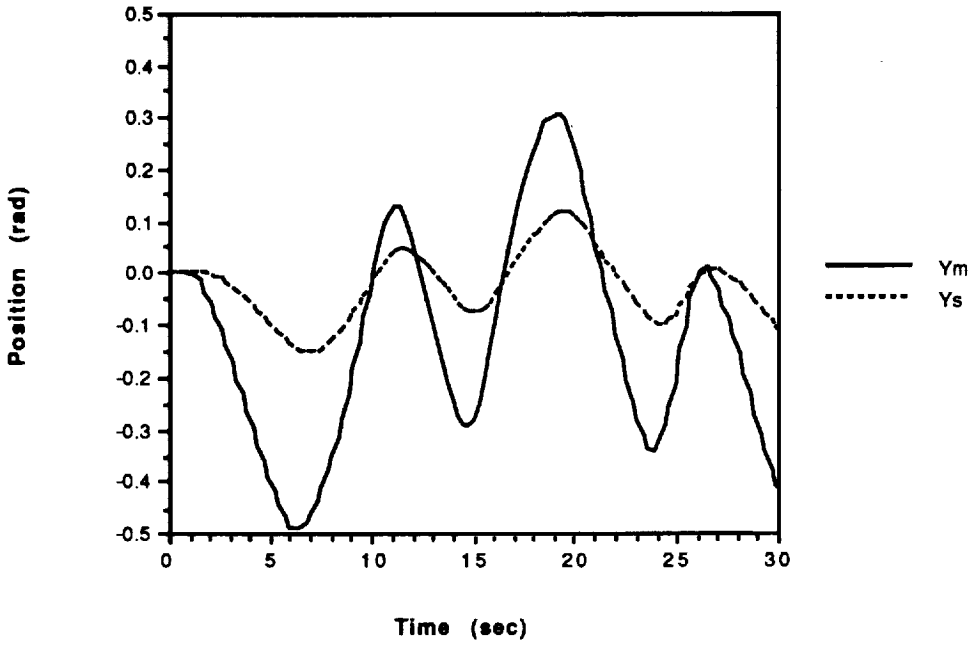

Figure 5.24: Position vs. Time
Elbow Yaw; R_y = 1:3

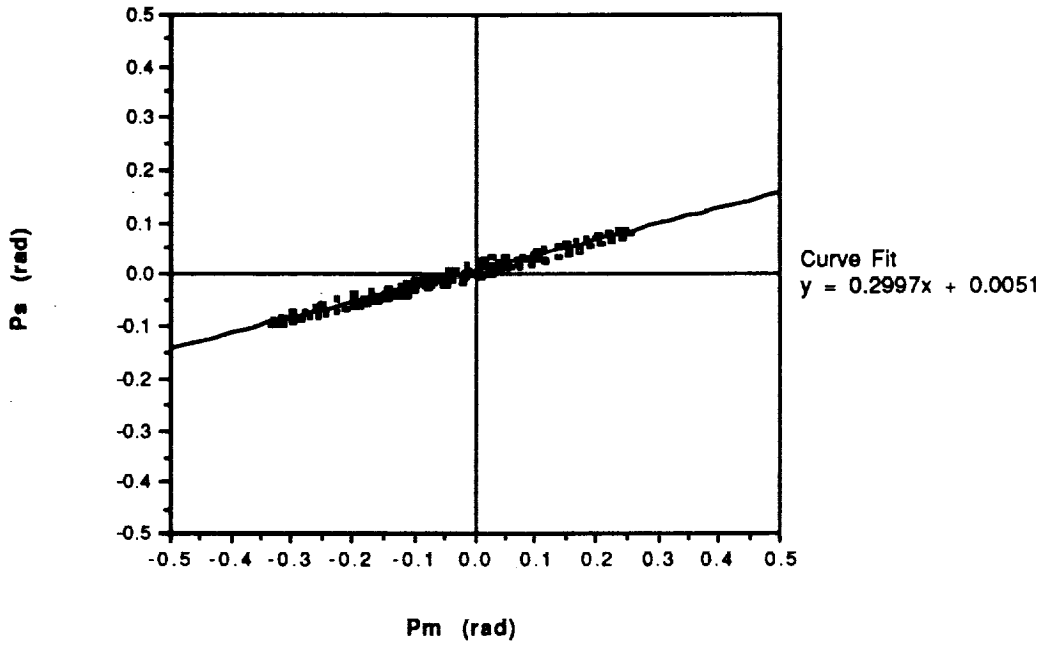

Figure 5.25: Slave Position vs. Master Position
Elbow Pitch; R_y = 1:3

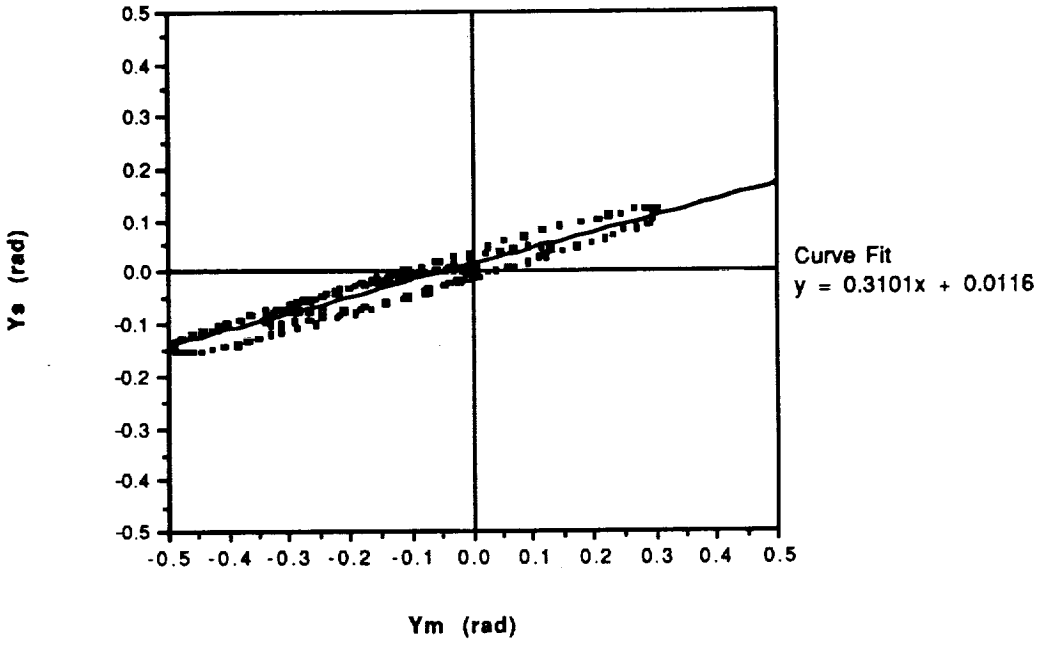

Figure 5.26: Slave Position vs. Master Position
Elbow Yaw; R_y = 1:3

5.6.3 Force Ratio

The performance parameter that relates the forces acting on the master and slave robots is known as the force ratio. For a single degree-of-freedom, it is defined as

$$R_f = \frac{f_s}{f_m} \tag{5.37}$$

For many tasks, it is desirable to specify the force ratio. This enables the human operator to exert large forces with the slave robot by applying small forces to the master robot. The force ratio can be expressed in terms of system variables as

$$R_f = \frac{-P_{21}E}{1 + P_{22}E} \tag{5.38}$$

The force ratio depends on the dynamics of the environment, and on the relationship between two elements in the H matrix. The compensator H_{21} filters the master force, while the compensator H_{22} filters the slave force. The outputs of both compensators are used to drive the slave robot. H_{21} couples the motion of the slave robot to that of the master robot. H_{22} determines the compliance of the slave robot to forces exerted on it by the environment. The force ratio can be arbitrarily specified by selecting the relative magnitudes of H_{21} and H_{22}.

In designing the H matrix, the gain of H_{22} is chosen to satisfy the requirements of system stability. Therefore, the gain of H_{21} is specified to achieve the desired force ratio. Substituting the definitions of the admittances into equation 5.38 and rearranging gives

$$H_{21} = \frac{R_f[1 + (G_sH_{22} + S_s)E]}{G_sE} \tag{5.39}$$

This expression relates H_{21} to known system variables. Given values for H_{22} and the desired force ratio R_f, equation 5.39 can be used to calculate the necessary gain of H_{21}. The magnitude of E has been determined experimentally for compression of a spring scale. The values of G_s and S_s have also been measured for small elbow pitch motions of the slave robot. It was found that $G_s = 0.0117$ rad/lbf, $S_s = 0.0033$ rad/lbf, and $E = 217.0$ lbf/rad.

For the first experiment, the force ratio was specified to be $R_f = 1{:}1$. In this case, the force exerted by the slave robot should be equal to the force applied to the master robot. The H matrix had the following structure:

$$H = \begin{bmatrix} H_{11}=0.20 & H_{12}=0 \\ H_{21}=0.78 & H_{22}=0.10 \end{bmatrix}$$

The gain of H_{22} was selected to insure that the impedance of the slave robot was greater than the impedance of the environment. This is a necessary requirement for system stability. The gain of H_{21} was calculated from equation 5.39 using the values given above for the system variables. The elbow of the master robot was moved through a series of pitch motions. The slave robot pushed down against a spring scale that was fixed at its base to a table. The spring scale simulated a compliant environment with linear stiffness. The end-point forces of both robots were recorded for 20 seconds.

Figure 5.27 is a plot of robot force versus time. It can be seen that the slave force tracks the master force as the spring scale is alternately compressed and released. The magnitude of the force ratio can be determined from Figure 5.28, which is a plot of slave force versus master force. A least-squares curve fit yields a slope of $R_f = 1.02$.

For the second experiment, the force ratio was specified to be $R_f = 2{:}1$. In this case, the force exerted by the slave robot should be twice as large as the force applied to the master robot. The desired force ratio was achieved by calculating the required magnitude for H_{21}. The H matrix had the following structure:

$$H = \begin{bmatrix} H_{11}=0.20 & H_{12}=0 \\ H_{21}=1.55 & H_{22}=0.10 \end{bmatrix}$$

The robot forces are plotted versus time in Figure 5.29. The slave force varies in phase with the master force. However, the amplitude of the slave force is double the amplitude of the master force. Figure 5.30 is a graph of slave force versus master force. The measured force ratio is $R_f = 2.04$.

Two force ratios have been demonstrated: $R_f = 1{:}1$ and $R_f = 2{:}1$. The slave force tracks the master force when the slave robot is constrained by a compliant environment. The measured force ratios agree well with theoretical predictions. To simplify the experiments, only one performance parameter, the force ratio, was specified at a time. The general case where three performance parameters are specified simultaneously will be demonstrated in the next section.

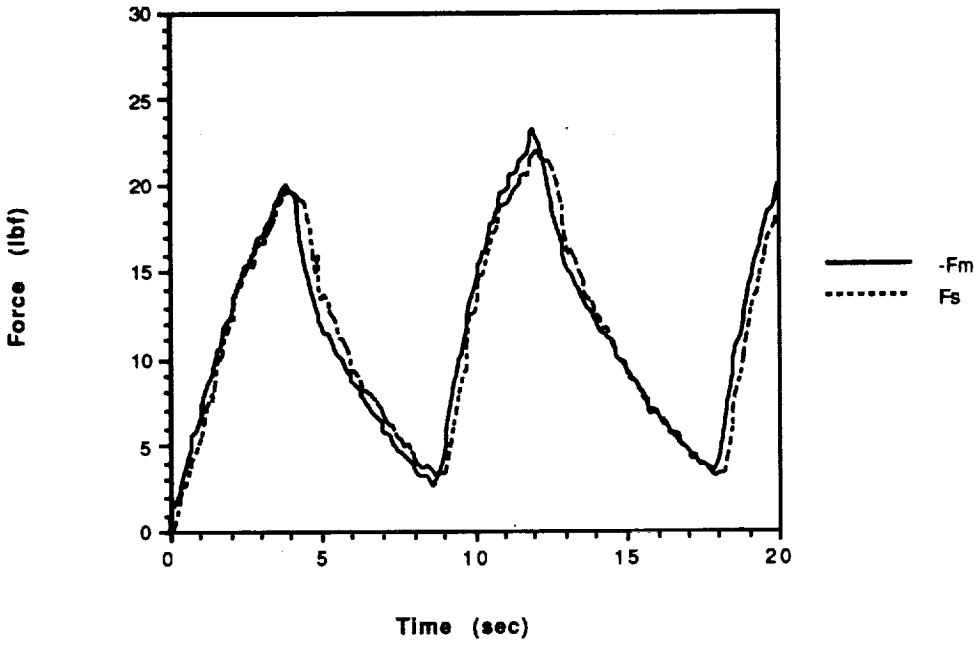

Figure 5.27: Force vs. Time;
R_f =1:1

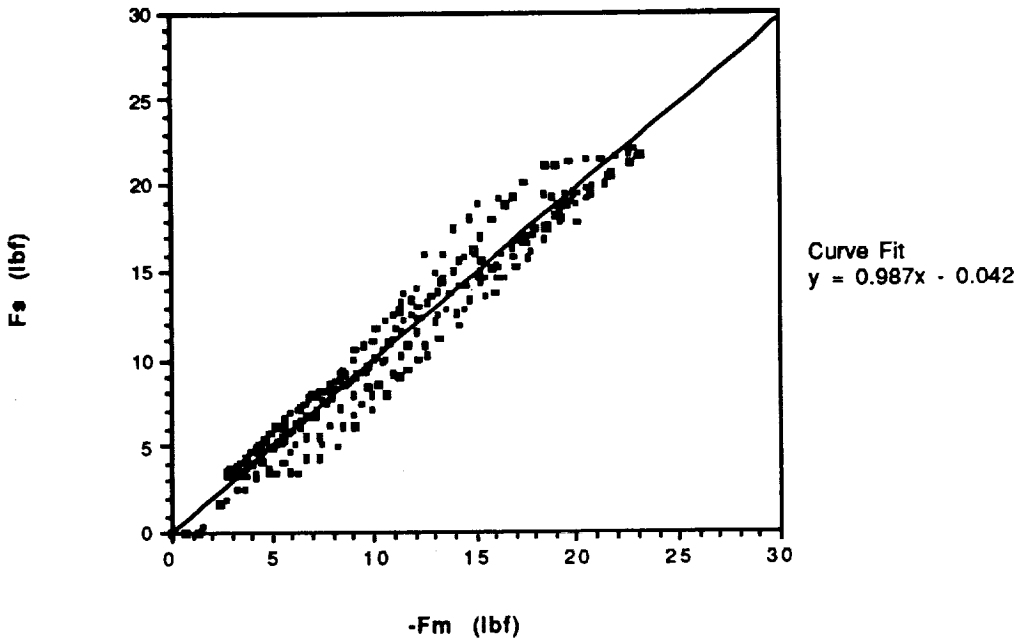

Figure 5.28: Slave Force vs. Master Force;
R_f = 1:1

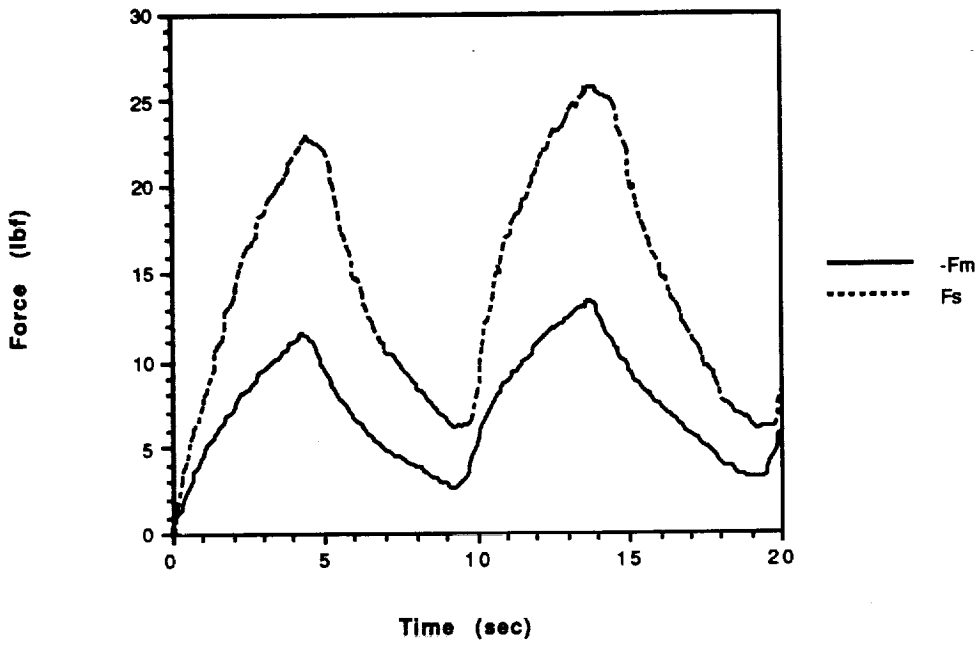

Figure 5.29: Force vs. Time;
$R_f = 2:1$

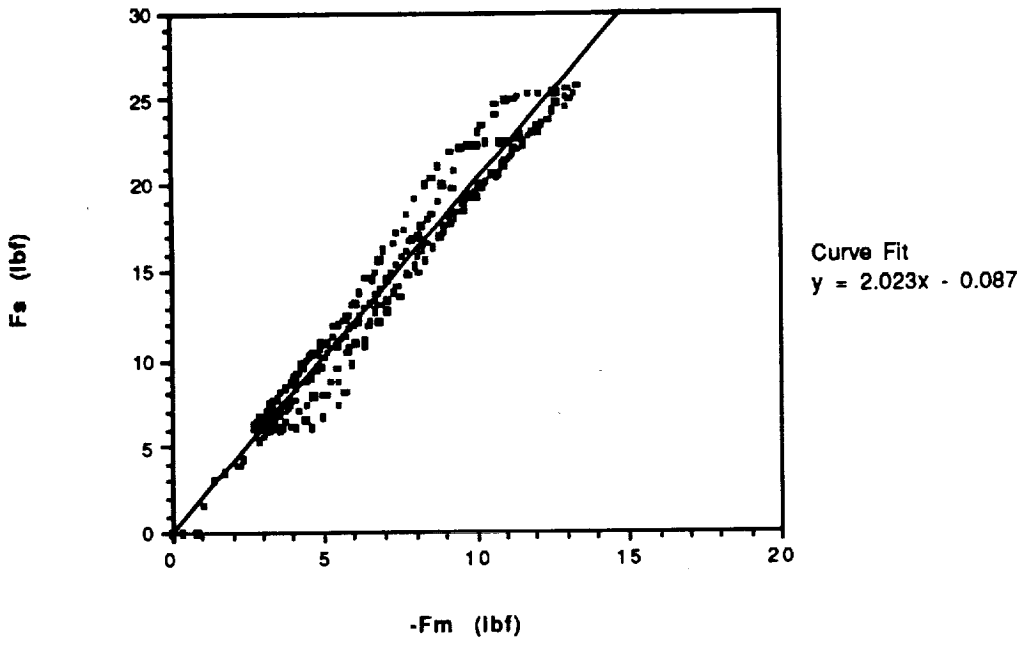

Figure 5.30: Slave Force vs. Master Force;
$R_f = 2:1$

5.6.4 Simultaneous Specification

In the previous experiments, only one performance parameter was specified at a time. It was necessary to assume that either the robot motion was unconstrained, or that there was no force reflection from the environment. These special cases illustrated the relationships between the performance parameters, the system variables, and the H matrix. In this section, the general case where three performance parameters are specified simultaneously will be demonstrated. The telerobotic system will be completely bilateral because force reflection will be included. The H matrix will be designed for both performance and stability.

The performance parameters were measured when the slave robot was compressing a spring scale. The spring scale simulated a compliant environment with linear stiffness. The master robot was moved through a series of elbow pitch motions by the human operator. The end-point forces and joint positions of both robots were recorded for 20 seconds.

The desired performance characteristics for the telerobotic system were:

$$R_f = 2 \quad R_y = 1 \quad Z_s > E$$

The first performance specification states that the force exerted by the slave robot should be twice the force applied to the master robot. The second performance specification requires that the positions of both robots be identical. The third performance specification is necessary to satisfy the requirements of system stability.

The equations that relate the performance parameters to known system variables are

$$R_f = -\frac{P_{21}E}{1 + P_{22}E} \tag{5.40}$$

$$R_y = \frac{P_{21}}{P_{11} + DPE} \tag{5.41}$$

$$Z_s = \frac{1 + P_{11}S_h}{P_{22} + DPS_h} \tag{5.42}$$

Given desired values for the performance parameters, equations 5.40 through 5.42 can be solved for the four unknown elements H_{11}, H_{12}, H_{21}, and H_{22}. Since there are only three

equations involving the performance parameters, one of the elements in the H matrix must be chosen arbitrarily.

Design of the H matrix begins by selecting a sufficiently small value for H_{22}. This insures that the slave impedance will always be greater than the impedance of the environment, no matter what value is assumed by the highly variable human arm sensitivity, S_h. The minimum slave impedance occurs when $S_h = 0$. In that case,

$$Z_s = \frac{1}{P_{22}} = \frac{1}{G_s H_{22} + S_s} \tag{5.43}$$

The stability condition $Z_s > E$ will be satisfied when

$$H_{22} < \frac{1/E - S_s}{G_s} \tag{5.44}$$

The static values of the system variables have been previously determined. It was found that $G_m = 0.0117$ rad/lbf, $S_m = 0.0033$ rad/lbf, $G_s = 0.0117$ rad/lbf, $S_s = 0.0033$ rad/lbf, and $E = 217.0$ lbf/rad. Substituting these values into equation 5.44 yields $H_{22} < 0.11$. Therefore, to guarantee stability for all possible values of the human arm sensitivity, the value of H_{22} is chosen to be 0.10.

The next step in the design of the H matrix is the specification of the desired force ratio. Solving equation 2 for H_{21} gives

$$H_{21} = \frac{R_f [1 + (G_s H_{22} + S_s)E]}{G_s E} \tag{5.45}$$

Since the value of H_{22} has already been determined, this expression can be used to calculate the gain of H_{21} necessary to achieve any desired force ratio. For a force ratio of $R_f = 2$, the required gain is $H_{21} = 1.55$.

Finally, the position ratio will be specified by selecting the relative values of the two remaining elements in the H matrix, H_{11} and H_{12}. One of these elements must be chosen arbitrarily, so H_{11} is set to unity for convenience. The value of H_{12} necessary to achieve the desired position ratio can then be determined from equation 5.41. It can be shown that

$$H_{12} = \frac{1}{G_s}\left[\frac{G_m H_{11} + S_m}{R_f} - \frac{1}{R_y E}\right] \tag{5.46}$$

where equation 5.40 for the force ratio has been used to simplify the expression. Since R_f depends on the magnitudes of H_{21} and H_{22}, equation 5.46 relates H_{12} to the other three elements in the H matrix. For a force ratio of $R_f = 2$ and a position ratio of $R_y = 1$, the required gain is $H_{12} = 0.25$.

The design of the H matrix to meet the specified performance criteria is now complete. To summarize, the H matrix has the following structure:

$$H = \begin{bmatrix} H_{11}=1 & H_{12}=0.25 \\ H_{21}=1.55 & H_{22}=0.10 \end{bmatrix}$$

The robot forces are plotted versus time in Figure 5.31. The slave force varies in phase with the master force as the spring scale is alternately compressed and released. The amplitude of the slave force is double the amplitude of the master force. The force ratio can be determined from Figure 5.32, which is a plot of slave force versus master force. A least-squares curve fit yields a slope of $R_f = 2.02$. The robot positions are plotted versus time in Figure 5.33. The slave robot tracks the master robot closely. Figure 5.34 is a plot of slave position versus master position. The measured position ratio is $R_y = 0.98$. The actual values of the force ratio and the position ratio agree well with their specified values.

The purpose of placing the performance criterion on the slave impedance was to guarantee stability of the telerobotic system during the experiment. However, it was not possible to measure the magnitude of Z_s because the slave robot was constrained by the environment. The only conclusion that can be inferred is that the slave impedance was greater than the impedance of the environment. Otherwise, the system would have been unstable. It will be shown that this must be true in a later section.

Desired values were specified for the force ratio, the position ratio, and the slave impedance. All three performance specifications were achieved by selecting the relative magnitudes of the elements in the H matrix. It has been demonstrated that three performance parameters can be specified simultaneously for the most general case of a bilateral telerobotic system.

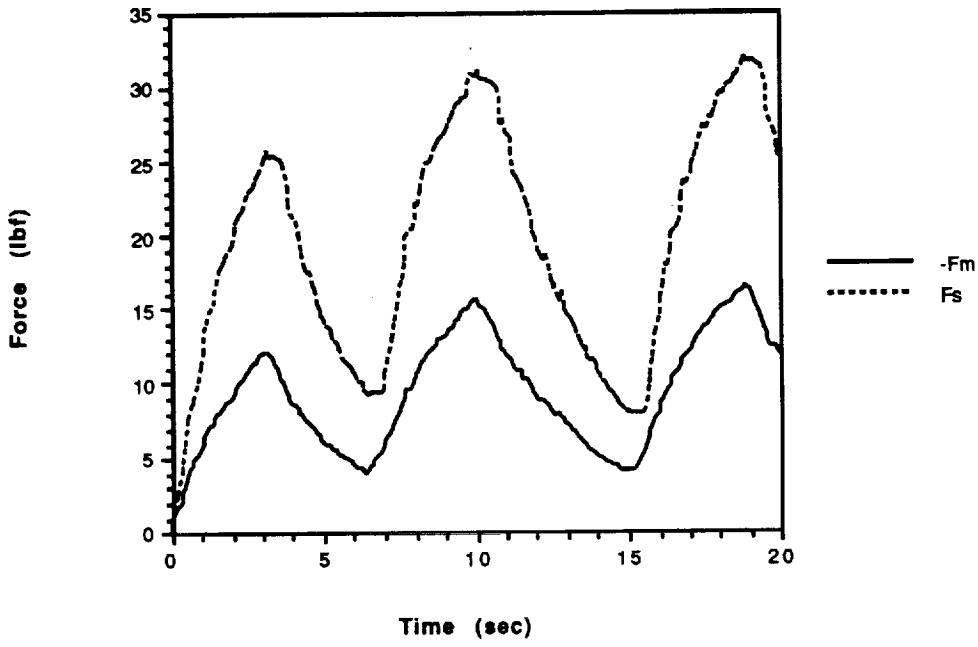

Figure 5.31: Force vs. Time
$R_f = 2:1$

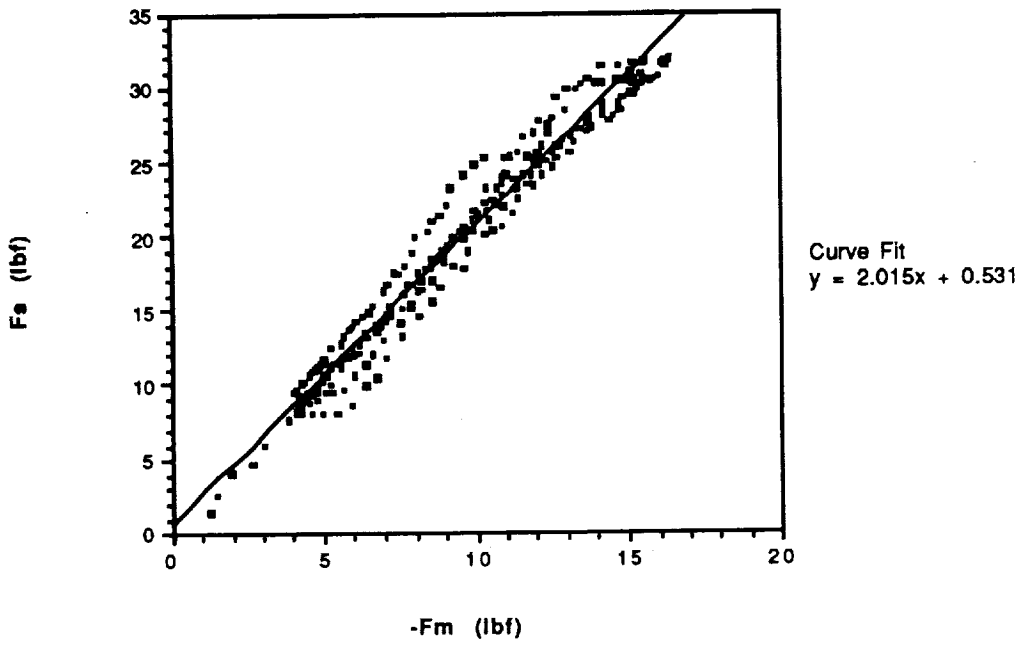

Figure 5.32: Slave Force vs. Master Force
$R_f = 2:1$

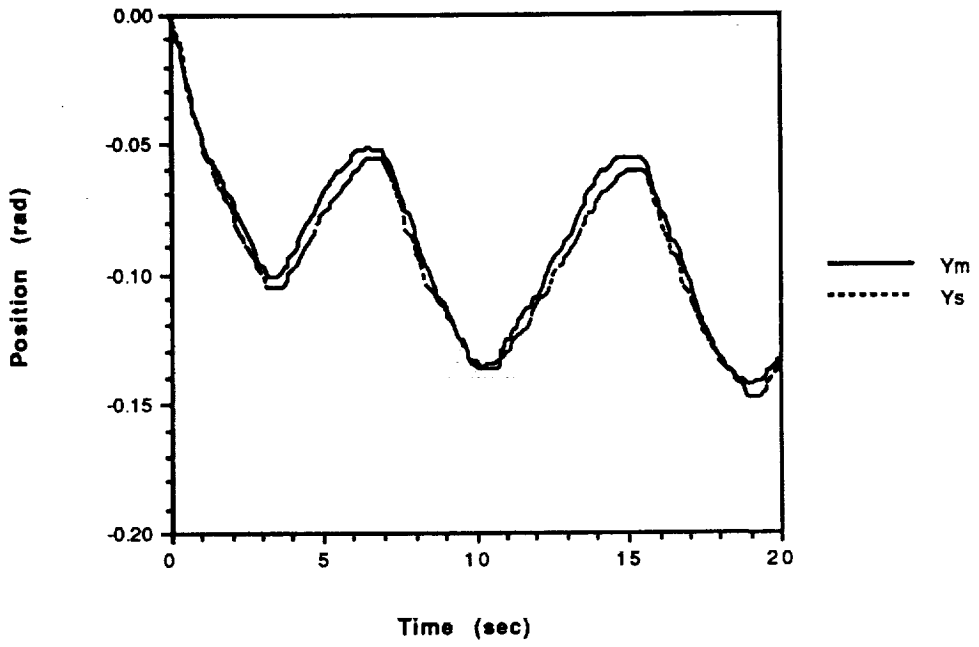

Figure 5.33: Position vs. Time
$R_y = 1:1$

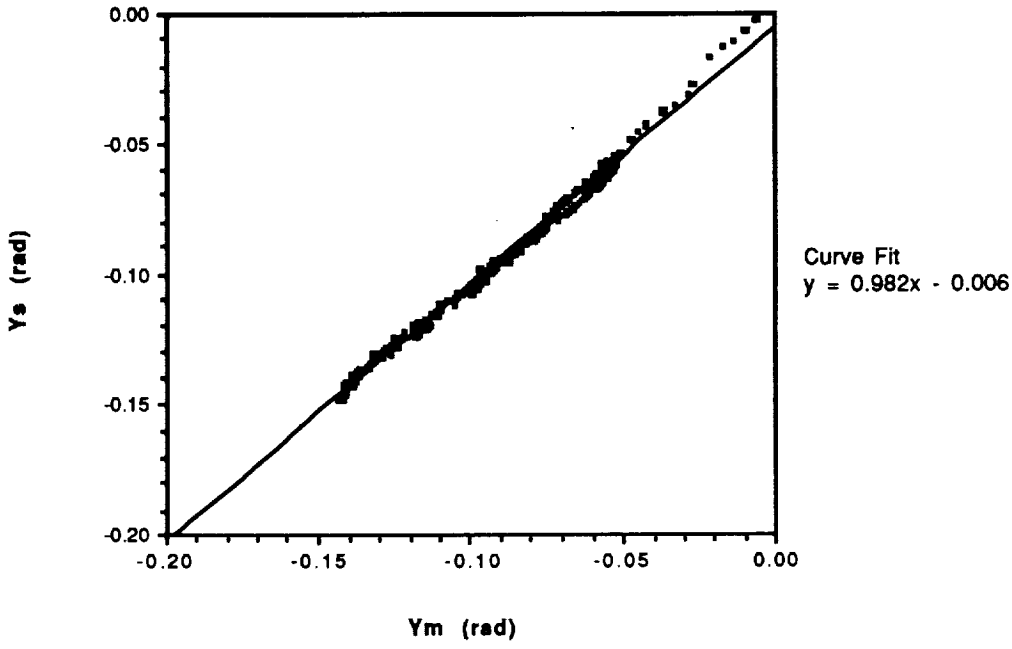

Figure 5.34: Slave Position vs. Master Position
R_y = 1:1

5.7 System Identification and Robustness

Robustness of the control architecture will be demonstrated by quantifying acceptable uncertainties in the telerobotic system's dynamic model. Knowledge of the dynamic model and its associated uncertainties is essential in the design of the H matrix. The process of determining the dynamic model from observed behavior is known as system identification.

There are two basic approaches to system identification. The first approach involves applying a sinusoidal input to the system at various frequencies and measuring the amplitude and phase of the corresponding output. The measured frequency response is then used to estimate the order and structure of the dynamic model. In the second approach, the dynamic model is represented by a parametric difference equation. The parameters in the difference equation are selected to minimize the error between the actual system response and the response predicted by the model. Once the model structure has been identified by parameter estimation, the frequency response can be calculated. In both approaches, the frequency response is used to determine the model uncertainties. While the first approach is a direct measurement of the frequency response, it has the disadvantage that large amounts of experimental data must be collected to yield accurate results. In addition, the sinusoidal inputs can lead to cyclic fatigue of the robotic hardware. In contrast, the second approach permits the determination of the dynamic model from a single set of random inputs. For these reasons, the parametric approach to system identification will be used in the following experiments.

Consider the linear time-invariant system depicted in Figure 5.35. The input signal is u(t), and the output signal is y(t). The output is related to the input by the impulse response function g(t) such that

$$y(t) = \int_0^\infty g(\tau)\, u(t-\tau)\, d\tau \tag{5.47}$$

If the impulse response function is known, the output corresponding to any input can be calculated. Thus, $g(\tau)$ is a complete characterization of the system (Ogata 1970).

Typically, both the input and output signals are sampled at discrete time intervals T. The behavior of the system is observed at the sampling instants

$$t = kT,\ k = 1, 2, \ldots$$

For notational convenience, it will be assumed that the sampling interval is equal to one time unit so that

$$t = 1, 2, \ldots$$

In discrete time, the integral in equation 5.47 can be replaced by the sum over all sampling instants. That is

$$y(t) = \sum_{k=1}^{\infty} g(k)\, u(t-k) \tag{5.48}$$

A realistic system is affected by disturbances such as measurement noise and uncontrollable inputs from the environment. The disturbances are usually only noticeable through their effects on the output. Thus, it will be assumed that the disturbances can be represented by an additive term v(t) at the output as shown in Figure 5.36. When the system is influenced by disturbances, equation 5.48 becomes

$$y(t) = \sum_{k=1}^{\infty} g(k)\, u(t-k) + v(t) \tag{5.49}$$

Many types of disturbances can be described as filtered random noise. If e(t) is a sequence of random variables with zero mean values, the disturbance can be expressed in a form similar to equation 5.48

$$v(t) = \sum_{k=0}^{\infty} h(k)\, e(t-k) \tag{5.50}$$

Substituting equation 5.50 into equation 5.49 yields the basic description of a linear system with additive disturbance

$$y(t) = \sum_{k=1}^{\infty} g(k)\, u(t-k) + \sum_{k=0}^{\infty} h(k)\, e(t-k) \tag{5.51}$$

The previous equation can be expressed in a simpler form by introducing the shift operator q^{-1} defined as

$$q^{-1}u(t) = u(t - 1)$$

Now equation 5.51 can be written as

$$y(t) = G(q)\, u(t) + H(q)\, e(t) \tag{5.52}$$

where

$$G(q) = \sum_{k=1}^{\infty} g(k)\, q^{-k}$$

$$H(q) = \sum_{k=0}^{\infty} h(k)\, q^{-k}$$

In equation 5.52, G(q) is known as the transfer function of the linear system (MATLAB User's Guide 1989).

The problem of system identification is to estimate the functions G and H from observations of u and y. To perform the estimation, the functions are expressed in terms of a finite number of coefficients. These coefficients are the parameters to be determined. The simplest parametric relationship between the inputs and outputs is a difference equation of the form

$$y(t) + a_1 y(t-1) + \ldots + a_{na} y(t-na) = b_1 u(t-1) + \ldots + b_{nb} u(t-nb) + e(t) \tag{5.53}$$

where the random noise e(t) appears as a direct error. Using the shift operator, the difference equation can be written as

$$A(q)\, y(t) = B(q)\, u(t) + e(t) \tag{5.54}$$

where

$$A(q) = 1 + a_1 q^{-1} + \ldots + a_{na} q^{-na}$$

$$B(q) = b_1 q^{-1} + \ldots + b_{nb} q^{-nb}$$

Equation 5.54 is known as an autoregressive or ARX model (Ljung 1987). Note that the ARX model corresponds to equation 5.52 if

$$G(q) = \frac{B(q)}{A(q)} \quad \text{and} \qquad H(q) = \frac{1}{A(q)}$$

The order of the denominator polynomial is na, while nb is the order of the numerator polynomial. The signal flow diagram for the ARX model is shown in Figure 5.37. The random noise goes through the characteristic dynamics of the system before being added to the output.

Sometimes, the system dynamics contain a delay of nk samples between the input and the output. In that case, some of the leading coefficients of B are zero since the input affects the output only after nk samples. Consequently, the ARX model is modified by the shift operator q^{-nk} as follows

$$A(q)\, y(t) = q^{-nk}\, B(q)\, u(t) + e(t) \tag{5.55}$$

In the previous equation, the variable e(t) represents the part of the output that cannot be predicted from past data. Given a model for the system, the prediction error can be calculated from

$$e(t) = A(q)\, y(t) - q^{-nk}\, B(q)\, u(t) \tag{5.56}$$

The most common method of parameter estimation is to choose the polynomials A and B such that the square of the prediction error is minimized for all sampling instants. That is, if

$$V_N(A, B) = \frac{1}{N} \sum_{t=1}^{N} e^2(t) \tag{5.57}$$

then

$$[A, B] = \arg\min V_N(A, B)$$

where N is the total number of samples. This is known as the least-squares estimate of the model parameters (MATLAB User's Guide 1989).

Many different model structures are possible, depending on the choices made for the orders of the polynomials and the number of delays. The question then arises of how to

select the best model to represent the observed data. One method of evaluating the candidate models is called the Akaike Final Prediction Error Criterion (FPE). The FPE is based on the minimum value of the criterion function V_N defined in equation 5.57. The FPE is given by

$$FPE = \frac{1 + n/N}{1 - n/N} V_N \tag{5.58}$$

where n is the number of estimated parameters in the model (Ljung 1987). The theory says that the model with the smallest value of FPE should be chosen. Another method of evaluating models is called cross-validation. The candidate model is used to calculate a simulated output from a new set of input data. The new input data is data that was not used in the parameter estimation. If the model is a good one, the simulated output will match the actual output corresponding to the new input data. If several models remain candidates after cross-validation, the simplest model is usually selected.

In the bilateral impedance control architecture, the H matrix is designed to achieve specified values of the performance parameters. Deviations from the desired performance are caused by uncertainties in the dynamic model used to design the H matrix. A measure of robustness to model uncertainties can be obtained from the frequency response of the performance parameters. The frequency response is calculated from an ARX model found through system identification.

For the system identification experiments, a random binary input signal was generated in the computer. A random binary signal shifts between two fixed values in a random manner. The input signal to the robot control system was a virtual force. In other words, the input did not result from the application of a real force on the robot's force sensor. The output of the control system was the robot position. For each experiment, two sets of input-output data were acquired. The data sets had different input signals. The first data set was used for parameter estimation of the dynamic model, while the second data set was used for cross-validation. The parameter estimation was done with MATLAB software (The MathWorks, Inc. 1989).

The purpose of the first experiment was to determine the frequency response of the performance parameter Z_s. The slave robot was free to move without constraint. The H matrix had the following structure:

$$H = \begin{bmatrix} H_{11}=0 & H_{12}=0 \\ H_{21}=0 & H_{22}=1 \end{bmatrix}$$

Since all elements in the H matrix except H_{22} are zero, the relationship between the force input and the position output is

$$y_S = (G_S H_{22} + S_S) f_S \tag{5.59}$$

However, there is no transfer of mechanical power to the robot from externally applied forces because the force input signal is generated in the computer. Therefore, the sensitivity S_S can be eliminated from the previous equation to give

$$y_S = G_S f_S \tag{5.60}$$

where it has been assumed that $H_{22} = 1$. Thus, system identification yields the transfer function of the primary closed-loop system, G_S. The primary closed-loop system consists of the slave robot and the stabilizing position controller. From the definition of the slave impedance

$$y_S = (1/Z_S) f_S \tag{5.61}$$

Comparing equations 5.60 and 5.61, it is apparent that

$$G_S = 1/Z_S \tag{5.62}$$

Thus, the frequency response calculated from the ARX model is equivalent to the frequency response of the inverse slave impedance, $1/Z_S$.

The two data sets acquired in the first experiment contained 376 samples each. The sampling interval was T = 0.04 seconds. The input-output data used for the parametric estimation of G_S are plotted versus time in Figure 5.38. The random binary input signal is a square wave with an amplitude of 5 lbf. The output signal is the elbow pitch position of the slave robot. The input-output data used for cross-validation of the dynamic model are plotted in Figure 5.39.

The FPE criterion was used to evaluate the candidate models. A second-order model was selected as the simplest representation of the slave robot dynamics. The ARX model has the following parameters:

$$na = 2, nb = 1, nk = 2, FPE = 1.33 \times 10^{-4}$$

Written explicitly in the form of a difference equation, the model is

$$y(t) = 1.333\ y(t-1) - 0.5911\ y(t-2) + 0.003\ u(t-2)$$

The corresponding transfer function in continuous time is

$$G_S(s) = \frac{-0.0560\ s + 2.4978}{s^2 + 13.1445\ s + 213.396} \tag{5.63}$$

The model was used to calculate the simulated output from the second set of input data. The cross-validation is shown in Figure 5.40 where the simulated output and the actual output are plotted versus time. The model predicts the response to a different input signal fairly well, so it must be a reasonably accurate representation of the system dynamics.

The static gain is the magnitude of the transfer function at zero frequency. The static gain was measured in a previous section by different methods, and it was found to be $G_S = 0.0117$ rad/lbf. Setting $s = 0$ in equation 5.63 yields exactly the same value. This check provides additional confidence in the model.

The closed-loop frequency response of G_S is shown in Figure 5.41. The frequency response has been normalized so that the static gain is 0 dB. This normalization does not affect the shape of the frequency response, only its magnitude. The frequency at which the magnitude falls below -3 dB defines the bandwidth of the system. High system bandwidth is desirable for good tracking and speed of response. For the slave robot control system, the bandwidth is about 20 rad/s.

When a human operator is interacting with the telerobotic system, she tends to adapt her own dynamics to compensate for the dynamics of the robots. An important consequence of the human's adaptability is that the maximum attainable bandwidth of the telerobotic system is limited to about 4.5 rad/s (Sheridan and Ferrell 1974). Since the human is the limiting factor, increasing the performance of the robots will have almost no effect on the overall system performance.

The closed-loop frequency response of G_S remains fairly flat out to 4 rad/s. This verifies the assumption made in previous experiments that the static value of G_S can be used to design the H matrix if the robot motion is slow. Furthermore, the magnitude of G_S is constant over nearly the same frequency range as the maximum attainable bandwidth of the telerobotic system. Thus, little is gained by using the closed-loop transfer function for H matrix design because the human determines the overall system dynamics. The slight improvement in accuracy does not warrant the additional complexity involved.

Now that a dynamic model has been identified for the slave robot, it is possible to quantify the model uncertainties. Consider a closed-loop system with unity feedback like the one depicted in Figure 5.42. The system dynamics are represented by G_n, which is the nominal open-loop transfer function. The nominal output of the system is y_n. It is related to the reference input command r by

$$y_n = \left\{ \frac{G_n}{1 + G_n} \right\} r \tag{5.64}$$

where the term in brackets is the closed-loop transfer function. An uncertainty of ΔG in the dynamic model causes a change of Δy in the nominal output. That is

$$y_n + \Delta y = \frac{(G_n + \Delta G)}{1 + (G_n + \Delta G)} r \tag{5.65}$$

Subtracting equation 5.64 from equation 5.65 gives

$$\Delta y = \frac{\Delta G}{[1 + (G_n + \Delta G)]\,(1 + G_n)} r \tag{5.66}$$

Dividing equation 5.66 by equation 5.64 yields

$$\frac{\Delta y}{y_n} = \frac{\Delta G}{G_n\,[1 + (G_n + \Delta G)]} \tag{5.67}$$

If the magnitude of the uncertainty is small compared to the magnitude of G_n, equation 5.67 can be rearranged so that

$$\frac{\Delta y / y_n}{\Delta G / G_n} = \frac{1}{1 + G_n} \tag{5.68}$$

This is an expression for the fractional change in the nominal output due to a fractional uncertainty in the model. Robustness to model uncertainties is usually specified as a maximum acceptable deviation in the system's nominal output over a certain frequency range. If the maximum acceptable deviation per unit of model uncertainty is denoted by Δ_m, then the robustness specification in the frequency domain becomes

$$\left|\frac{1}{1+G_n}\right| < \Delta_m \qquad \text{for } 0 < \omega < \omega_m \tag{5.69}$$

If the gain of G_n is much greater than one, equation 5.69 can be written in the simpler form

$$|G_n| > 1/\Delta_m \qquad \text{for } 0 < \omega < \omega_m \tag{5.70}$$

Thus, the system is robust to modeling uncertainties on the order of $1/\Delta_m$ if its open-loop frequency response satisfies equation 5.70. Conversely, equation 5.70 can be used to calculate the model uncertainties from the measured open-loop frequency response of the system.

To demonstrate robustness of the slave robot impedance, it is necessary to determine the open-loop transfer function of $1/Z_S$. Equation 5.63 is the closed-loop transfer function of G_S. From equation 5.64, the relationship between the open and closed-loop transfer functions is

$$(G_S)_{CL} = \frac{(G_S)_{OL}}{1 + (G_S)_{OL}} \tag{5.71}$$

Since $G_S = 1/Z_S$, the open-loop transfer function of the inverse slave impedance is

$$(1/Z_S)_{OL} = \frac{(G_S)_{CL}}{1 - (G_S)_{CL}} \tag{5.72}$$

The open-loop frequency response of $1/Z_S$ is shown in Figure 5.43. It was calculated from equation 5.72 using the normalized transfer function of G_S.

Suppose that the uncertainty in the dynamic model is on the order of 10 percent. That is, $\Delta G/G_n = 0.10$. If it is desirable to insure that the actual value of Z_S will remain within one percent of its nominal specified value in the presence of this uncertainty, then $\Delta y/y_n = 0.01$. Therefore, the robustness specification is chosen to be $\Delta_m = 0.10$. Equation 5.70 implies that

$$|1/Z_S| > 10 \qquad (= 20 \text{ dB})$$

This robustness specification is represented by the shaded region in Figure 5.43. It can be seen that the robustness specification is satisfied over the frequency range $0 < \omega < 1$ rad/s. Notice that the uncertainties in the slave impedance must become greater as the frequency

range increases because the magnitude of $1/Z_s$ constantly decreases at 20 dB/decade. When the frequency range is equal to 4.5 rad/s, which is the maximum attainable bandwidth of the telerobotic system, the magnitude of $1/Z_s$ is 8 dB. This implies that the uncertainty in the slave impedance for a 10 percent uncertainty in the model is approximately 4 percent. Thus, the slave impedance is fairly robust to large uncertainties in the H matrix at low frequencies.

The purpose of the second experiment was to determine the frequency response of the performance parameter Z_m. The second experiment was identical to the first experiment except that it was performed on the master robot. The H matrix had the following structure:

$$H = \begin{bmatrix} H_{11}=1 & H_{12}=0 \\ H_{21}=0 & H_{22}=0 \end{bmatrix}$$

System identification yields the closed-loop transfer function of the master robot control system, G_m. Using the definition of the master impedance, it can be shown that $G_m = 1/Z_m$. Thus, the frequency response calculated from the dynamic model for G_m is equivalent to the frequency response of the inverse master impedance, $1/Z_m$.

As before, two sets of input-output data were acquired. One set was used for parameter estimation, and the other set was used for cross-validation. Each data set contained 376 samples, and the sampling interval was 0.04 seconds. A second-order ARX model was selected as the simplest representation of the master robot dynamics. The model has the following parameters:

$$na = 2,\ nb = 1,\ nk = 2,\ FPE = 3.04 \times 10^{-4}$$

Written explicitly in the form of a difference equation, the model is

$$y(t) = 1.6487\ y(t-1) - 0.7657\ y(t-2) + 0.0014\ u(t-2)$$

The corresponding transfer function in continuous time is

$$G_m(s) = \frac{-0.0206\ s + 0.9737}{s^2 + 6.6734\ s + 84.2817} \qquad (5.73)$$

The model was used to calculate the simulated output from the second set of input data. The cross-validation is shown in Figure 5.44 where the simulated output and the actual output are plotted versus time. The agreement is not as good as it was for the slave robot, but the model is still a reasonably accurate representation of the system dynamics. The

static gain of the transfer function is 0.0116 rad/s. In a previous section, the static gain of G_m was found by different methods to be 0.0117 rad/s. This check provides additional confidence in the model.

The closed-loop frequency response of G_m is plotted in Figure 5.45. The frequency response has been normalized so that the static gain is 0 dB. The bandwidth of the master robot control system is about 12 rad/s. Note that the bandwidth of the master robot is less than that of the slave robot. In addition, the peak magnitude at resonance is greater, and occurs at a lower natural frequency. These observations seem to indicate that the master robot is less rigid and has lower damping. The closed-loop frequency response remains fairly flat out to 3 rad/s. The range in which the static value of the transfer function can be used for H matrix design is more restricted than it was for the slave robot.

The open-loop frequency response of $1/Z_m$ is shown in Figure 5.46. It was calculated from the normalized closed-loop transfer function of G_m. Suppose that the robustness specification is chosen to be $\Delta_m = 0.10$. This means that a ten percent uncertainty in the model will cause a change in the nominal master impedance of less than one percent. The robustness specification is represented by the shaded region in Figure 5.46. It can be seen that the robustness specification is satisfied over the frequency range $0 < \omega < 1$ rad/s. When the frequency range is equal to 4.5 rad/s, which is the maximum attainable bandwidth of the telerobotic system, the magnitude of $1/Z_m$ is 6 dB. This implies that the uncertainty in the master impedance for a 10 percent uncertainty in the model is approximately 5 percent. Thus, the master impedance is fairly robust to large uncertainties in the H matrix at low frequencies.

Now that dynamic models have been found for the master and slave robots, they can be used to calculate the frequency response of the performance parameter R_y. The position ratio defines a relationship between the robot forces such that

$$y_s = R_y\, y_m \tag{5.74}$$

Since y_m is an output of the control system instead of an input, it is not possible to determine the transfer function R_y directly by system identification. However, when the slave robot is not interacting with the environment, y_m is related to the system input f_m by the master robot dynamic model

$$y_m = (G_m H_{11} + S_m)\, f_m \tag{5.75}$$

Similarly, y_s is related to f_m by the slave robot dynamic model

$$y_s = (G_s H_{21})\, f_m \tag{5.76}$$

If f_m is a virtual force generated in the computer, the master robot sensitivity can be eliminated from equation 5.75 to give

$$y_m = (G_m H_{11})\, f_m \tag{5.77}$$

The position ratio is obtained by dividing equations 5.76 and 5.77. If the position ratio is specified to be $R_y = 1.00$, both elements in the first column of the H matrix will have unity gain. Therefore, when

$$H = \begin{bmatrix} H_{11}=1 & H_{12}=0 \\ H_{21}=1 & H_{22}=0 \end{bmatrix}$$

the position ratio becomes

$$R_y = \frac{G_s}{G_m} \tag{5.78}$$

The closed-loop transfer functions G_s and G_m have already been determined through system identification. Substituting equations 5.63 and 5.73 into equation 5.78 and simplifying yields

$$R_y = \frac{-0.0560s^3 + 2.1241s^2 + 11.9490s + 210.519}{-0.0206s^3 + 0.7029s^2 + 8.4028s + 207.784} \tag{5.79}$$

The simplest representation of the dynamics that determine the position ratio is a third order equation. The static gain of the transfer function is $R_y = 1.01$, which is almost the same as the specified value of $R_y = 1.00$. Equation 5.79 can be used to calculate the frequency response of R_y. The frequency response is shown in Figure 5.47, where the static gain has been normalized to 0 dB. The position ratio remains constant out to 4 rad/s, which is nearly equal to the maximum attainable bandwidth of the telerobotic system. The position ratio does not fall off at higher frequencies because the dynamic responses of the master and slave robots decrease at the same rate.

In the third experiment, the frequency response of the performance parameter R_f was determined. The force ratio defines a relationship between the robot forces such that

$$f_s = R_f f_m \tag{5.80}$$

If the input signal is the master force f_m, and the output signal is the slave force f_s, system identification yields the transfer function R_f directly.

A random binary input signal was generated in the computer to simulate a vertical force acting on the master robot's force sensor. The simulated master force was used to drive the slave robot, which was compressing a spring scale. The spring scale exerted a reaction force on the slave robot. The virtual master force and the actual slave force were recorded.

Using previously measured static values of the system parameters, the H matrix was designed to achieve a force ratio of $R_f = 1.00$. The H matrix had the following structure:

$$H = \begin{bmatrix} H_{11}=0 & H_{12}=0 \\ H_{21}=0.78 & H_{22}=0.10 \end{bmatrix}$$

The master robot was not driven. The slave robot's motion resulted from the combined action of the virtual force from the master robot, and the actual force from the spring scale.

Two sets of input-output data were acquired. Each data set contained 376 samples, and the sampling interval was T = 0.04 seconds. The input-output data used for parametric estimation of R_f are plotted versus time in Figure 5.48. The amplitude of the random binary input signal alternates between -15 and -20 lbf. This negative amplitude variation insures that the spring scale is always in compression. The output signal is positive because the spring scale pushes up against the slave robot. The input-output data used for cross-validation of the dynamic model are plotted in Figure 5.49.

A second-order ARX model was selected as the simplest representation of the observed input-output behavior. The model has the following parameters:

na = 2, nb = 1, nk = 2, FPE = 1.603

In difference equation form, the model is

y(t) = 1.2065 y(t-1) - 0.5134 y(t-2) - 0.2611 u(t-2)

The FPE was considerably higher than it was for the parametric estimation of the robot dynamics. This is probably a result of the model's inability to predict the high-frequency

oscillations in the noisy slave force signal. However, the model does predict the large-scale dynamic behavior of the robot forces fairly well. This is evident from the cross-validation shown in Figure 5.50.

The continuous-time transfer function corresponding to the ARX model of the force ratio is

$$R_f(s) = \frac{5.3507s - 231.8675}{s^2 + 16.6666s + 272.5188} \tag{5.81}$$

The static gain of the transfer function is $R_f = 0.85$. This is 15 percent lower than the specified value of $R_f = 1.00$. The discrepancy may result from hysteresis in the measured reaction force. The hysteresis is caused by backlash in the slave robot's wrist joint. The wrist joint is normally locked to prevent rotation. However, a significant amount of backlash was observed in the wrist joint during the experiment. The force ratio is approximately equal to its specified value when the spring scale is compressed to 20 lbf. This can be seen by comparing the input and output signals in Figures 5.48 and 5.49. In contrast, the force ratio is only about 75 percent of its specified value when the spring scale is released to 15 lbf. While a nonlinear effect like hysteresis cannot be completely characterized by a linear model, the transfer function correctly predicts the average force ratio over the entire cycle.

The frequency response of R_f can be calculated from equation 5.81. The frequency response is shown in Figure 5.51, where the static gain has been normalized to 0 dB. The force ratio remains constant out to 4 rad/s, which is nearly equal to the maximum attainable bandwidth of the telerobotic system. At higher frequencies, the force ratio falls off rapidly because the slave robot cannot move fast enough in response to the force input from the master robot.

The robustness experiments have demonstrated that the performance parameters Z_m, Z_s, R_y, and R_f remain nearly constant over the full range of human capability. Static values of the system variables can be used to design the H matrix for adequate performance within the bandwidth $0 < \omega < 4.5$ rad/s. At low frequencies, the robot impedances are robust to modeling uncertainties on the order of 10 percent. As the frequency range increases, the dynamic models used for H matrix design must be known more precisely.

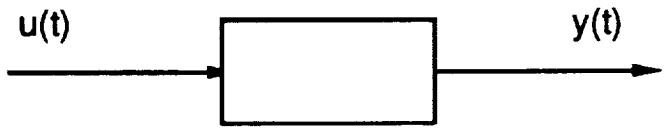

Figure 5.35: Linear System

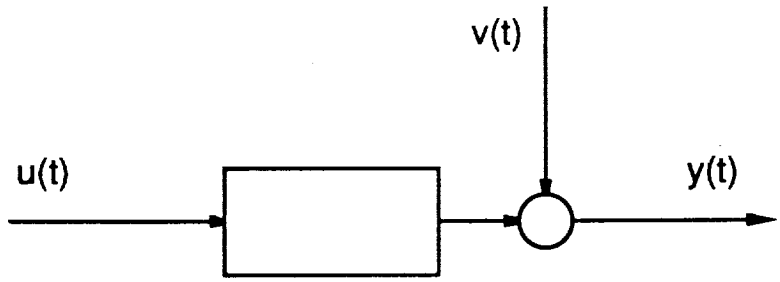

Figure 5.36: Linear System with Additive Disturbance

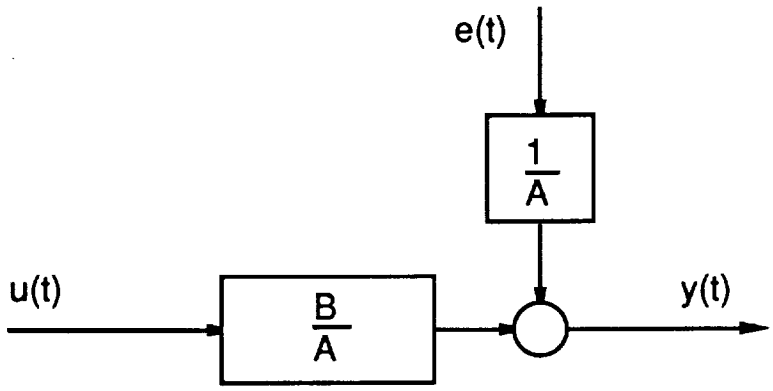

Figure 5.37: ARX Model

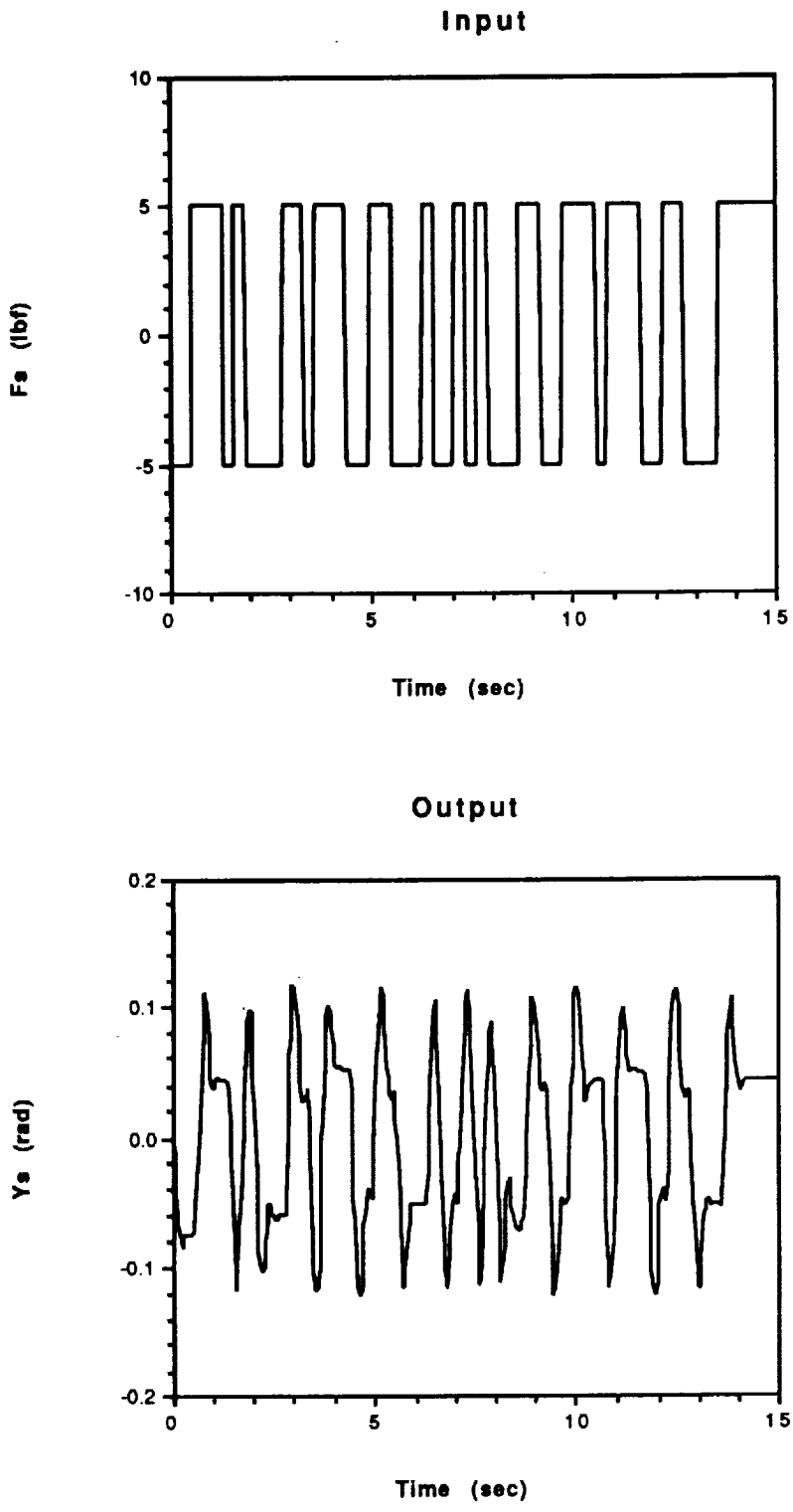

Figure 5.38: Input-Output Data for Parameter Estimation of G_s

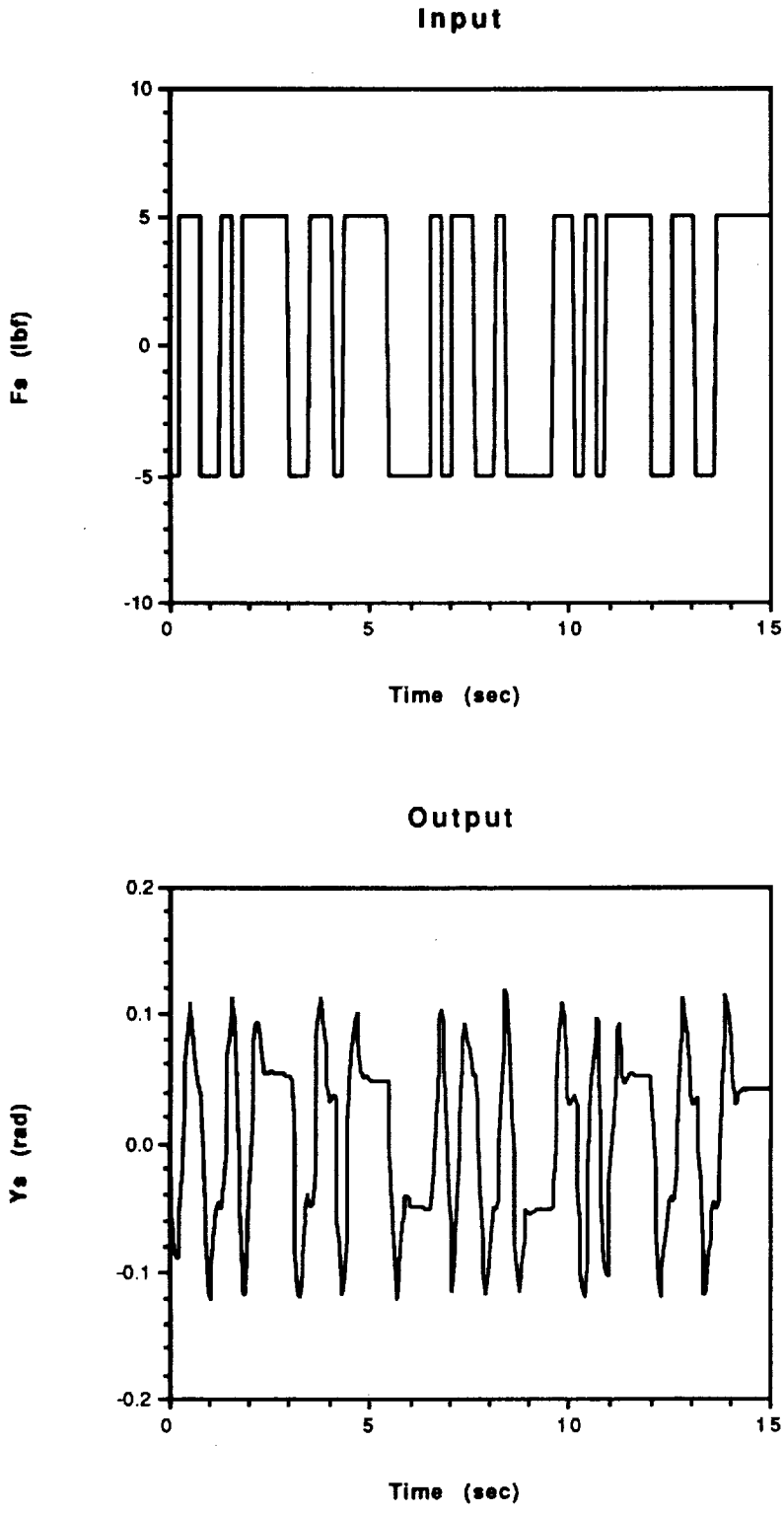

Figure 5.39: Input-Output Data for Cross-Validation of G_s

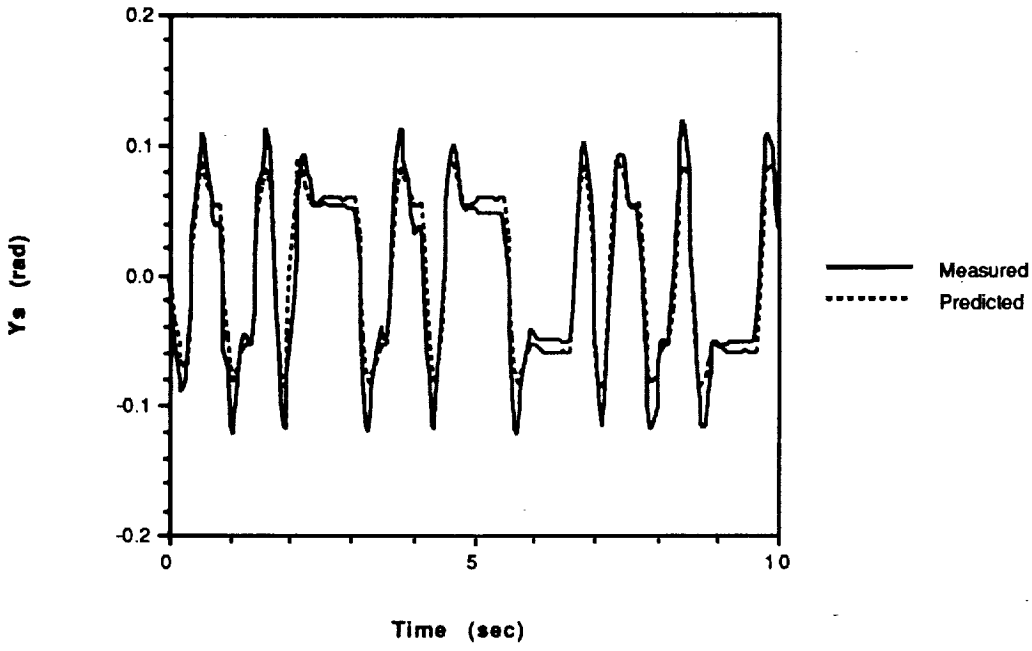

Figure 5.40: Cross-Validation of G_s

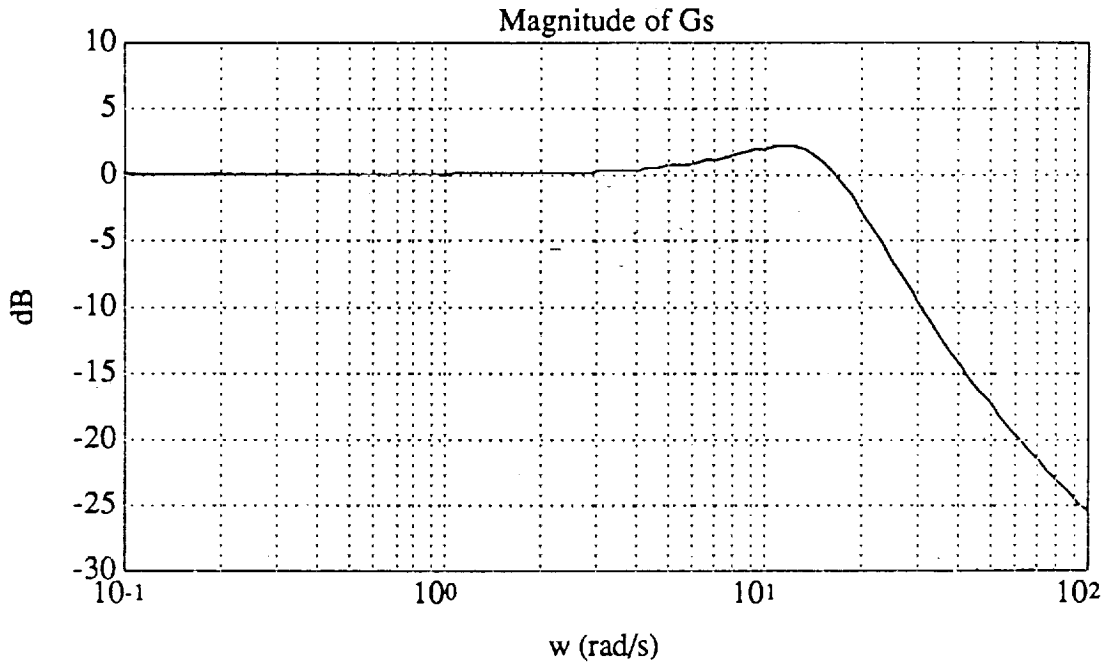

Figure 5.41: Normalized Closed-Loop Frequency Response of G_s

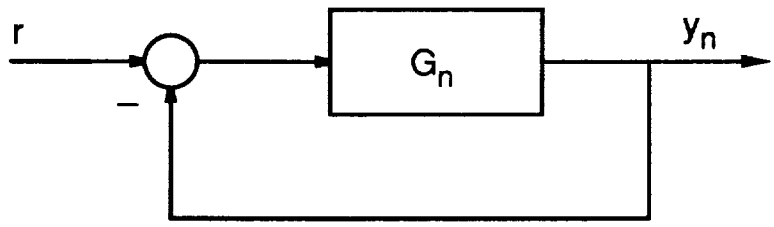

Figure 5.42: Closed-Loop System

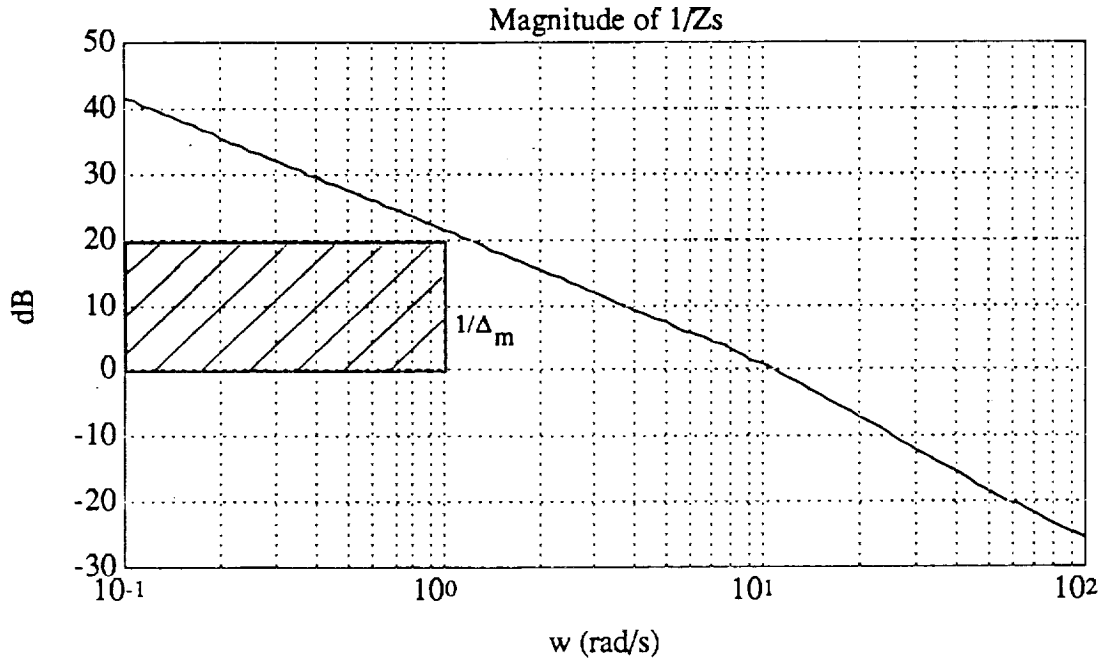

Figure 5.43: Open-Loop Frequency Response of $1/Z_s$

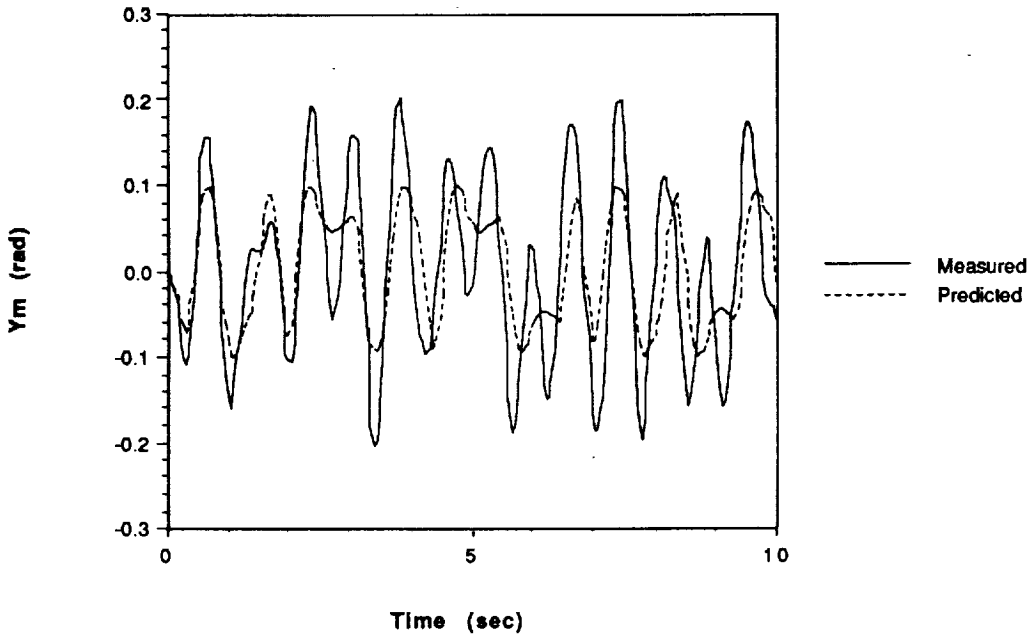

Figure 5.44: Cross-Validation of G_m

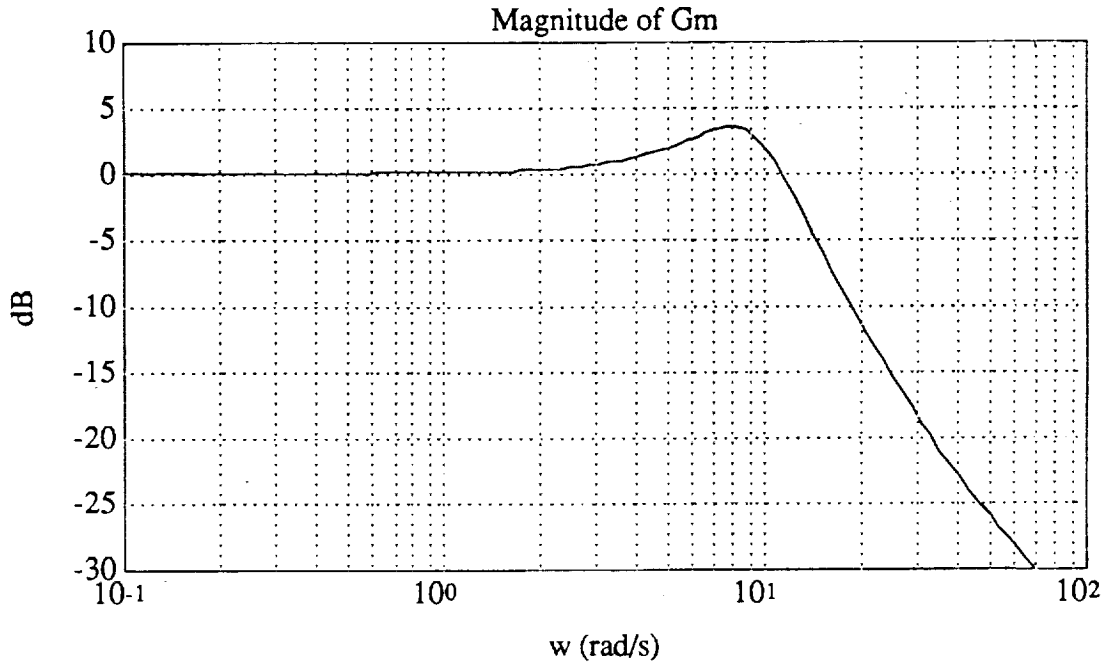

Figure 5.45: Normalized Closed-Loop Frequency Response of G_m

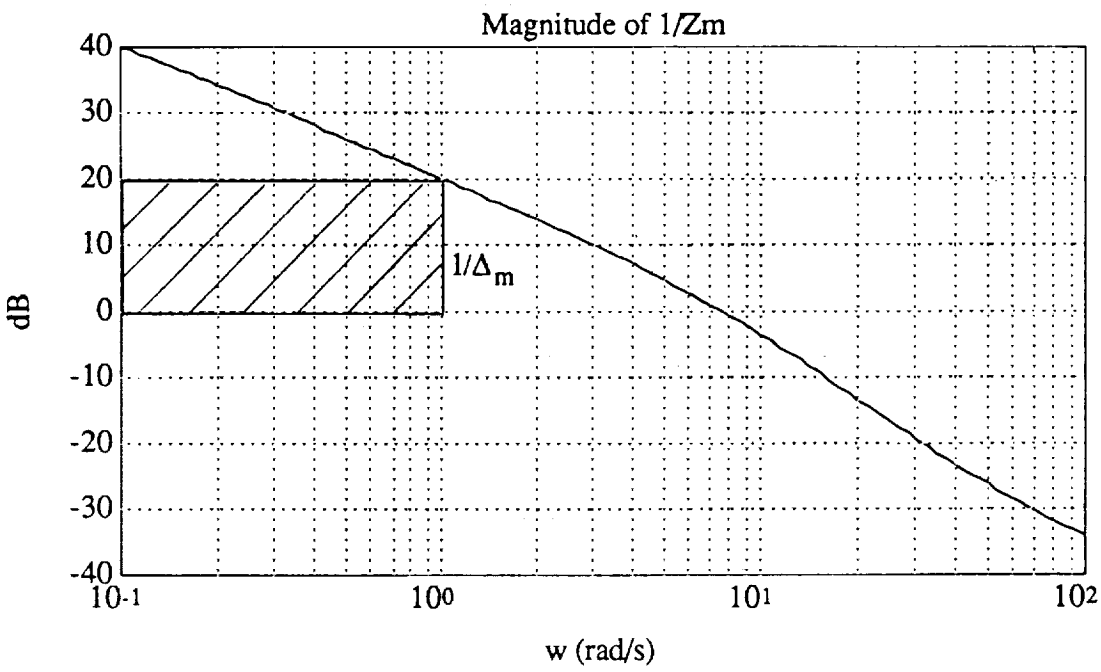

Figure 5.46: Open-Loop Frequency Response of $1/Z_m$

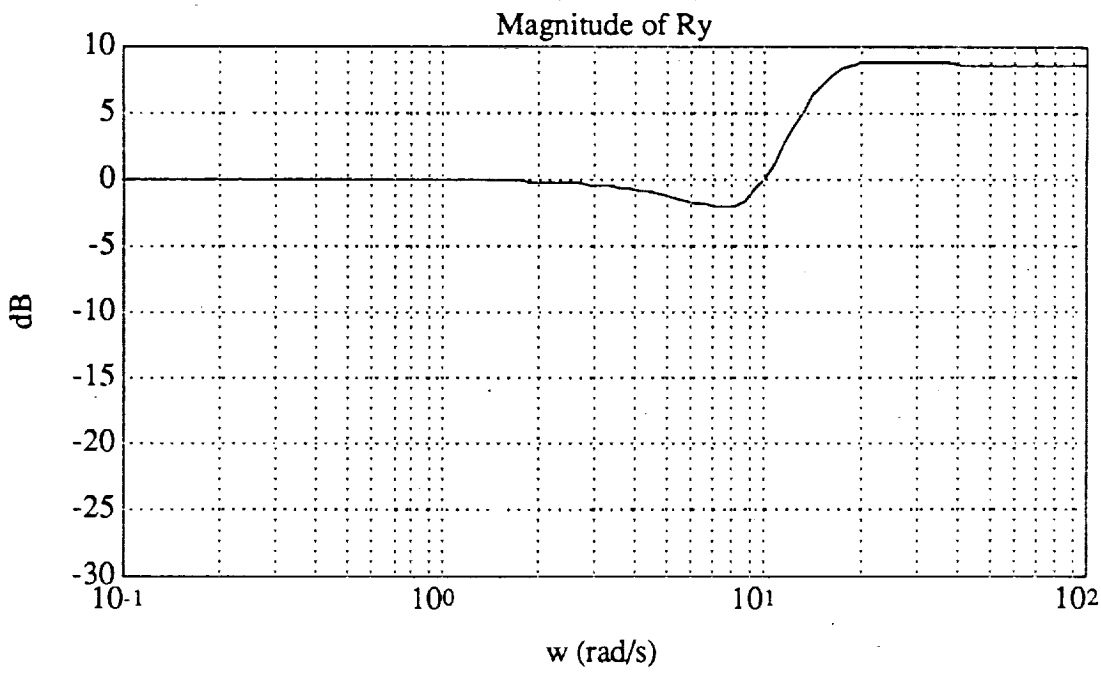

Figure 5.47: Normalized Frequency Response of Ry

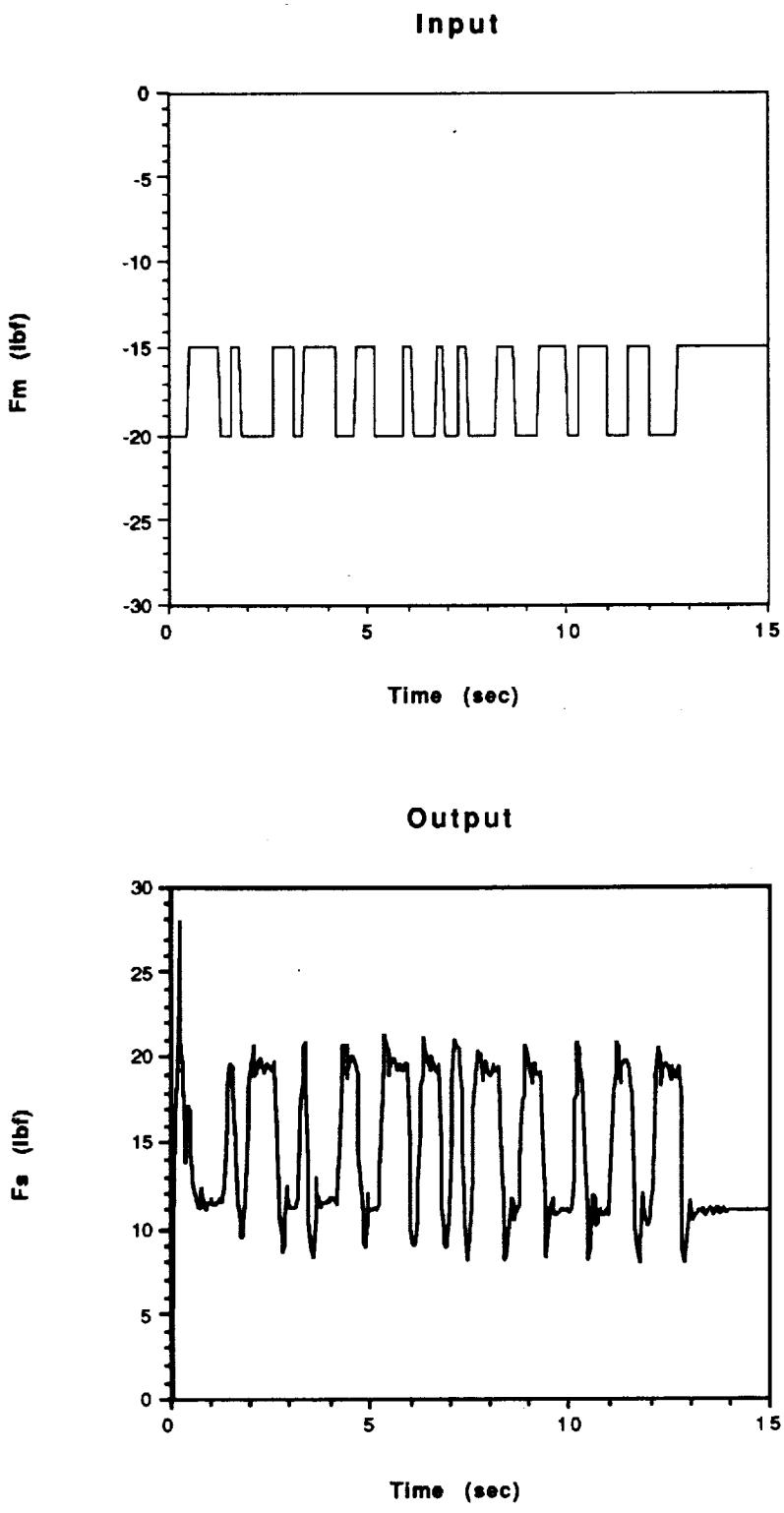

Figure 5.48: Input-Output Data for Parameter Estimation of R_f

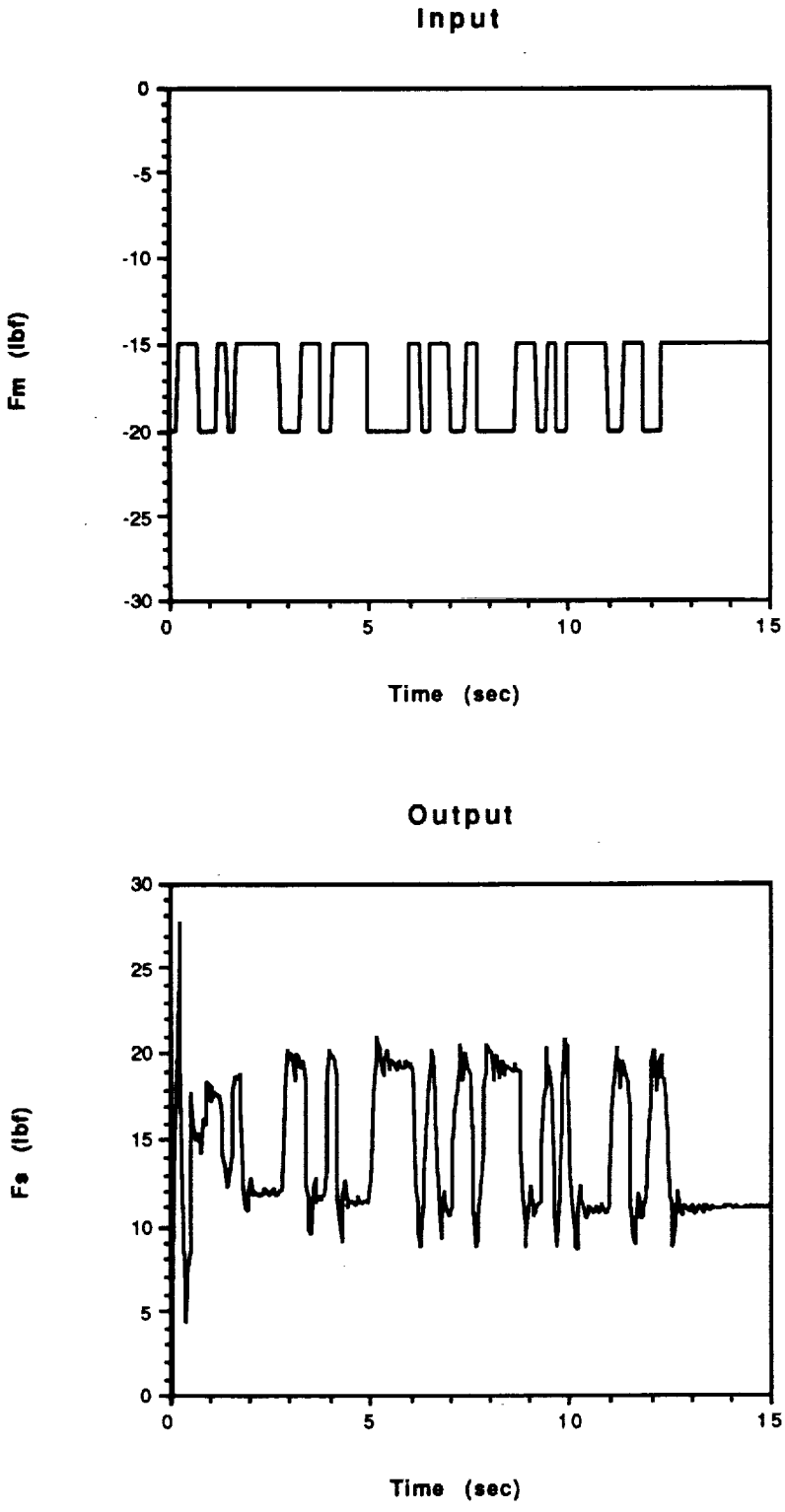

Figure 5.49: Input-Output Data for Cross-Validation of R_f

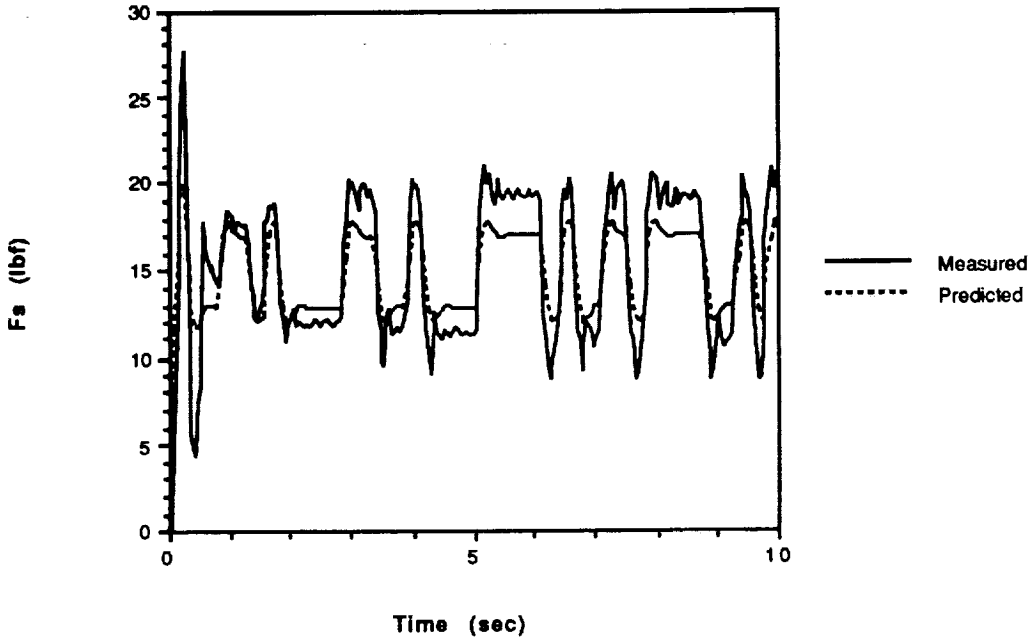

Figure 5.50: Cross-Validation of R_f

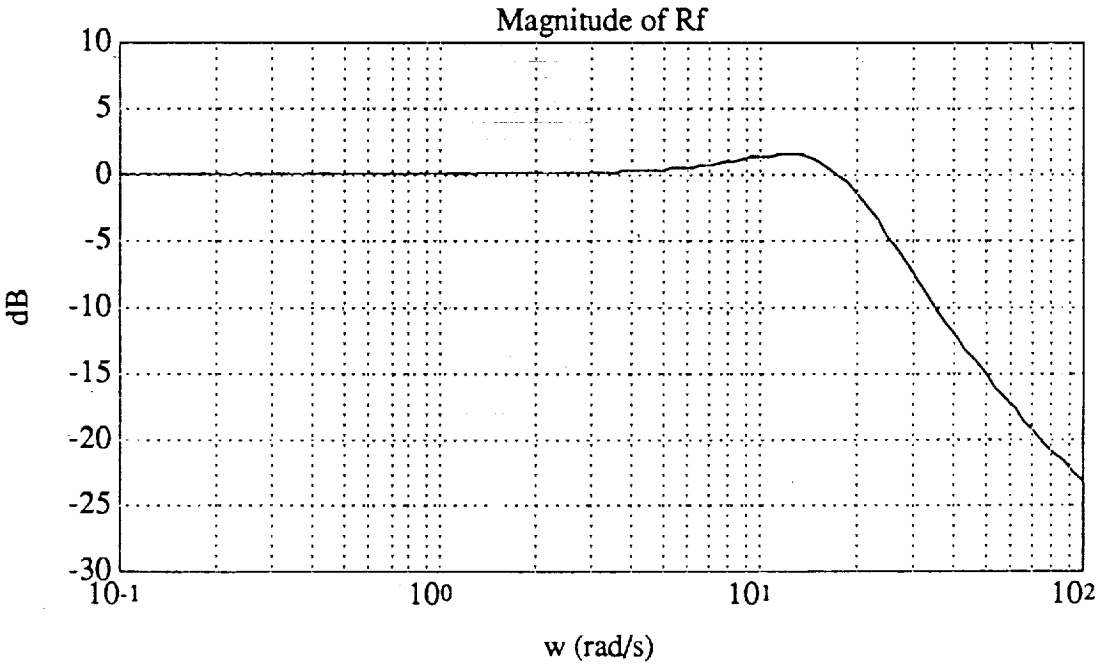

Figure 5.51: Normalized Frequency Response of R_f

5.8 Stability Conditions

The stability of the telerobotic system depends on the relationship of the H matrix to the dynamics of the human arm and the environment. System stability is guaranteed if the following conditions are satisfied:

$$|P_{11}| < \frac{1}{|S_h|} \tag{5.82}$$

$$\left| \frac{1 + P_{11}S_h}{P_{22} + \Delta P S_h} \right| > |E| \tag{5.83}$$

The first stability condition applies to the interaction between the master robot and the human arm. The second stability condition applies to the interaction between the slave robot and the environment. The physical meaning of the stability conditions can be appreciated if they are expressed in terms of the robot impedances. The impedance of the master robot is given by

$$Z_m = \frac{1 + P_{22}E}{P_{11} + \Delta P E} \tag{5.84}$$

For unconstrained motion, $E = 0$ and the master robot impedance becomes

$$Z_m = \frac{1}{P_{11}} \tag{5.85}$$

Using this expression in equation 5.82, the first stability condition can be rewritten as

$$|Z_m| > |S_h| \tag{5.86}$$

The impedance of the human arm is the sensitivity S_h. Therefore, the first stability condition states that for unconstrained motion, the impedance of the master robot must be greater than the impedance of the human arm. Equation 5.86 is a sufficient but not an absolutely necessary condition for stability of the master robot. In other words, the robot may be stable if $|Z_m| < |S_h|$, but it can never be unstable if $|Z_m| > |S_h|$.

The impedance of the slave robot is given by

$$Z_s = \frac{1 + P_{11}S_h}{P_{22} + \Delta P S_h} \tag{5.87}$$

Substituting this expression into equation 5.83 yields

$$|Z_s| > |E| \tag{5.88}$$

The impedance of the environment is E. Therefore, the second stability condition states that for constrained motion, the impedance of the slave robot must be greater than the impedance of the environment. Equation 5.88 is a sufficient but not an absolutely necessary condition for stability of the slave robot. In other words, the robot may be stable if $|Z_s| < |E|$, but it can never be unstable if $|Z_s| > |E|$.

The first stability condition will be verified by finding a lower bound on the master robot impedance at which the system exhibits stable behavior. To prove the stability condition, it is only necessary to show that the lower bound is no greater than the impedance of the human arm.

The master impedance is a performance parameter that can be arbitrarily specified by adjusting the H matrix. The H matrix is designed by expressing the master impedance in terms of known system parameters. If the slave robot is free to move without constraint, the master impedance can be written as

$$Z_m = \frac{1}{G_m H_{11} + S_m} \tag{5.89}$$

by substituting the definition of P_{11} into equation 5.85. Solving the previous equation for H_{11} yields

$$H_{11} = \frac{1/Z_m - S_m}{G_m} \tag{5.90}$$

This equation can be used to calculate the magnitude of H_{11} necessary to achieve any desired impedance Z_m. The master impedance is specified as a fraction of the human arm impedance S_h. The values of G_m, S_m, and S_h have been measured experimentally for a

particular configuration of the master robot and the human arm. It was found that G_m = 0.0117 rad/lbf, S_m = 0.0033 rad/lbf, and S_h = 115.5 lbf/rad for small elbow pitch movements near the horizontal.

For the first experiment, the master impedance was specified to be $Z_m = S_h$. The objective was to demonstrate stable behavior. The H matrix had the following structure:

$$H = \begin{bmatrix} H_{11}=0.46 & H_{12}=0 \\ H_{21}=0 & H_{22}=0 \end{bmatrix}$$

The magnitude of H_{11} was calculated from equation 5.90 using the values given above for the system variables. Since the first stability condition applies to the interaction between the master robot and the human arm, it is not necessary to drive the slave robot. Only the master robot was driven. This was done by setting all gains in the H matrix except H_{11} to zero. An increasing vertical force was applied to the master robot so that its elbow moved in pitch. The human arm was kept rigid during the maneuver. The applied force was recorded over a 5-second period. Figure 5.52 is a plot of the master force versus time. Since the force increases smoothly without oscillation, the master robot is stable. This experiment establishes a lower bound for stability on Z_m. The lower bound is at most equal to S_h. Therefore, the first stability condition is verified.

To demonstrate unstable behavior, the master impedance was specified to be $Z_m = 0.5S_h$ in the second experiment. The desired impedance was achieved by calculating the required magnitude for H_{11}. The H matrix had the following structure:

$$H = \begin{bmatrix} H_{11}=1.20 & H_{12}=0 \\ H_{21}=0 & H_{22}=0 \end{bmatrix}$$

The master force is plotted as a function of time in Figure 5.53. The force increases smoothly at first, then suddenly undergoes large amplitude oscillations. It is obvious that the robot is unstable. Since the master impedance is much smaller than the human arm impedance, this result is expected.

The first stability condition is conservative. That is, it guarantees stability if it is satisfied, but it does not predict the onset of instability. As illustrated in the previous two experiments, the transition from stable to unstable behavior occurs somewhere in the region $0.5S_h < Z_m < S_h$.

The second stability condition will be verified in the same manner as the first stability condition. That is, a lower bound for stability will be established on the slave robot

impedance. To prove the stability condition, it is only necessary to show that the lower bound is no greater than the impedance of the environment.

The slave impedance is a performance parameter that can be arbitrarily specified by adjusting the H matrix. The H matrix is designed by expressing the slave impedance in terms of known system parameters. When there is no force reflection from the environment, the gain of H_{12} is zero. Consequently, the admittance $P_{12} = 0$, and equation 5.87 can be simplified to

$$Z_s = \frac{1}{P_{22}} \tag{5.91}$$

Note that by assuming no force reflection, the dependence of Z_s on the human arm impedance S_h has been eliminated. Substituting the definition of P_{22} into the previous equation gives

$$Z_s = \frac{1}{G_s H_{22} + S_s} \tag{5.92}$$

Solving this equation for H_{22} yields

$$H_{22} = \frac{1/Z_s - S_s}{G_s} \tag{5.93}$$

Equation 5.93 can be used to calculate the magnitude of H_{22} required to achieve any desired impedance Z_s. The slave impedance is specified as a fraction of the environmental impedance E. The magnitude of E has been determined experimentally for compression of a spring scale. The values of G_s and S_s have also been measured for small elbow pitch motions of the slave robot. It was found that $G_s = 0.0117$ rad/lbf, $S_s = 0.0033$ rad/lbf, and $E = 217.0$ lbf/rad.

For the third experiment, the slave impedance was specified to be $Z_s = E$. The objective was to demonstrate stable behavior. The H matrix had the following structure:

$$H = \begin{bmatrix} H_{11}=0.20 & H_{12}=0 \\ H_{21}=1 & H_{22}=0.11 \end{bmatrix}$$

Because H_{12} is zero, there is no force reflection, and the slave impedance depends solely on H_{22}. The magnitude of H_{22} was calculated from equation 5.93 using the values given above for the system variables. H_{21} was given a unity gain so that the slave robot would move in

response to an increasing vertical force exerted on the master robot. The slave robot compressed a spring scale that simulated a compliant environment. The reaction force on the slave robot was recorded over a 5-second period. Figure 5.54 is a plot of the slave force versus time. The slave force increases steadily without significant oscillation. Thus, the slave robot is stable. This experiment establishes a lower bound for stability on Z_S. The lower bound is at most equal to E. Therefore, the second stability condition is verified.

The purpose of the fourth experiment was to demonstrate an unstable interaction with the environment. The slave impedance was specified to be $Z_S = 0.5E$. The desired impedance was achieved by calculating the required magnitude for H_{22}. The H matrix had the following structure:

$$H = \begin{bmatrix} H_{11}=0.20 & H_{12}=0 \\ H_{21}=1 & H_{22}=0.51 \end{bmatrix}$$

The measured reaction force is plotted as a function of time in Figure 5.55. The slave force oscillates violently, indicating that the slave robot is unstable. Since the slave impedance is much smaller than the environmental impedance, this result is expected.

Like the first stability condition, the second stability condition is conservative. Stability is guaranteed if the condition is satisfied, but the system may not become unstable if the condition is violated. It can be concluded from the previous two experiments that the transition from stable to unstable behavior occurs somewhere in the region $0.5E < Z_S < E$.

These experiments have demonstrated that stability depends on the relative magnitude of the impedance at both ends of the telerobotic system. For stable behavior, the master impedance should be greater than the impedance of the human arm, while the slave impedance should be greater than the impedance of the environment. These results are consistent with theoretical predictions.

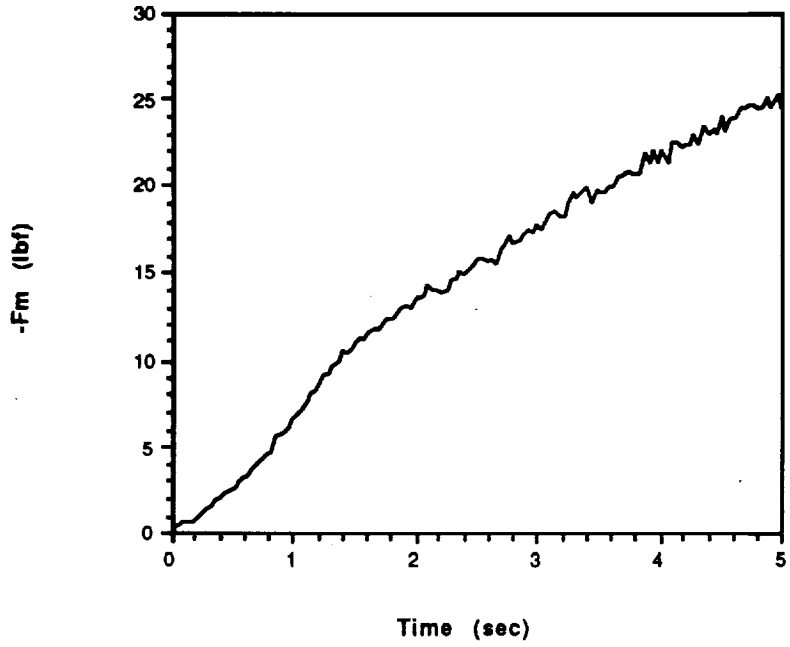

Figure 5.52: $Z_m = S_h$;
Master Force vs. Time

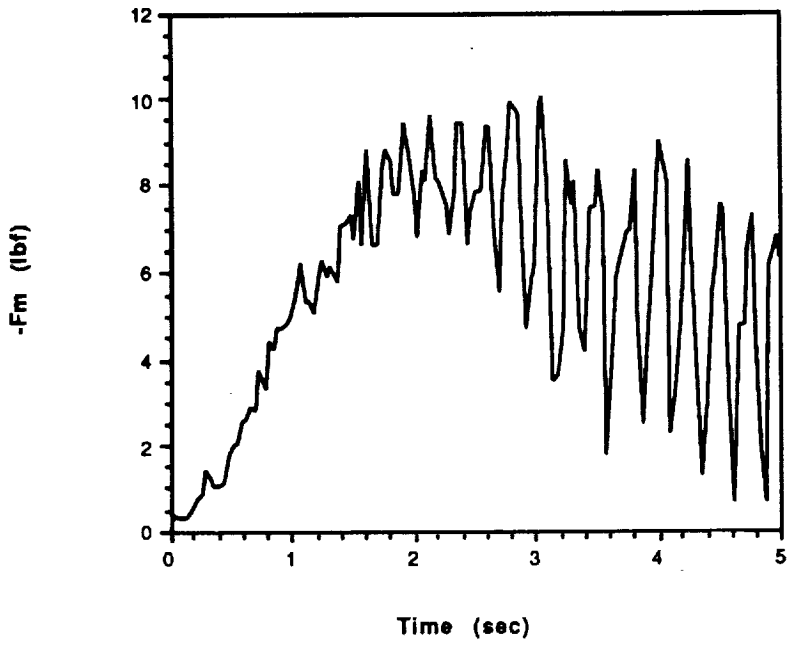

Figure 5.53: $Z_m = 0.5S_h$;
Master Force vs. Time

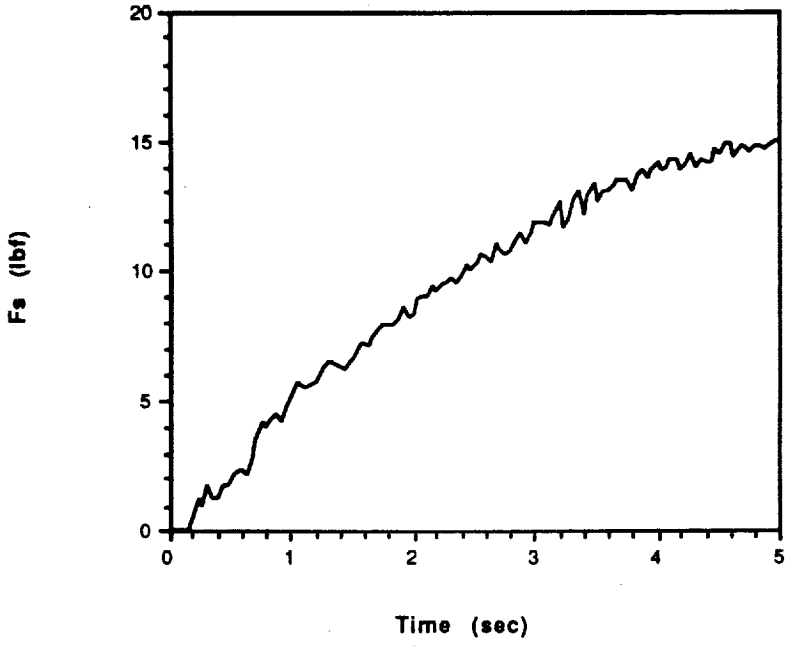

Figure 5.54: $Z_S = E$;
Slave Force vs. Time

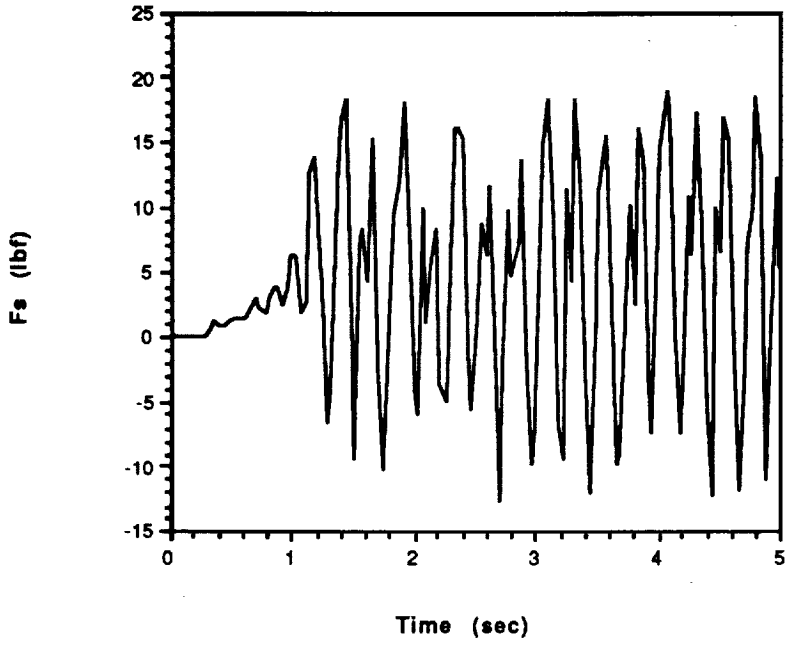

Figure 5.55: $Z_S = 0.5E$;
Slave Force vs. Time

5.9 Summary

The bilateral impedance control architecture was successfully implemented on a telemanipulator having seven degrees of freedom. The H matrix was modified to include force transformation terms. These additional terms were necessary to map forces measured in Cartesian space into input commands to the stabilizing position controllers in joint space. The force transformation scheme was based on the transpose of the manipulator Jacobian.

Static values were determined for the system variables G_m, S_m, G_s, S_s, S_h, and E. These values were used in the design of the H matrix to achieve desired performance characteristics. The performance parameters were measured and compared to their specified values.

The robot impedance was modulated by changing the gain and structure of the compensators in the H matrix. A stiffness impedance was obtained when the H matrix had constant gain. A damping impedance was produced when the H matrix integrated the force input.

The position ratio was measured for unconstrained motion in two degrees of freedom. Three position ratios were demonstrated: R_y=1:1, R_y=2:1, and R_y=1:3. In all cases, the actual position ratio was within 10 percent of its specified value. The error seemed to increase as the difference in robot positions increased.

The force ratio was measured when the slave robot was compressing a spring scale. Two force ratios were demonstrated: R_f=1:1 and R_f=2:1. In both cases, the actual force ratio was within 2 percent of its specified value.

It was shown that the force ratio, the position ratio, and the slave impedance can be specified at the same time.

Second-order dynamic models were obtained for G_m, G_s, and R_f by the ARX parametric estimation technique. A random binary input signal was applied to the system, and the resulting output signal was recorded. The dynamic models were cross-validated by calculating a simulated output and comparing it to the observed output.

The frequency response of the performance parameters was derived from the dynamic models found through system identification. The performance parameters were nearly constant over the full range of human capability, $0 < \omega < 4.5$ rad/s. This implies that static values of the system variables can be used for H matrix design at low frequencies.

Robustness to modeling uncertainties was determined from the shape of the calculated frequency response. At low frequencies, the robot impedances will remain within one percent of their nominal specified values if the modeling uncertainties are no more than

10 percent. However, as the frequency range increases, the dynamic models used for design of the H matrix must be known more precisely.

The stability conditions were verified by establishing lower bounds on the robot impedances. For unconstrained motion, the transition from stable to unstable behavior occurred somewhere in the region $0.5S_h < Z_m < S_h$. For constrained motion, the transition occurred in the region $0.5E < Z_s < E$.

The experimental results for performance and stability were consistent with theoretical predictions.

Chapter 6
CONCLUSIONS

The bilateral impedance control architecture differs from previous approaches in that force signals travel in both directions between the master and slave robots. The communication of force signals within the system is regulated by the H matrix. By tailoring the structure of the H matrix, it is possible to arbitrarily specify desired system performance characteristics. This is the primary advantage of bilateral impedance control.

System performance can be completely described by a set of three independent parameters. These parameters may be the force ratio, the position ratio, or the impedance of either robot. To form an independent set, one of the parameters must be the slave impedance. The performance parameters are functions of the system variables that govern the dynamic behavior of the robots, the human arm, and the environment.

The performance parameters are fundamentally related to the elements in the H matrix. The compensator H_{11} determines the master impedance, while the compensator H_{22} determines the slave impedance. The compensator H_{21} couples the motions of the robots, and the compensator H_{12} controls force reflection. By selecting the relative magnitudes of these four elements, three performance parameters can be specified simultaneously.

The only limitations on the choice of performance parameters are imposed by the requirements for system stability. There are two conditions that are sufficient to guarantee stability for both linear and nonlinear systems. For unconstrained motion, the master impedance must be greater than the impedance of the human arm. For constrained motion, the slave impedance must be greater than the impedance of the environment. The system may be stable when the conditions are violated, but it can never be unstable when the conditions are satisfied. Since both the master and slave impedances are performance parameters that can be arbitrarily specified, it is not necessary to trade off performance and stability in most cases.

Power is generated in the telerobotic system by the human arm and the control system actuators. The human arm is an independent source of effort, while the actuators are dependent sources of effort. There is no transfer of power between the master and slave robots. Only information is exchanged by the transmission of force signals. The system's order is equal to the number of independent energy storage elements. The bilateral impedance control architecture can be modeled as a sixth-order system. Potential energy is stored in the stiffness of the human arm, the environment, and the stabilizing control systems. Kinetic energy is stored in the inertia of the robots.

When the bilateral impedance control is implemented on a multi-degree-of-freedom telemanipulator, force transformation terms must be added to the H matrix. These additional terms map forces measured in Cartesian space into input commands to the stabilizing position controllers in joint space. The transpose of the manipulator Jacobian can be used to transform force.

In practice, the specified performance characteristics can be achieved fairly accurately. However, the deviation of the performance parameters from their desired values tends to grow as the difference between the master and slave variables gets larger. This could result from small errors being amplified across the system. Additional errors are introduced because the zero readings of the force sensors drift over time. Since these errors are cumulative, the force sensor zeros must be reestablished periodically.

The form of the robot impedance depends on the structure chosen for the compensators in H matrix. If the compensators have constant gain, force is proportional to position and a stiffness impedance is obtained. If the compensators integrate the force input, a damping impedance is obtained where force is proportional to velocity.

If the motion of the robots is relatively slow, the H matrix can be designed using static values of the system variables. The performance parameters are nearly constant over the full range of human capability. The control architecture is robust to small modeling uncertainties at low frequencies. However, as the frequency range increases, the system variables must be known more precisely.

The main disadvantage of bilateral impedance control is that values must be determined for the system variables before the H matrix can be designed. The variables that describe the dynamic behavior of the human arm and the environment are continually changing. These variables must be revised for each new task or configuration. In a complex world, the control architecture would require some form of adaptive control to make it truly practical.

The major goal of the research program was attained. Theories of performance and stability were developed and verified experimentally. This work has shown that bilateral impedance control holds promise as a new control method for telerobotic systems.

REFERENCES

Anderson, R. J., *A Network Approach to Force Control in Robotics and Teleoperation*, Ph. D. Thesis, University of Illinois, January 1989.

Anderson, R. J., and Spong, M. W., "Asymptotic Stability for Force Reflecting Teleoperators with Time Delay," in *Proceedings of the IEEE International Conference on Robotics and Automation*, 1989.

Barker, L. K., and McKinney, Jr., W. S., "Optimized Resolved Rate Control of Seven-Degree-of-Freedom Laboratory Telerobotic Manipulator (LTM) with Application to Three-Dimensional Graphics Simulation," NASA Technical Paper 2938, October 1989.

Craig, J. J., *Introduction to Robotics; Mechanics and Control*, Addison-Wesley Publishing Company, 1988.

Hannaford, B., "Stability and Performance Tradeoffs in Bi-Lateral Telemanipulation," in *Proceedings of IEEE International Conference on Robotics and Automation*, Scottsdale, AZ, May 1989.

Hannaford, B., "A Design Framework for Teleoperators with Kinesthetic Feedback," *IEEE Transactions on Robotics and Automation*, Vol. 5, No. 4, August 1989.

Herndon, J. N., Hamel, W. R., and Meintel, A. J., "Robotic Systems for NASA Ground-Based Research," *Robotics*, Vol. 4, No. 1, March 1988.

Herndon, J. N., Babcock, S. M., Butler, P. L., Costello, H. M., Glassell, R. L., Kress, R. L., Kuban, D. P., Rowe, J. C., Williams, D. M., and Meintel, A. J., "Telerobotic Manipulator Developments for Ground-Based Space Research", paper presented to ANS Meeting on Robotics and Remote Systems, Charleston, SC, March 1989.

Jansen, J. F., and Herndon, J. N., "Design of a Telerobotic Controller with Joint Torque Sensors," in *Proceedings of the IEEE International Conference on Robotics and Automation*, 1990.

JR3 Universal Force-Moment Sensor System Operation Manual, JR3, Inc., Woodland, CA, 1988.

Karnopp, D., and Rosenberg, R., *System Dynamics: A Unified Approach*, John Wiley and Sons, New York, 1975.

Kazerooni, H., Sheridan, T. B., and Houpt, P. K., "Robust Compliant Motion for Manipulators," *IEEE Journal of Robotics and Automation*, Vol. 2, No. 2, June 1986.

Kazerooni, H., "Compliant Motion Control for Robot Manipulators," *International Journal of Control*, Vol. 49, No. 3, pp. 745-760, 1989.

Kazerooni, H., "Human-Robot Interaction via the Transfer of Power and Information Signals", *IEEE Transactions on Systems, Man, and Cybernetics*, Vol. 20, No. 2, March 1990.

Kernighan, B. W., and Ritchie, D. M., *The C Programming Language*, Second Edition, Prentice Hall, Englewood Cliffs, NJ, 1988.

Lehtomaki, N. A., Sandell, N. R., and Athans, M., "Robustness Results in Linear-Quadratic Gaussian Based Multivariable Control Designs," *IEEE Transactions on Automatic Control*, Vol. 26, No. 1, pp. 75-92, February 1981.

Ljung, L., *System Identification: Theory for the User*, Prentice-Hall, Englewood Cliffs, NJ, 1987.

Ogata, K., *Modern Control Engineering*, Prentice-Hall, Englewood Cliffs, NJ, 1970.

MATLAB System Identification Toolbox User's Guide, The MathWorks, Inc., S. Natick, MA, 1989.

Raju, G. J., Verghese, G. C., and Sheridan, T. B., "Design Issues in 2-port Network Models of Bilateral Remote Manipulation," in *Proceedings of the IEEE International Conference on Robotics and Automation*, 1989.

Sheridan, T. B., and Ferrell, W. R., *Man-Machine Systems: Information, Control, and Decision Models of Human Performance*, MIT Press, Cambridge, MA, 1974.

Sheridan, T. B., "Telerobotics," in *Proceedings of the Workshop on Shared Autonomous and Teleoperated Manipulator Control*, Philadelphia, PA, 1988.

Spong, M. W., and Vidyasagar, M., "Robust Nonlinear Control of Robot Manipulators," IEEE Conference on Decision and Control, December 1985.

Vidyasagar, M., and Desoer, C. A., *Feedback Systems: Input-Output Properties*, Academic Press, 1975.

Vidyasagar, M., *Nonlinear Systems Analysis*, Prentice-Hall, 1978.

Whitney, D. E., "Historical Perspective and State of the Art in Robot Force Control," *The International Journal of Robotics Research*, Vol. 6, No. 1, Spring 1987.